Principles and Applications of Semiconductor Photoelectrochemistry

MING X. TAN, PAUL E. LAIBINIS, SONBINH T. NGUYEN, JANET M. KESSELMAN, COLBY E. STANTON, *and* **NATHAN S. LEWIS***

Division of Chemistry and Chemical Engineering
California Institute of Technology
Pasadena, California

CONTENTS

I. INTRODUCTION

II. ELECTRONIC PROPERTIES OF SEMICONDUCTORS

A. Crystal Structures of Some Selected Semiconductors
B. Band Structure and Optical Properties of Semiconductors
1. The Molecular Orbital Description of Semiconducting Solids
2. Optical Characteristics of Semiconductor Materials
3. Carrier Statistics for Semiconductors

III. EQUILIBRIUM STATE AT A SEMICONDUCTOR/LIQUID JUNCTION

A. Depletion
1. Qualitative Description of Interfacial Charge Equilibration
2. Quantitative Description of Interfacial Charge Equilibration
B. Accumulation
C. Fermi Level Pinning

IV. CHARGE TRANSFER AT A SEMICONDUCTOR/LIQUID JUNCTION

A. Current–Voltage Behavior for a Semiconductor/Liquid Interface
1. Charge Transfer at Equilibrium
2. The Dark Current–Voltage Characteristics of a Junction
B. Current–Voltage Characteristics of a Semiconductor Electrode Under Illumination
1. Basic *I–V* Equations for Illuminated Semiconductor/Liquid Junctions
2. Energy Conversion Properties
C. Photoelectrosynthetic and Photocatalytic Cells

*Author to whom correspondence should be addressed.
Progress in Inorganic Chemistry, *Vol. 41*, Edited by Kenneth D. Karlin.
ISBN 0-471-59699-X © 1994 John Wiley & Sons, Inc.

V. STRATEGIES FOR THE DESIGN OF SEMICONDUCTOR/LIQUID JUNCTIONS FOR ENERGY CONVERSION

A. Photoelectrochemical Cells Employing Large Band Gap Semiconductors
B. Advances in Semiconductor/Liquid Junctions Employing Small Band Gap Semiconductors
1. Strategies for the Generation of Stable Aqueous Photoelectrochemical Cells
2. Energetics of Aqueous Photoelectrochemical Cells: Fermi Level Pinning
3. Photoelectrochemical Generation of Fuels Using Small Band Gap Semiconductors
4. Semiconductor/Liquid Junctions in Nonaqueous Solvents
5. Hot Electrons in Photoelectrochemical Cells
6. Surface Modification of Small Band Gap Semiconductors
C. Dye Sensitization of Semiconductor Electrodes

VI. RECENT ADVANCES IN APPLICATIONS OF LARGE BAND GAP SEMICONDUCTOR/LIQUID JUNCTIONS

A. Photodegradation of Organic Waste Waters with Large Band Gap Semiconductors
B. Use of Large Band Gap Semiconductors to Catalyze New Synthetic Oxidation Reactions

VII. SUMMARY

ABBREVIATIONS

SYMBOLS

ACKNOWLEDGMENTS

REFERENCES

I. INTRODUCTION

Photoelectrochemical cells are the most efficient chemical means known for converting solar energy. These devices are simple to construct, and often consist of nothing more than two electrodes, one metallic and one semiconducting, that are immersed into a liquid and exposed to sunlight. Using a fascinating process to be described in this chapter, the semiconducting electrode can efficiently absorb sunlight, create delocalized charges, effect the separation of these charges with high yield, and produce an electrical current that leads to energy conversion. Such devices can be extremely effective at converting solar energy into electrical and/or chemical energy, with efficiencies exceeding 15% in state-of-the-art systems (1–4). The goal of this chapter is to elucidate the operating principles of such cells and to describe current frontiers in semiconductor photoelectrochemistry.

At present, there are three methods by which light can be converted into industrially useful energy sources (Fig. 1). *Photosynthesis* is Nature's method

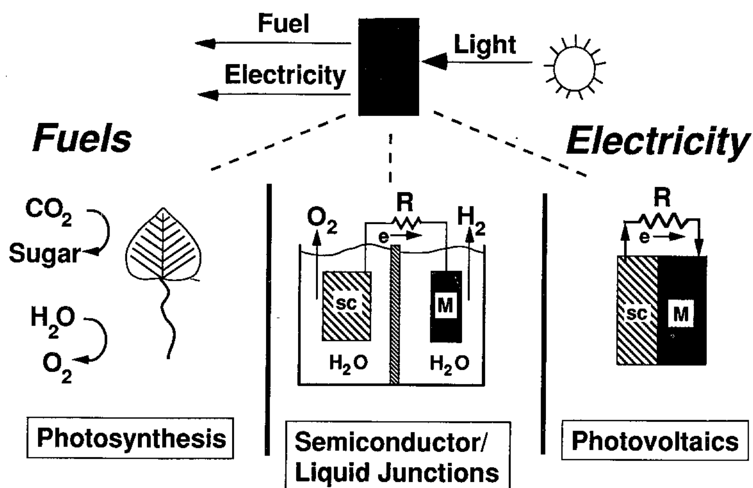

Figure 1. Methods of solar energy conversion.

of solar energy conversion, and is ultimately responsible for the chemical fuels that sustain life on this planet. The basic photosynthetic process involves conversion of carbon dioxide and water to sugars and dioxygen. In this process, the incident solar radiation provides the energy source, and some of this solar energy is stored in the form of chemical fuels that are produced by the photosynthetic cycle. Although natural photosynthetic systems can form a variety of chemical products (among them, methane, alcohol, and sugars), all photosynthetic systems found in nature operate similarly, in that they ultimately convert incident photon energy into stored fuels. Typical photosynthetic processes do not store a large amount of the incident solar energy. Generally, only 3–5% of the total incident power is stored as Gibbs free energy in the fuels of plants during an optimal growing season, yet this level of power storage is sufficient to support life on earth.

Photovoltaic cells are solid state devices that convert solar illumination into electrical energy. Photovoltaic cells have been recognized as a feasible energy conversion technology only within the last 20 years, although devices with efficiencies of 1–4% were constructed as early as 1954 (5). A basic photovoltaic cell consists of two different types of solids that are connected at an abrupt, defined junction (5). This junction provides the cell with the ability to direct electrical current flow in only one direction through the external circuit, and to produce electrical power. In contrast to the process of photosynthesis, photovoltaics cannot directly convert the incident photon energy into chemical fuels, but instead lead only to the production of electricity. Modern photovoltaics are quite efficient, and state-of-the-art devices are capable of converting over 25%

of the incident solar energy into electrical energy (6–8). These devices are also extremely durable and can have lifetimes that exceed 20 years under many types of environmental stresses (9).

The third type of energy conversion system, which is the topic of this chapter, is a *photoelectrochemical cell.* Photoelectrochemical cells are also relatively recent energy conversion devices. In fact, photoelectrochemical cells with solar energy conversion efficiencies greater than 10% have only been developed within the past 15 years (10–12). The semiconducting electrode is the key to the operation of a photoelectrochemical cell. The semiconductor is responsible for the absorption of the incident light, while the interface between the semiconductor and the liquid is the key factor in the subsequent chemical steps that lead to energy conversion. Photoelectrochemical cells can be thought of as hybrids between photovoltaics and photosynthesis, in that they can be constructed either to produce electricity or to store chemical fuel, or both. Their solar energy conversion efficiencies are also typically between those of photosynthesis and photovoltaics, with values ranging from less than 1% to as high as 17% (10).

Before proceeding into the details of the photoelectrochemical process, it is instructive to draw some additional comparisons between the energy conversion processes involved in photosynthetic reaction centers, photovoltaics, and photoelectrochemical cells. In the photosynthetic reaction center, light is absorbed by an antenna system, and the initial excitation energy eventually gets transferred to a specific site, the chlorophyll dimer, which is often referred to as the "special pair" (13). While the absorption of light by the antenna and chlorophyll pigment is a requirement for energy conversion, it is not sufficient to insure the success of the process. The excited state of this special pair, which consists of an electron and an electron vacancy (a hole), could just return to the ground state and release the absorbed optical energy as heat unless another competing chemical pathway can direct the electron elsewhere to perform useful work. In the photosynthetic reaction center, this separation of the excited electron from its vacancy is accomplished by the presence of a series of electron acceptors that are strategically located within the protein. In a series of steps, the excited electron moves from one pigment to the next, losing a small amount of free energy in every step (14, 15). Eventually, the electron is spatially separated sufficiently far away from its site of excitation that even though recombination with the electron vacancy is thermodynamically feasible, it is kinetically slow. The remaining energy of the excited electron can then be used to drive the chemical reactions in photosynthesis.

Photovoltaics also use a free energy gradient to separate photogenerated charges. However, in photovoltaics, the free energy gradient is produced by an electric potential energy gradient at the junction between two solids. The purpose of this energy gradient is similar to that in photosynthesis, because it directs the charges (electrons and holes) through the solid. The electric potential

energy gradient attracts electrons to one side of the device, while driving holes to the other side of the system. This separation of the photogenerated charges thereby prevents "short circuiting" of the device that would result from a random flow of charge to either side of the photovoltaic cell.

Semiconductor/liquid junctions also utilize a free energy gradient to promote charge separation. By a process to be explained later in this chapter, immersion of the semiconductor into a solution produces an electric field at the solid/liquid interface. When light is incident on the photoelectrochemical cell, the semiconductor electrode absorbs photons and creates excited electrons. These electrons sense the electric field present at the solid/liquid interface, and are either attracted or repelled by this field (depending on its sign), to produce a directional flow of current through the cell. The free energy gradient at the semiconductor/liquid interface is thus very similar to that in photovoltaics and in the machinery of photosynthesis, because it is responsible for separating the charges that will ultimately lead to energy conversion. Chemical control over the electric field at a semiconductor/liquid interface is therefore one of the key concerns in the area of semiconductor photoelectrochemistry.

In operation, a photoelectrochemical cell can produce electricity, chemical fuels, or both. The overall process that occurs in such a cell depends not only on the electrochemical reactions at the semiconductor electrode, but also on the reactions that take place at the metallic counter electrode. If the reactions at the metallic counter electrode are the reverse of those at the semiconductor electrode, then no net chemical change will take place in the cell. In this mode of operation, the light-induced current will only result in the production of electrical power in the circuit. For instance, consider the case in which the semiconductor electrode effects the oxidation of water to produce O_2(g) (Fig. 1). If O_2(g) is simultaneously reduced at the counter electrode, then the only mechanism by which energy can be extracted from this system is by collection of the excess energy from the light-generated electrons. This extraction of energy can be accomplished by forcing the charges through a resistive load in the external circuit, leading to the net production of electrical energy from the incident light energy. This type of photoelectrochemical cell thus acts similarly to a photovoltaic cell as an energy conversion device.

Alternatively, if sufficient energy is available from the electrons, it might be possible to reduce water to H_2(g) at the counter electrode instead of reducing O_2(g). In this system, water is electrolyzed to produce O_2(g) and H_2(g), and fuels will be produced from the incident photon energy. As in the process of photosynthesis, this type of photoelectrochemical cell will have converted the incident solar energy into chemical fuels. If even more energy is available from the electrons, then electrical work through a resistive load and H_2(g) production are possible, and both electricity and chemical fuels would be produced. This latter ability is unique to photoelectrochemical cells.

In general, there are three quantities that characterize the performance of a

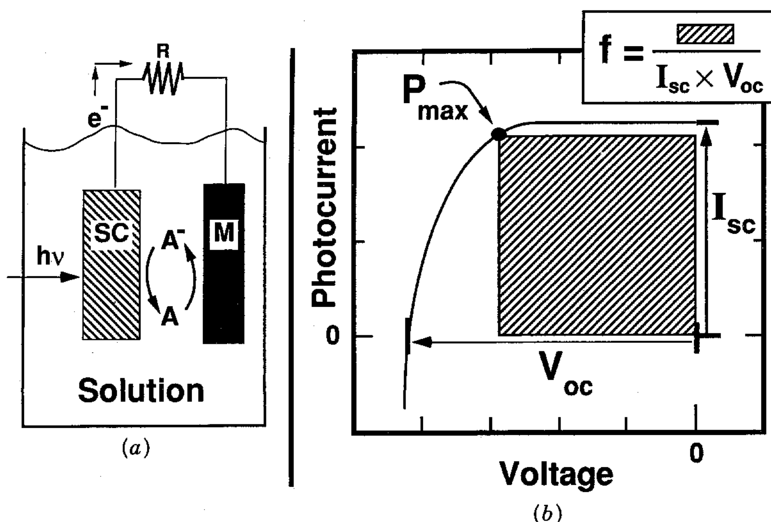

Figure 2. (*a*) A photoelectrochemical cell consists of two electrodes, an illuminated semiconductor electrode (SC) and a metal counter electrode (M) in a solution containing an electroactive species A/A^-. In a cell that converts light into electricity, the counter electrode performs the reverse reaction of the photoelectrode, and the incident photon energy is harvested as electrical energy through an external resistor (R). (*b*) *I–V* curve is generated by varying the magnitude of *R* in the external circuit. The electrical properties of a photoelectrochemical cell are quantified by the open circuit voltage (V_{oc}), the short circuit current (I_{sc}), the maximum power point (P_{max}), and the fill factor (f) of the cell. The definitions of these parameters can be found in the text.

photoelectrochemical energy conversion device (Fig. 2). The current through the external circuit represents one such parameter, since no energy can be extracted if no net current is present in the external circuit. The current is generally measured when negligible work is demanded through the measuring device, for example, when a simple low-resistance ammeter is connected between the two electrodes in the cell. This current is called the *short circuit current* (I_{sc}) because if measured correctly, it is the current that would flow when a direct short circuit is present between the two electrodes. The second parameter of interest is the voltage developed by the photoelectrochemical cell. This voltage is measured at open circuit with a voltmeter of extremely high resistance, so that negligible current can flow through the cell. The *open circuit voltage* (V_{oc}) is a measure of the maximum Gibbs free energy that can be obtained from the cell. The third parameter characterizes the rate at which the current approaches its limiting short circuit value, and is called the *fill factor* (f). This parameter allows the calculation of the maximum power that can be produced by a given photoelectrochemical cell. The challenge in this area is to understand how to optimize simultaneously the open circuit voltage, the short circuit current, and the fill

factor of a given photoelectrochemical cell. Taken together, these three quantities are the key variables that are measured in, and are the focus of, experimental investigations in photoelectrochemistry.

In almost all potential applications of photoelectrochemical cells, fundamental questions and practical problems still must be addressed before these systems can compete favorably as a practical energy conversion technology. For example, corrosion and passivation processes of the semiconductor electrode often compete with the desired energy conversion reactions. These degradation reactions seriously limit the lifetime of most photoelectrochemical devices. In other systems, unidentified chemical species on the semiconductor surface are believed to trap photogenerated electrons before they can be separated by the electric field. These traps are deleterious because they induce loss mechanisms that lower the energy conversion efficiency of the entire photoelectrochemical cell. In still other systems, the contact between the solid and the liquid does not lead to large electric field strengths, so that the free energy gradient is not sufficient to achieve an effective charge separation at the solid/liquid interface. All of these features are, in principle, under chemical control. Thus, the understanding and manipulation of these phenomena form the basis for the concepts in this chapter and for current research in the area of semiconductor photoelectrochemistry.

The primary focus of this chapter is the development of semiconductor electrodes for solar energy conversion applications. The electrochemistry and photoelectrochemistry of semiconductors are also important in several other technologies, and we will discuss these relationships whenever appropriate. For example, electrochemical etching and corrosion reactions at semiconductor/liquid interfaces are essential processes in integrated circuit technology (16, 17). Similarly, the expanding field of chemically sensitive semiconductor-based sensors depends on an understanding and control of the properties of the semiconductor/liquid interface (18, 19). One recent application that we will discuss in detail is the use of large band gap semiconductors as catalysts for useful chemical reactions. Of particular note in this context is the use of suspensions of TiO_2 particles for toxic waste treatment and for novel synthetic oxidations. These technologies are among the numerous reasons to understand the behavior of semiconductor/liquid junctions; thus, our focus on energy conversion should be viewed from this perspective.

In order to understand in more detail how semiconductor/liquid junctions operate, it will be necessary to review some basic concepts in the fields of solid state physics, electrochemistry, and surface chemistry. Generally, some of these topics are new material to most scientists that are interested in semiconductor photoelectrochemistry. Although useful reference information on the behavior of a variety of semiconductor electrodes is available in the recent book by Finklea (10), and although accessible articles on various aspects of research in the

area have been written by several authors, including Rajeshwar (20), Wrighton (21), Bard (22), Memming (23, 24), Heller (11), Fox (25, 26), Parkinson (12), Gerischer (27, 28), Lewis (29), and Koval and Howard (30), there is no one place in which a general, accessible introduction to all of the required concepts can be found. In this chapter, we have specifically written Sections II, III, and IV as a primer that should be useful to those without a background in any of these areas. These sections should also enable the reader to gain a historical perspective, as well as to approach current research problems, in the area of semiconductor photoelectrochemistry. In Sections V and VI, we will use this essential background to discuss the progress that has been made in this area, the problems that remain, and the current strategies that show particular promise for future developments.

II. ELECTRONIC PROPERTIES OF SEMICONDUCTORS

One of the main differences between energy storage processes in molecular-based systems, such as photosynthesis, and energy storage processes in photoelectrochemical cells concerns the mobility of the charge carriers that are created by light excitation. In the photosynthetic process, a localized electron is created by the initial excitation event. This electron is then separated from the electron vacancy through a molecular "hopping" mechanism, in which the mobility of the photogenerated charge carrier is limited by the ability of the electron to jump from site to site in the photosynthetic reaction center. In contrast, the carriers created by photoexcitation in semiconductors are highly delocalized and are extremely mobile. Consequently, these photogenerated carriers can rapidly move through large distances with a minimum of energy loss, thus avoiding recombination. In the semiconductor-based system, the ability of the semiconductor to transport charges will depend critically on the electronic properties of the semiconducting solid. To understand these effects from a chemical viewpoint, we need to first explore the various types of physical structures that are commonly adopted by semiconducting solids. Knowledge of these structures will then be used to explain the key electronic properties of semiconductors in energy conversion schemes.

A. Crystal Structures of Some Selected Semiconductors

Semiconductors constitute a diverse group of inorganic solids, and therefore, as a class, they have a variety of different crystal structures. The most basic semiconductor structure is based on the interpenetration of two *face-centered cubic* (fcc) lattices. A familiar, nonsemiconducting solid that adopts this structure is NaCl, where the Na^+ cations constitute one fcc lattice and the Cl^- anions

constitute the other (Fig. 3*a*). Many specific crystal structures of semiconductors are based on variants of this basic fcc lattice. Covalent semiconductors, such as the elemental semiconductors Si and Ge, have structures in which the tetrahedral atoms attempt to achieve maximum bonding between nearest neighbor atoms. In these solids, maximum bonding implies that the atoms are positioned as closely as possible within the fcc structure while still maintaining a tetrahedral environment. These solids therefore adopt the *cubic diamond* lattice, in which one-half of the tetrahedral holes in the fcc lattice are filled with atoms (Fig. 3*b*). A related structure is adopted by covalent, binary semiconducting solids having elements of similar electronegativities. For example, GaAs adopts the *zinc blende* structure, which is simply the cubic diamond structure with adjacent atoms throughout the structure being of opposite type (Fig. 3*c*). The compounds InAs, InP, and GaP are other examples of common covalent binary semiconductors that adopt the zinc blende structure.

In certain cases, when the semiconductor is composed of elements with very different radii and electronegativities, the lattice site in the tetrahedral position of a fcc structure becomes too small to accommodate one of the ions in the semiconductor. To maintain a lattice with a 1 : 1 cation–anion stoichiometry, the solid adopts a structure in which the atoms are instead hexagonally close-packed. As in the zinc blende structure, only one-half of the possible tetrahedral sites in this hexagonal structure are filled with atoms. Such a structure is called the *wurtzite* structure. The wurtzite structure is adopted by semiconductors such as ZnO and CdSe (Fig. 3*d*), whereas the semiconductor ZnS can be found in either the zinc blende or the wurtzite structure. Comparison between these lattices shows that the wurtzite structure is more open, and the bonding is more ionic, than in the zinc blende structure.

Taken together, these three structures (cubic diamond, zinc blende, and wurtzite) encompass the majority of the common semiconductor materials in use today. These three structures belong to a group of materials called the *adamantine solids* and share the common feature of having an average of four valence electrons per atom (31). This set of structures is by far the most important class considered in the remainder of our discussion of semiconductor photoelectrochemistry.

In several semiconducting solids, steric or electronic factors can result in the adoption of nonadamantine structures. Semiconductors that adopt nonadamantine structures include the metal oxides Fe_2O_3, TiO_2, and $SrTiO_3$, and transition metal dichalcogenides such as MoS_2, WS_2, and WSe_2. Titanium dioxide, an important semiconductor in photoelectrochemical applications, occurs in three modifications, only two of which are used in photoelectrochemical research: rutile and anatase (32). Figure 3*e* and *f* shows the structures of both of these forms of TiO_2. The *rutile* lattice is derived from a body-centered cubic (bcc) structure. To maintain a 1 : 2 cation–anion stoichiometry in the rutile structure,

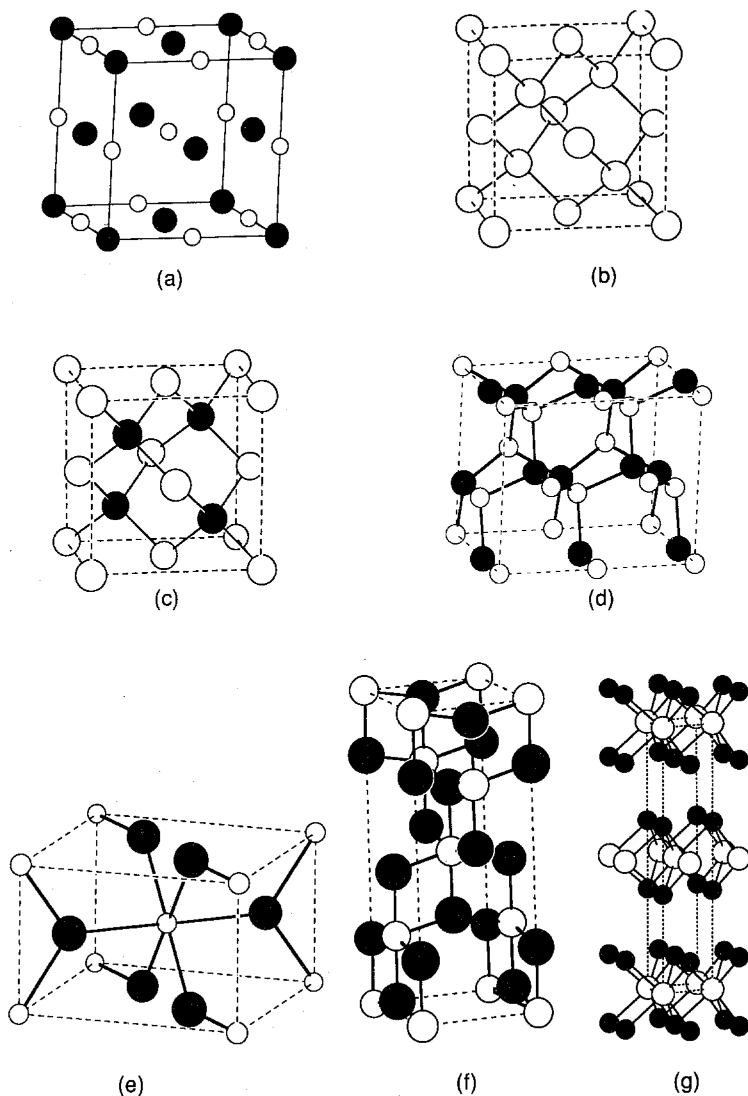

Figure 3. Structures of some common crystal lattices. (*a*) NaCl. (*b*) Si. (*c*) GaAs. (*d*) ZnO. (*e*) TiO_2, rutile. (*f*) TiO_2, anatase. (*g*) MoS_2. For the binary materials, the black circles represent the more electronegative elements (i.e., Cl, As, O, and S) and the white circles represent the less electronegative elements (i.e., Na, Ga, Zn, Ti, and Mo).

one-half of the trigonal sites are occupied by anions. The *anatase* lattice is derived from the NaCl structure, but only one-half of the sites in one fcc lattice are occupied by Ti^{4+} cations. To date, large single crystals of TiO_2 have only been prepared in the rutile structure, while TiO_2 powders commonly contain both anatase and rutile components (32). The compound Fe_2O_3 has been found to occur in many lattice structures, the most important of which is the α form. In this particular modification, the oxide anions adopt hexagonal close packing and the metal cations occupy two-thirds of the octahedral sites within this anion lattice.

Figure 3*g* illustrates an additional structure, which is commonly found for transition metal dichalcogenide compounds such as MoS_2, WS_2, and WSe_2. These semiconductors adopt a layer structure in which the transition metal is "sandwiched" between two layers of chalcogenide atoms. In this *layer-type* structure, there is no covalent bonding between adjacent chalcogenide layers. A useful feature of this structure is that the weak van der Waals interactions between chalcogenide planes allow high quality surfaces to be prepared merely by peeling layers of the crystalline sample apart, thereby revealing atomic planes that are of interest to photoelectrochemists.

B. Band Structure and Optical Properties of Semiconductors

One of the key properties of semiconductors that makes them useful for energy conversion is the delocalization of electrons throughout the semiconducting solid. To understand the origin of these delocalized orbitals, we need to examine the nature of the bonding within semiconductor crystals. The basic model that has been successfully used to describe the electronic structure of semiconductors is the band theory of solids. Our treatment of band theory will be qualitative, and the interested reader is encouraged to read more about this subject in the excellent reviews by Hoffmann (33–35) and in the classic texts by Ashcroft and Mermin (36), Harrison (37), Kittel and Kroemer (38), Kittel (39), Seitz (40), and Goodstein (41).

1. The Molecular Orbital Description of Semiconducting Solids

The process of obtaining molecular orbitals (MOs) for solids is similar to the approach that chemists use to describe the bonding in simple diatomic molecules. However, when the orbital theory is used to describe the electronic properties of a collection of atoms within a solid lattice, different terminology is generally used. To demonstrate these differences, we will first illustrate the process on a chemically familiar system, consisting of polyenes of varying chain lengths. We will then generalize this methodology to include the bonding description of inorganic semiconducting solids.

a. Band Structure in Linear Conjugated Polyenes. We begin with an orbital description of the bonding in ethylene, which is the repeating unit in a straight-chain polyene. In the Hückel molecular orbital description of ethylene, the carbon atoms are sp^2 hybridized into a σ-orbital framework. The remaining carbon p orbitals interact to yield two orbitals of π symmetry, one of which is bonding and one of which is antibonding with respect to the C–C interaction. This situation is qualitatively represented in Fig. 4. In the ground state of ethylene, the bonding π orbital is occupied by two electrons, and this orbital is lower in energy than the empty antibonding orbital. A discrete optical transition exists between the highest occupied molecular orbital (HOMO) and lowest unoccupied molecular orbital (LUMO) of ethylene, because these two orbitals are separated by a well-defined energy gap.

As the basic ethylene units are coupled together to form a larger molecule, the π bonding will become more delocalized, and more atomic orbitals must be included in the overall MO description. In 1,3-butadiene, the four valence $2p$ orbitals of C that are not incorporated into the σ-bonding framework will produce four π-type MOs. Two of these orbitals are bonding in character and are occupied by electron pairs, while the other two are antibonding and are empty (Fig. 4). Reference to the energy scale shows that the HOMO–LUMO gap of butadiene is slightly smaller than that of ethylene. This reduced energy gap is

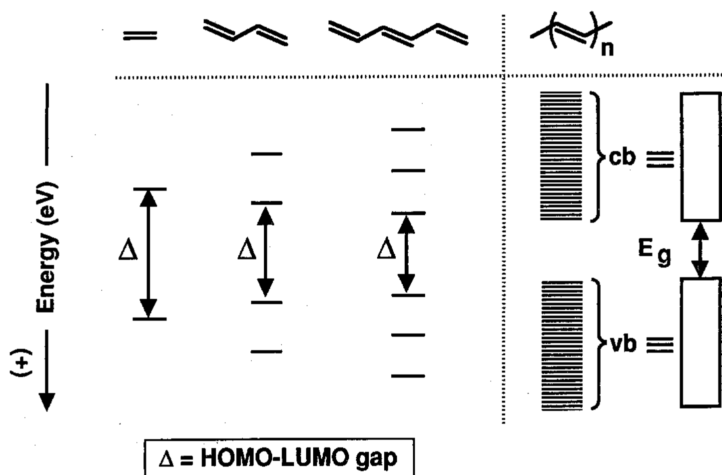

Figure 4. The development of a polyene band structure from the MOs of ethylene. From left to right, the MOs progressively develop into a band structure as the length of the conjugated chain is increased. For shorter polyene chains, Δ represents the HOMO–LUMO gap. For the infinite polyene chain, vb and cb denote the valence band and the conduction band, respectively, and $\mathbf{E}_g$ is the band gap energy.

a consequence of the extended conjugation in this π system relative to that in ethylene.

Addition of another ethylene unit to 1,3-butadiene creates 1,3,5-hexatriene, a molecule with three fully occupied π-bonding orbitals and three empty π-antibonding orbitals. Again, the highest bonding MO and the lowest antibonding MO are separated by the HOMO–LUMO gap. As this process of adding ethylene units is continued, longer conjugated systems will be created until an infinite one-dimensional polyene chain has been formed. This chain will contain an infinite number of bonding and antibonding MOs. In this infinite chain, the bonding orbitals will tend to cluster together into a tightly packed group, and the antibonding orbitals will cluster into another tightly packed group. Although it is not obvious that the bonding and antibonding groups will not overlap in energy, it can be shown that these two groups are well separated even in the infinite polyene (33, 34). It can also be shown that this separation produces a well-defined HOMO–LUMO energy gap, just as in the cases of ethylene, 1,3-butadiene, 1,3,5-hexatriene, and other molecular oligomers that are precursors to the infinite chain polyene (Fig. 4).

Because the fully developed polyene has an extremely large number of MOs, a description of the π bonding in this molecule can be simplified by considering groups of orbitals together as sets. Even though each of the MO distributions in the polyene consists of a large number of orbitals that are packed tightly together into a finite energy interval, for most purposes we can ignore the energy spacing between the individual orbitals. We can therefore consider the orbitals as forming "continuous" *bands* of energy levels. A shorthand notation for this assumption is to draw the band as a single block in energy. In this notation, there is an implicit understanding that there are actually a large number of states clustered together within this block (Fig. 4). The cluster of fully occupied bonding orbitals is referred to as the *valence band* (vb), and the cluster of vacant antibonding orbitals is called the *conduction band* (cb). Under this scheme, the HOMO–LUMO gap is called the *band gap*.

b. Band Structure in Inorganic Semiconducting Crystals. Band structures for three-dimensional solids such as semiconductor crystals can be obtained in a similar fashion to that for polyenes. Localized MOs are constructed based on an appropriate set of valence atomic orbitals, and the effects of delocalization are then incorporated into the molecular structure as the number of repeat units in the crystal lattice is increased to infinity. This process is widely known to the chemical community as extended Hückel theory. It is also called the tight binding theory by physicists who apply these methods to calculate the band structures of semiconducting and metallic solids.

We will not describe this process in detail for inorganic solids, because there are complications that result from the different symmetry types of various unit

cells, as well as from spin–orbit coupling considerations. These factors tend to increase the complexity of the MO description of inorganic solids relative to the simple MO treatment of organic polyenes. However, the principles of the procedure are the same as those outlined for the organic polyene example, with each individual atom in the lattice contributing a set of atomic orbitals toward the formation of crystal orbitals. These crystal orbitals will extend throughout the solid, and will yield discrete energy bands when represented on an energy diagram (Fig. 5), just as in our polyene example.

To understand the electronic structure of these solids, the electron occupancy of these bands must be considered. The number of valence electrons on the

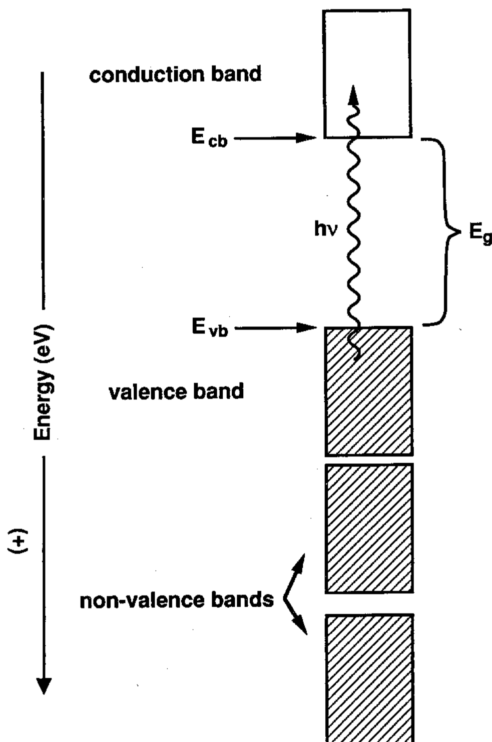

Figure 5. A schematic representation of the orbital band structure of a semiconductor. The shaded area denotes a fully occupied band and the unshaded area denotes an empty band. Two nonvalence bands are also drawn to stress the point that the valence band of a semiconductor is the highest occupied band. The parameters E_{cb} and E_{vb} represent the energies of the conduction band edge and the valence band edge, respectively, and E_g is the band gap energy. When photons with energy greater than the band gap are absorbed by the semiconductor, electrons are excited from the semiconductor valence band into the conduction band.

atomic constituents of the semiconductor will determine the electron occupancy of each band in the resulting solid. By definition, the highest filled band is called the valence band of the semiconductor. Similarly, the lowest vacant band is called the conduction band. Associated with each band is a *bandwidth*, which is simply the energy difference between the orbitals of highest and lowest energy in the band. Thus, we obtain an energy diagram for semiconductor crystals that is similar to the one presented in Fig. 4 for the organic polyenes, with the valence band containing the HOMO and the conduction band containing the LUMO for the solid of concern (Fig. 5).

In semiconductor terminology, the top of the valence band and the bottom of the conduction band are called the *valence band edge* and the *conduction band edge*, respectively. The energy of the conduction band edge is denoted as $\mathbf{E}_{cb}$; similarly, the energy of the valence band edge is denoted as $\mathbf{E}_{vb}$. The energy difference between these levels is called the *semiconductor band gap*. The size of this band gap is perhaps the most important characteristic of a semiconducting solid, as it influences all of the important electronic properties of a semiconductor. In this chapter, we will abbreviate the band gap energy as $\mathbf{E}_g$. In general, semiconducting solids have band gaps that range from 0.3 to 3.5 eV; Table I lists the values of $\mathbf{E}_g$ for a variety of common semiconductors.

It should be noted that the positions of the crystal orbitals on the energy scale in Figs. 4 and 5 are located with respect to the vacuum level as reference. The *vacuum level* is defined as the energy level of an electron in vacuum, and is taken to be 0 eV on the energy scale. Note also that although the physics convention assigns more negative energies to electrons that are more tightly bound relative to vacuum (e.g., the energy of a 1*s* orbital in the H atom is -13.6 eV), the energy scale used by most electrochemists is opposite in sign, with more tightly bound electrons having more positive energies relative to the vacuum level. This assignment on the electrochemical energy scale is based on a "work function" convention, which refers to the energy required to remove an electron from a particular electronic state in the solid. This convention will be useful later in this chapter when we will relate the energies of bands to those of the solution electrochemical potential scale.

c. Chemical Properties of Inorganic Semiconductors. In general, semiconductors can have different types of valence band and conduction band structures. These differences can affect the chemical reactivity of the photogenerated carriers in solids. For example, in a covalent solid, such as Si, the valence and conduction bands can be thought of as crystal orbitals that are either bonding or antibonding combinations of hybridized Si atomic orbitals. This situation is closely related to our polyene example, where the valence band consisted of bonding π orbitals and the conduction band consisted of antibonding π^* orbitals. However, in an ionic crystal, such as TiO_2, the valence band is composed

TABLE I
Properties of Some Common Semiconductors[a]

Semiconductor	Crystal Structure	Band Gap (eV)[b]	Type of Band Gap
Si	Diamond	1.12	Indirect
Ge	Diamond	0.70	Indirect
Se	Hexagonal	1.77	Direct
GaP	Zinc blende	2.26	Indirect
GaAs	Zinc blende	1.42	Direct
InP	Zinc blende	1.35	Direct
InAs	Zinc blende	0.36	Direct
ZnS	Zinc blende	3.58	Direct
	Wurtzite	3.70	Direct
ZnSe	Wurtzite	2.67	Direct
ZnTe	Wurtzite	2.26	Direct
CdS	Wurtzite	2.42	Direct
CdSe	Wurtzite	1.70	Direct
CdTe	Zinc blende	1.56	Direct
MoS_2	layer-type	1.17	Indirect
$MoSe_2$	layer-type	1.06	Indirect
$MoTe_2$	layer-type	1.00	Indirect
WS_2	layer-type	1.30	Indirect
WSe_2	layer-type	1.16	Indirect
ZnO	Wurtzite	3.35	Direct
TiO_2	Rutile	3.02	Indirect
	Anatase	3.2	Indirect
$BaTiO_3$	Perovskite	3.3	Indirect
$SrTiO_3$	Perovskite	3.2	Indirect
α-Fe_2O_3	Corundum	2.2	Indirect
SnO_2	Rutile	3.5	Indirect
In_2O_3	Cubic	2.62	Indirect
WO_3	Perovskite	2.7	Indirect

[a]Data compiled from (10, 42–45).
[b]At 300 K.

of crystal orbitals that are derived from the filled $2p$ orbitals of O^{2-}, while the conduction band is composed of crystal orbitals that are derived from the empty $3d$ orbitals of Ti^{4+} (46–49). The band gap in this case is obviously not an energy gap between bonding and antibonding bands of the same symmetry. Rather, it is the energy gap between two very different types of bands. This band structure has implications for the chemical behavior of the excited state of TiO_2 versus that of Si, as will be discussed later in this chapter.

Many other chemical properties of semiconductor materials can be explained by reference to their electronic band structure. For example, ionic semiconductors are generally found to be more stable towards corrosion and passivation

than covalent semiconductors (cf. Section V). This observation can easily be rationalized using the frontier molecular orbital argument, which states that chemical reactivities are often controlled by the size of the HOMO–LUMO gap (50, 51). For semiconductors, the HOMO–LUMO gap is the band gap and, therefore, the chemical reactivity of semiconductors should be related to the value of $\mathbf{E}_g$. In a covalent semiconductor, the crystal orbitals that comprise the valence band and the conduction band are reasonably close in energy. This result implies that the band gap is relatively small and the semiconductor is thus expected to be chemically reactive. This prediction is in agreement with experiment. In fact, one of the key problems in using small band gap semiconductors in energy conversion applications is their tendency to undergo corrosion and passivation reactions (cf. Section V). In contrast, the crystal orbitals that make up the valence and conduction bands of ionic semiconductors (TiO_2, $SrTiO_3$, etc.) are generally very different in energy, so the band gaps of these materials are usually very large. These solids should therefore be less prone to undergo oxidation or corrosion reactions. This prediction is also consistent with experimental results and accounts for the emphasis on the use of metal oxides in water photoelectrolysis (cf. Section V).

The orbital character of the valence and conduction bands can also be used to understand trends in the electronic properties of semiconductors. For example, even though the value of $\mathbf{E}_g$ varies a great deal in metal oxide semiconductors (Table I), the energies of the valence band edges are quite similar throughout this series of solids. This similarity can also be understood from our MO–band structure treatment since calculations have shown that the valence bands of these semiconductors are all constructed predominantly from the 2*p* orbitals of O^{2-} (52). The MOs that arise from these atomic orbitals should therefore be similar in bonding character and in energy. Within this framework, changes in the lattice cation will primarily affect the energy of the conduction band edge. This prediction is consistent with experimental data for metal oxide semiconductors (52–56).

This latter behavior has been generalized to extend beyond the metal oxide semiconductor series. A general guideline has been proposed that the valence band character of most semiconductors is dominated by orbitals that are derived from atomic orbitals of the lattice anion (57). To the extent that this generalization is valid, it predicts that semiconductors with a given lattice anion will have valence band edge energies similar to other materials with the same lattice anion. This rule also predicts that changes in the lattice cation will be reflected primarily in the energy of the conduction band edge (and, therefore, also in the band gap energy). This generalization is called the *common anion rule* (57). Although the common anion rule has received some experimental and theoretical support (56, 58–65), it is at best a rough generalization in chemical behavior. This generalization is not expected to be rigorously valid for any wide series

of materials, especially for solids with differing crystal structures and lattice stoichiometries.

Another analogy to chemical systems can be made when considering the reactivity of excited states of semiconductors. In molecular systems, it is well known that the types of orbitals in the HOMO and LUMO can determine the chemical reactivity of the excited electronic states of a molecule. A similar argument can be applied to predict the reactivity of semiconductors. For example, it has been suggested that layer-type semiconductors, such as MoS_2, should be more stable towards corrosion and passivation reactions than II–VI semiconductors, such as CdS (66, 67). This prediction was based on calculations which revealed that the valence and conduction bands of MoS_2 are both largely Mo 3*d* in character. In contrast, the valence band in CdS is S^{2-} in character, and the conduction band is Cd^{2+} in character. For CdS, excitation of an electron from the valence band to the conduction band is expected to remove an electron from the S^{2-}-derived orbitals, and should provide an initial step towards the dissolution of the lattice anion as the neutral S^0 species. For MoS_2, excitation of an electron is expected to merely result in the transfer of an electron from one metal derived orbital set (in the valence band) to another metal derived orbital set (in the conduction band), so no photocorrosion processes should be initiated. These predictions have been partially verified by experiment, as metal dichalcogenide electrodes are often more stable in contact with aqueous electrolytes than are II–VI compounds (cf. Section V).

2. *Optical Characteristics of Semiconductor Materials*

a. The Optical Absorption Threshold of Semiconductors. Now that we have described the bonding in semiconductors, we are in a position to investigate the electronic transitions that result from this orbital structure. In a semiconductor, the most important electronic transition for energy conversion applications is the optical excitation of an electron across the semiconductor band gap. This excitation leads to promotion of an electron from an orbital in the valence band into an orbital in the conduction band. This fundamental and extremely important process represents the first step in the photoelectrochemical conversion of optical energy to electrical and/or chemical energy.

The light absorption process in semiconductors has a definite energy threshold associated with it. The value of this threshold is the band gap energy ($\mathbf{E}_g$). Large band gap materials, such as TiO_2, will therefore only absorb at short wavelengths, and will not absorb as many photons from sunlight as small band gap semiconductors, such as Si. This threshold behavior is extremely important in photoelectrochemistry, because it is one of the main constraints that limits the efficiency of solar energy conversion devices.

Figure 6 depicts the power distribution of the solar spectrum versus photon

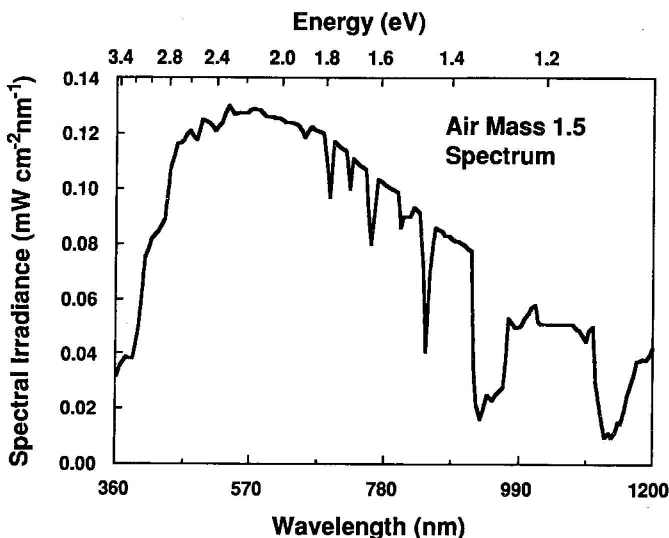

Figure 6. The spectral distribution of sunlight under Air Mass 1.5 conditions (68). Air Mass (AM) 1.5 refers to a standard measurement condition when the sun is 48° above the horizon. It should be noted that the majority of the solar irradiation is concentrated in the region between 1 and 3 eV.

energy. This plot shows that the majority of the solar irradiance is centered in the region between 1 and 3 eV. Thus, large band gap semiconductors (i.e., those with $\mathbf{E}_g > 2.2$ eV) will be ineffective at harvesting a substantial fraction of the solar spectrum, and will not provide the most efficient solar energy conversion devices.

From this analysis, it would appear that the use of a semiconductor with a small band gap ($\mathbf{E}_g \leq 1$ eV) would be advantageous for solar energy conversion, because such a semiconductor would be able to absorb most of the solar spectrum. Unfortunately, materials with very small band gaps also are not optimal for use in solar energy conversion. In most semiconductors, the absorption of photons with energy $h\nu = \mathbf{E}_g$ leads to an optical transition that produces an electron at the conduction band edge. This excitation energy is then available as the potential energy to drive a chemical reaction. In contrast, absorption of photons with $h\nu > \mathbf{E}_g$ leads to excited states with electron energies greater than the conduction band edge. Unfortunately, this extra energy is usually wasted, because the highly excited electrons readily thermalize to the energy of the conduction band edge. Thus, regardless of the actual energy of the incident light, a semiconductor with band gap energy $\mathbf{E}_g$ is usually only capable of producing excited states with a potential energy of $\mathbf{E}_g$. In general, semiconductors with band gap energies that are very small can absorb a large number of photons

from the solar spectrum, but will waste a significant amount of that energy as heat, greatly reducing their effectiveness in harvesting the incident solar energy.

The optimal trade-off between effective photon absorption and maximization of the excited state potential energy per absorbed photon can be calculated through a straightforward analysis of the solar spectrum displayed in Fig. 6. This analysis leads to the conclusion that materials with band gaps between 1.1 and 1.7 eV are the best absorbers for solar energy conversion devices (11, 68–70). Such materials not only can absorb a significant fraction of the solar spectrum, but also can deliver a significant amount of excited state energy from these absorbed photons. It is often thought that in order to drive high-energy chemical processes, visible light absorption is the most desirable property of a molecular photocatalyst for solar energy storage. However, an absorption threshold in the near-IR region is optimal for solar energy conversion applications. Common semiconductor materials with such absorption thresholds include Si, GaAs, InP, $MoSe_2$, and CdTe. Other materials, such as TiO_2, have too large a band gap to be efficient absorbers. Still others, such as Ge, have band gaps that are too small for an optimal match to the solar spectrum. This restriction on the band gap of useful materials will be addressed in more detail in Section V, but it is important to keep this critical constraint in mind throughout the remainder of our discussion of semiconductor photoelectrochemistry.

b. Depth of Light Absorption in Semiconductors. In addition to calculating the maximum photon absorption that can be obtained with a specific material, it is also important to consider how effectively the incident light will be absorbed near the surface of a semiconductor sample. In general, from Beer's law, the absorbance and transmittance of a material can be expressed as

$$A = \ln\frac{I_0}{I} = \varepsilon c\ell \quad \text{and} \quad T = \frac{I}{I_0} = \exp(-\varepsilon c\ell) \tag{1}$$

where I is the transmitted light intensity, I_0 is the incident light intensity, ε is the molar extinction coefficient, ℓ is the optical path length, and c is the concentration of absorbing material. For solids, the concentration of the absorber is a constant, so Beer's law can be rewritten as follows

$$A = \ln\frac{I_0}{I} = \alpha\ell \quad \text{and} \quad T = \frac{I}{I_0} = \exp(-\alpha\ell) \tag{2}$$

where $\alpha \equiv \varepsilon c$ is the *absorption coefficient* of the material. This latter equation is the form that is usually used for expressing light absorption in solids. In this expression, A and α are a function of the wavelength at which the light absorption is measured.

For molecules, the extinction coefficient of an electronic transition can vary over a wide range of values, depending on whether the transition is optically and/or spin allowed. For semiconductors, the same restrictions apply. At the wavelength of interest, the electronic transition from one band to another must be optically allowed and spin allowed to have a high extinction coefficient, that is, to have a large absorption coefficient. Semiconductors that display a fully allowed transition between the valence band and the conduction band are referred to as *direct band gap semiconductors*. In these materials, such as GaAs and CdTe, the absorption coefficients are large, and the light is strongly absorbed close to the surface of the solid. Typical values of α for these materials are 10^4–10^5 cm^{-1}, indicating that light cannot penetrate deeper than 1 μm before it is essentially completely absorbed by the solid. A plot of the absorption coefficient versus wavelength for a typical direct band gap semiconductor, GaAs, is depicted in Fig. 7.

For other semiconductor materials, such as Si, the lowest energy electronic transition between the valence band and the conduction band is formally optically forbidden. These materials are said to have an *indirect band gap*. Indirect band gap materials generally display small absorption coefficients for photons near the band gap energy. This behavior is analogous to a *d–d* electronic absorption band in an octahedral transition metal complex, which is formally optically forbidden due to the inversion symmetry of the *d* orbitals. In octahedral

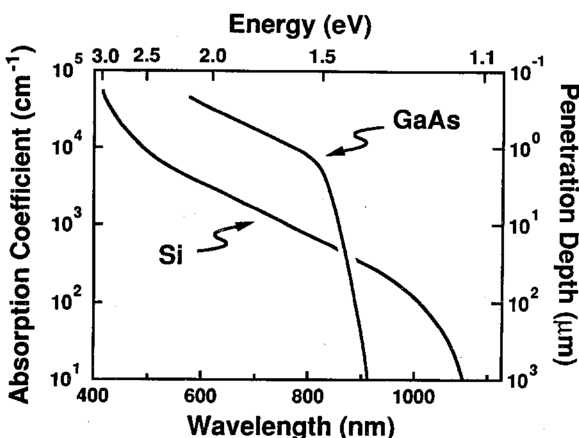

Figure 7. A plot of absorption coefficient versus photon wavelength for Si and GaAs (45). A direct band gap semiconductor, such as GaAs (E_g = 1.42 eV), has a sharp onset of absorption at photon energy = E_g and a large absorption coefficient for $h\nu > E_g$. The indirect band gap semiconductor Si (E_g = 1.12 eV) has a broad, weak onset of absorption, which begins at photon energies $\leq E_g$ due to vibrational coupling with the crystal lattice. For Si, note the low value of the absorption coefficient at photon energies substantially higher than the band gap energy.

transition metal complexes, *d–d* transitions are generally observed experimentally, albeit with weak extinction coefficients, because other mechanisms allow the light absorption process to conserve momentum when the entire molecular wavefunction is considered. Similarly, for indirect band gap semiconductors, light absorption is allowed only when the momentum of the photon is coupled both to lattice vibrations and electronic transitions. Because of the requirement to have this additional coupling term, the photon absorption process is less likely to occur. Indirect band gap semiconductors therefore have relatively small absorption coefficients. For example, although the band gap energy for Si is 1.12 eV, the absorption coefficient at 1.3 eV is only 10^2 cm^{-1} (Fig. 7). This contrasts with the value of 10^4 cm^{-1} that is typically displayed by direct band gap materials at photon energies 0.1–0.2 eV higher than $\mathbf{E}_g$ (43). Examples of other indirect band gap semiconductors include GaP and TiO_2.

For direct band gap materials, the absorption coefficient generally increases rapidly when $h\nu \approx \mathbf{E}_g$, and it then remains at large values when $h\nu >> \mathbf{E}_g$. For indirect band gap materials, the absorption coefficient is generally a much more slowly rising function of energy, with $\alpha \propto (\mathbf{E}-\mathbf{E}_g)^2$ (for $\mathbf{E} \geq \mathbf{E}_g$) being a typical dependence of the absorption coefficient on the energy of the incident photon (43). In both cases, all of the incident light can be absorbed if the sample is sufficiently thick, because as illustrated in Eq. 2, increases in ℓ will produce increases in A. Note, however, that as the photon energy increases, the indirect band gap material will eventually enter a regime where it absorbs light almost as effectively as a material with a direct band gap.

A related, useful quantity to characterize the absorption of light by semiconductors is the *optical penetration depth* (Fig. 7). This quantity is defined to be equal to the inverse of the absorption coefficient; that is, penetration depth $\equiv$ α^{-1}. From Eq. 2, it can be seen that the penetration depth is the distance into the semiconductor at which the transmitted light intensity reaches 1/e of the incident light intensity at the surface of the solid. In general, when compared to direct band gap materials, indirect band gap semiconductors have larger penetration depths and, therefore, require thicker samples to fully absorb the incident light. This requirement is extremely important with respect to the design of an actual photoelectrochemical energy conversion system.

To optimally create charge and effectively produce a photocurrent, the semiconductor needs to be thick enough to absorb essentially all the photons. For example, the indirect gap of Si results in $\alpha = 10^2$ cm^{-1} for photon energies near $\mathbf{E}_g$ (Fig. 7), which implies that more than 100 μm of Si must be used to absorb the incident light effectively in this energy range. This value places severe restrictions on the type of cells, and on the quality of crystals, that must be used in any efficient silicon-based solar energy conversion device. This situation contrasts with that for the direct band gap semiconductor GaAs, in which $\alpha \geq 10^4$ cm^{-1} near $\mathbf{E}_g$ (Fig. 7). The large absorption coefficient of this direct

band gap semiconductor implies that only 1–2 μm of GaAs are needed to harvest the incident photons near the GaAs band gap energy.

3. *Carrier Statistics for Semiconductors*

In the previous sections, we described the mechanism by which a semiconductor can absorb light. We also examined the properties a semiconductor must possess in order to harvest optical energy efficiently from the solar spectrum. These sections have further described how the structure and electronic properties of semiconductors enable them to create delocalized charge carriers for use in solar energy conversion. However, we have not discussed an additional property of semiconductors that is important in energy conversion devices, electrical conductivity. Even if light is effectively absorbed by the semiconductor, and even if this light absorption successfully creates free, delocalized charges in the semiconductor, the charge carriers must move through the solid in order to produce a photocurrent. If the semiconductor is too resistive, then energy will be lost as the carriers traverse the length of the semiconductor crystal to reach the electrical contacts. In order to control this undesirable resistive loss, as well as to control other important electronic properties of semiconductor junctions, impurities are usually intentionally introduced into semiconductor crystals. This process, which is called *doping*, serves to decrease the resistance of the crystal. Doping also allows control over the Fermi level (i.e., the electrochemical potential) of the semiconductor phase. The carrier concentrations that result from these chemical steps, as well as other relevant electrical variables for semiconductor systems, are discussed in Section II.B.3.

a. Carrier Concentrations in an Intrinsic Semiconductor. To start this discussion, we must first consider the properties of the undoped, *intrinsic* semiconductor (i.e., the pure semiconductor). Although we described a semiconductor as having a filled HOMO (the valence band) and an empty LUMO (the conduction band), this condition is only rigorously true at a temperature of absolute zero. At any finite, nonzero temperature, thermal excitation within the solid will result in promotion of carriers from one band to the other. This promotion of carriers produces a nonzero conductivity within the semiconductor. We wish to describe this situation quantitatively.

Before proceeding with this discussion, it is important to realize that there are two different types of charge carriers in a semiconductor: electrons and holes. The promotion of an electron from the valence band into the conduction band, either by thermal or optical excitation, produces a free electron in the conduction band and an electronic vacancy in the valence band. This electronic vacancy is commonly referred to as a *hole*. Although the motion of holes is actually specified by the motion of the remaining collection of valence band

electrons, a hole can formally be treated as a discrete particle with a positive electronic charge. Like an electron, a hole can act as a charge carrier. Thus, a hole moving towards a contact is physically identical to an electron moving away from that contact. Because both electrons and holes contribute to the current in a semiconductor sample, we will use the more general term *charge carriers* to refer to either electrons or holes in a semiconductor.

To describe the conductivity of a semiconductor sample quantitatively, we need to calculate the concentration of both types of charge carriers in the solid. The key quantity that controls the equilibrium concentration of electrons and holes in an intrinsic semiconductor is the band gap. Because the thermal excitation required to produce an electron and a hole is equal to $\mathbf{E}_g$, the equilibrium carrier concentrations can be related to $\mathbf{E}_g$ using the Boltzmann relationship (71).

$$n_i p_i = \text{``constant''} \exp\left(-\frac{\mathbf{E}_g}{kT}\right) \tag{3}$$

In this equation, k is the Boltzmann constant, T is the absolute temperature, and n_i and p_i are the electron and hole concentrations at equilibrium in the intrinsic semiconductor. Both n_i and p_i are expressed as particles per cubic centimeter, which is often abbreviated as "cm^{-3}." The constant in Eq. 3 will be defined below. However, it is clear that this type of Boltzmann relationship should correctly describe the concentrations of electrons and holes that exist as a result of thermal excitation across the band gap at any given temperature.

Realizing that the thermal excitation to promote an electron into the conduction band must also result in the formation of a hole in the valence band, we can set $p_i = n_i$. This equivalence leads to the following relationship between n_i and $\mathbf{E}_g$

$$n_i^2 = \text{``constant''} \exp\left(-\frac{\mathbf{E}_g}{kT}\right) \tag{4}$$

This equation is essentially an equilibrium constant relationship between the electron and hole concentrations in the semiconductor. It is much like the ionization constant expression for the dissociation of water, which can be related to the concentrations of H^+(aq) and OH^-(aq) through the relationship $[H^+][OH^-] = K_w = 1 \times 10^{-14}\ M^2$. The only difference between these two expressions is that the temperature dependence of the equilibrium constant is contained implicitly in the value of K_w, but is explicit in the relationship expressed by Eqs. 3 and 4. The most important point to keep in mind is that increases in the sample temperature will produce exponential increases in the electron and hole concentrations for an intrinsic semiconductor.

The value of the constant in Eq. 4 can be obtained from experimental measurements, just as K_w can be obtained from pH measurements of neutral water. In the case of semiconductors, however, the constant can also be calculated a priori from a knowledge of the band structure of the solid. This calculated constant is usually broken down into two quantities, one that describes the properties of the conduction band, and one that describes the properties of the valence band. The former is called the *effective density of states in the conduction band* (N_c), while the latter is called the *effective density of states in the valence band* (N_v). (The effective density of states is the number of crystal orbitals per cubic centimeter within 3 kT of the band edge.) We will not derive the relationship between the band structure and N_c (or N_v), but the interested reader can find this derivation in numerous solid state physics textbooks (36, 38, 39, 43). Generally, N_c and N_v have similar values, and are typically about 10^{19} cm^{-3}. This value implies that the constant in Eq. 4 has a typical value of "constant" $= N_cN_v = 10^{38}$ cm^{-6}.

We can now estimate the equilibrium carrier concentrations for semiconductors that are of interest in solar energy conversion. Recalling that the optimal value of $\mathbf{E}_g$ is between 1.1 and 1.7 eV, we can simply use a representative value for $\mathbf{E}_g$ in Eq. 4 to calculate n_i^2 for this particular material. Because kT is so much smaller than $\mathbf{E}_g$ for these optimal light absorbers, few electrons and holes are produced at room temperature in such semiconductors. For example, considering GaAs with $\mathbf{E}_g = 1.42$ eV and using the actual values of $N_c = 4 \times 10^{17}$ cm^{-3} and $N_v = 7 \times 10^{18}$ cm^{-3} for GaAs at $T = 300$ K in Eq. 4, we calculate that the equilibrium concentrations of electrons and of holes at room temperature are only 2×10^6 cm^{-3}. In general, samples with higher band gap energies will typically have much lower values of n_i^2. Even for Si, with $\mathbf{E}_g$ at the lower end of the acceptable range [$\mathbf{E}_g$(Si) $= 1.12$ eV], n_i is only 1.5×10^{10} cm^{-3}—an equilibrium electron concentration of less than 1 part per trillion! Such samples are far too resistive for the purposes of photoelectrochemistry.

b. Doping. Because the intrinsic carrier concentrations in semiconductors are so low, even impurity concentrations at the level of 1 part per billion can have a profound effect on the electrical properties of semiconductor samples. To increase the sample conductivity and to control other electronic properties of the semiconductor, low concentrations of specific impurity atoms are often introduced into the crystal lattice. The strategy for introducing *dopant atoms*, as well as some quantitative properties of doping statistics, are described in Section II.B.3.b.

Chemistry of Dopants: Donors versus Acceptors. Dopant atoms can be either *donors* or *acceptors*. Donors are readily ionized to produce an electron in the conduction band and a positive charge on the dopant atom; acceptors become

ionized to produce holes in the valence band and negative charges on the dopant site. A material that has been doped with donors is called an *n-type semiconductor*, while one that has been doped with acceptors is called a *p-type semiconductor*. These designations can be easily remembered by the sign of the predominant charge carrier. Donors create free electrons, which have a *n*egative charge, so the sample is denoted n-type. Similarly, acceptors create holes, which have a *p*ositive charge, so the sample is denoted p-type. The predominant charge carrier is called the *majority carrier*, so electrons are the majority carriers in an n-type sample and holes are the majority carriers in a p-type semiconductor.

Figure 8 displays the energy levels of common donors and acceptors with reference to the band edges of two semiconductors. If the energy levels of these donors and acceptors are close to the conduction or valence bands, respectively, they are called *shallow donors* or *acceptors*. Levels that are further away from either band are called *deep levels*. Although ionization of shallow dopants is usually complete at room temperature, ionization of deep dopants generally does not occur at room temperature. We will consider primarily shallow dopant materials in the remainder of Section II.B.3.b.

The properties of most common dopants can be surmised from simple atomic ionization energies and from trends in the periodic properties of the elements. For example, in Si, which is a Group 14 (IVA) element, Group 15 (VA) elements, such as P or As (which have lower ionization energies than Si), will act as donors. Since only four of the five valence electrons in P are required for tetrahedral bonding in the crystal, the fifth valence electron will be donated to the conduction band at room temperature. This situation will produce an n-type crystal, in which the majority carriers are electrons. To a good approximation, the Group 15 (VA) atom in the Si lattice could be considered as being a positively charged P core with a loosely bound electron, as depicted in Fig. 9*a*.

Conversely, Group 13 (IIIA) elements such as B or Al are acceptors in Si, since they require an additional electron from the valence band to satisfy the tetrahedral bonding requirement. The Group 13 (IIIA) atom in the Si lattice can be considered as a negatively charged B core with a loosely bound hole (Fig. 9*b*). Since the trapping of an electron by the Group 13 (IIIA) dopant atom results in the ionization of an electron from a lattice Si site, the doping process with the Group 13 (IIIA) element produces an excess number of holes in the valence band. Doping Si with B thus leads to a p-type Si sample. In such a p-type sample, the holes are the majority carriers, while the electrons are the *minority carriers* (i.e., the less abundant carriers).

Other impurity atoms, such as transition metals, can have deeper levels or multiple levels. In addition, interstitial atoms and crystal defects can also behave as dopants. All of these factors can significantly affect the electronic properties of the material, even if these atoms exist in the crystal in concentrations of parts per billion. The manufacturing and processing of most semiconductor

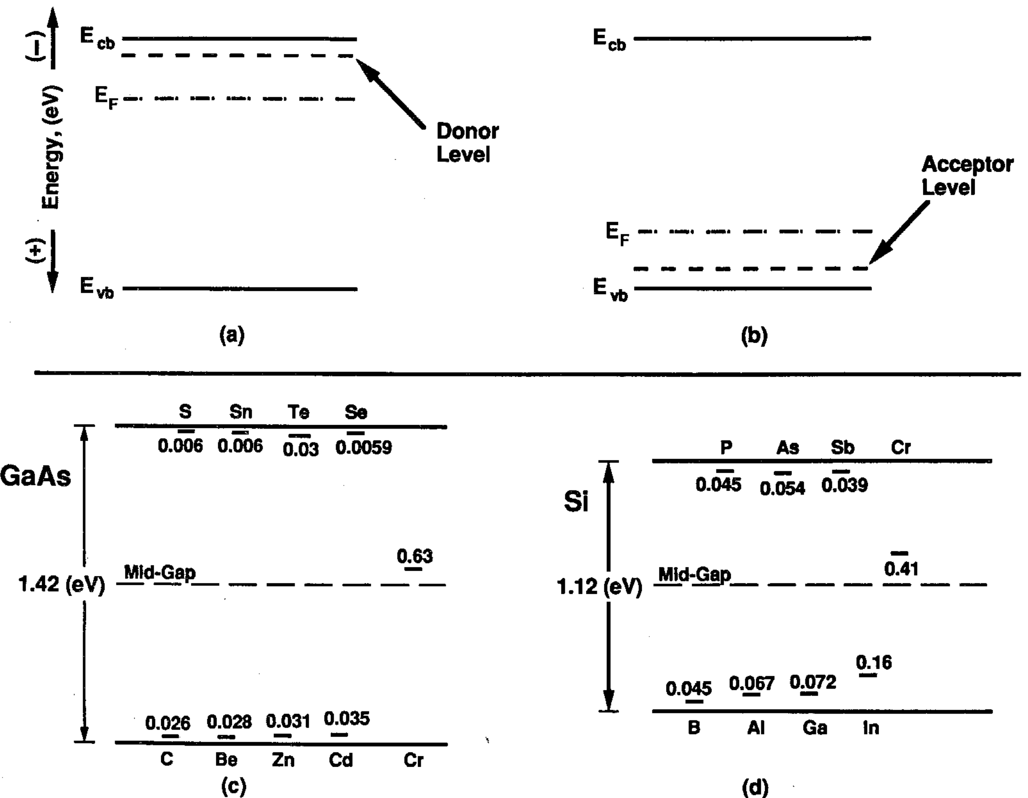

Figure 8. A schematic drawing of the energy levels of "shallow" (*a*) donor and (*b*) acceptor dopants. The parameters $\mathbf{E}_{cb}$ and $\mathbf{E}_{vb}$ represent the energies of the conduction band edge and the valence band edge, respectively. The parameter $\mathbf{E}_F$ is the Fermi level. For a semiconductor doped with donors, the Fermi level is closer to the conduction band edge, while $\mathbf{E}_F$ is closer to the valence band edge for a semiconductor doped with acceptors. A representation of typical dopant levels for (*c*) GaAs and (*d*) Si in relation to the band edges (43). The numbers near these levels denote the difference in energy (eV) away from the nearest band edge.

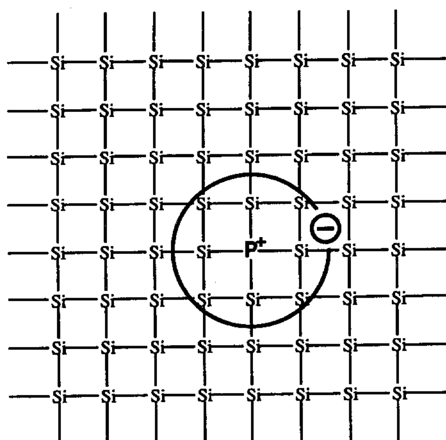

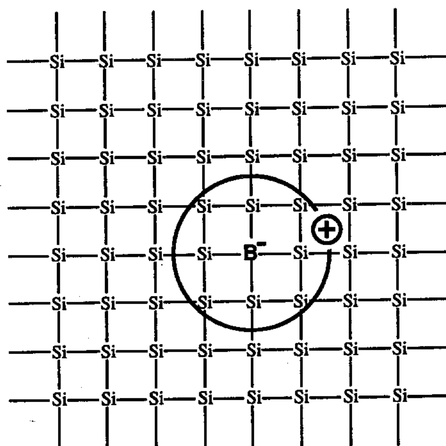

Figure 9. A schematic representation of dopant atoms in a Si lattice: (*a*) a P-doped Si lattice and (*b*) a B-doped Si lattice. The dopant atoms are shown as replacing a Si atom in the crystal lattice. The circles represent schematic Bohr radii of the carrier [i.e., an electron (−) or a hole (+)] around the dopant atom. Note that these orbits are not drawn to scale; in reality, the first Bohr radius of these carriers is about 12 Å (72), and a single carrier is spread over about 10^3 Si atoms.

materials and devices are therefore conducted under conditions of excruciating cleanliness in order to minimize the incorporation of unwanted impurities. For certain applications, impurities with deep levels are incorporated into the semiconductor to control properties that cannot be easily manipulated by shallow dopants (42, 43, 73). For most samples of concern in photoelectrochemistry, however, doping is performed using the straightforward concepts that have been described above.

Carrier Concentrations in a Doped Semiconductor. Because shallow dopant atoms are readily ionized at room temperature, the electron concentration (n) in an n-type semiconductor is closely approximated by the concentration of donor atoms (N_d) in the lattice. Rigorously, the electron concentration is given by the sum of the thermally generated electrons and those generated by the ionization of dopants. However, because n_i is so small for the semiconductors of concern in photoelectrochemistry, $n = n_i + N_d \cong N_d$ for any reasonable dopant concentration (10^{14}–10^{18} dopant atoms per cubic centimeter). Similarly, for a p-type semiconductor, the hole concentration is approximately equal to the acceptor concentration N_a. This approximation holds because shallow acceptors are essentially completely ionized at room temperature, and the intrinsic hole concentration p_i is generally negligible compared to the number of holes that result from the doping process. Clearly, control over the dopant density of a semiconductor allows the manipulation of the carrier concentrations.

It is also important to calculate the equilibrium concentration of holes in a doped n-type semiconductor and of electrons in a doped p-type semiconductor. These minority carrier concentrations are readily obtained using the concepts described above, because Eqs. 3 and 4 are actually more general than has been indicated. As pointed out above, the relationship between n_i and p_i in Eq. 3 is actually an equilibrium constant relationship between the electron and hole concentrations in the solid. In the discussion above, this expression was derived under the special constraint that $n_i = p_i$, that is, under thermal excitation conditions. However, the equilibrium constant relationship on the right-hand side of Eqs. 3 and 4 must hold regardless of the source of electrons and holes, so it applies to both doped and intrinsic semiconductor samples. We thus obtain

$$np = n_i^2 = N_c N_v \exp\left(-\frac{\mathbf{E}_g}{kT}\right) \tag{5}$$

as the general relationship between the electron and hole concentrations in any given semiconductor. In Eq. 5, n and p equal the equilibrium majority and minority carrier concentrations, respectively, for an n-type semiconductor.

This relationship is often called the *law of mass action*, when applied to semiconductor doping statistics (43). The situation is conceptually identical to that for the equilibrium constant relationship for aqueous acid–base dissociation. The relationship $K_w = [H^+(aq)][OH^-(aq)]$ holds not only for the neutral liquid (i.e., the "intrinsic," pH = 7 sample), but also for the proton and hydroxide concentrations in the presence of externally added sources of $H^+(aq)$ or $OH^-(aq)$ (i.e., the extrinsic or "doped" liquid). In the doped semiconductor, we are merely adding electrons or holes to control the carrier concentrations in the same way that the pH of water can be manipulated through addition of acid or base.

Use of numerical quantities in Eq. 5 indicates that for typical doping levels of 10^{15}–10^{17} cm^{-3}, the minority carrier concentrations are extremely low. For example, for n-Si, with $\mathbf{E}_g = 1.12$ eV, the hole concentration is 10^3–10^5 cm^{-3}. These extremely low levels will be insignificant compared to the minority carrier concentrations that will be created by the absorption of photons. The photocurrents will thus be essentially independent of the background minority carrier concentration in the semiconductor samples of interest. This point will be further elaborated in Section IV.

Conductivity. The doping process is also used to control the electrical conductivity of the sample. The conductivity (σ) of a semiconductor is related to the free carrier concentrations by Eq. 6.

$$\sigma = qn\mu_{\rm n} + qp\mu_{\rm p} \tag{6}$$

This equation states that the electrical conductivity due to a free carrier is the product of the charge on the carrier (q), its concentration in the solid, and a quantity called the mobility (μ). Since semiconductors have two different types of mobile charge carriers, electrons and holes, the total sample conductivity σ is simply the sum of the individual conductivities due to each carrier type. It should be noted that the conductivity depends only on the absolute number of carriers, and therefore is not affected by the signs of the carriers themselves. Carrier mobilities for electrons and holes in a variety of semiconductors can be measured experimentally. These values have been tabulated in various reference books (39, 42–44) and are available for many semiconductors of interest. Doping of a semiconductor therefore allows precise control over the conductivity of the sample to be used in photoelectrochemical experiments.

c. Fermi Levels and the Energetics of Semiconductor Samples. The last quantity that is needed to describe the important properties of an isolated semiconductor phase is the electrochemical potential, or *Fermi level* ($\mathbf{E}_F$), of the solid. The Fermi level determines the tendency of the semiconductor to transfer charges to other phases. For solutions that contain electroactive acceptors (A) and donors (A^-), the familiar Nernst equation (which can be written in the form of Eq. 7) quantitatively describes the electrochemical potential of the electrolyte phase.

$$\mathbf{E}(A/A^-) = \mathbf{E}^{\circ\prime}(A/A^-) + \frac{kT}{n_e} \ln \frac{[A]}{[A^-]} \tag{7}$$

In Eq. 7, $\mathbf{E}(A/A^-)$ is the actual electrochemical potential of the solution, $\mathbf{E}^{\circ\prime}(A/A^-)$ is the formal electrochemical potential of the redox couple (A/A^-), n_e is the number of electrons (per molecule of redox couple) that are exchanged during the reaction, and [A] and $[A^-]$ are the respective concentrations of the acceptor and donor species.

This relation is familiar to chemists, because solutions with more positive electrochemical potentials will tend to accept electrons from solutions with more negative values of $\mathbf{E}(A/A^-)$. Now that we have an expression for the electrochemical potential of the solution phase (namely, the Nernst equation), we need to evaluate the electrochemical potential of the doped semiconductor phase (i.e., the Fermi level) in order to describe the charge-transfer events at a semiconductor/liquid interface. A qualitative explanation of this concept is the subject of Section II.B.3.c.

As formally defined in statistical mechanics, the Fermi level of any phase is the energy level where the probability of finding an electron is one-half. In an intrinsic semiconductor crystal at absolute zero, the Fermi level would be located at the middle of the band gap. At absolute zero, the states in the valence band would be totally occupied, and the states in the conduction band would be completely empty. The probability of finding an electron therefore would go from 1.0 in the valence band to 0 in the conduction band, and would reach a value of $\frac{1}{2}$ at mid-gap (even though there are no actual electronic states at this energy).

For a doped semiconductor, the Fermi level position will be shifted from mid-gap, because the doping process will vary the tendency of the solid to either gain or lose electrons. For example, if donors are added to an intrinsic semiconductor, the solid phase will be more likely to lose electrons. The Fermi level of an n-type semiconductor will thus move closer to the vacuum level (i.e., will become more negative on the electrochemical potential scale). Similarly, if acceptors are added to an intrinsic material, the Fermi level will become more positive, because this phase will now have an increased tendency to accept electrons from another phase.

Using an analogy to the Nernst equation, the Fermi level of a semiconductor phase can be written as

$$\mathbf{E}_F = \mathbf{E}_{Fi} - kT\ln(n/n_i) \tag{8a}$$

or

$$\mathbf{E}_F = \mathbf{E}_{Fi} + kT\ln(p/p_i) \tag{8b}$$

More rigorous equations can be obtained by using Fermi–Dirac statistics on the electron occupancy of the filled and empty states of a semiconductor (43, 74).

However, the final results of such a treatment are identical to Eqs. 8a and b for most doping conditions. In these equations, the term $\mathbf{E}_{Fi}$ represents the Fermi level position in the intrinsic semiconductor (i.e., when $n = n_i$ in Eq. 8a or $p = p_i$ in Eq. 8b). This value serves as a reference energy, much as pH $= 7$ serves as a reference value for changes in the pH of a neutral aqueous solution. Physically, Eq. 8a states that doping a semiconductor with donors will produce a more negative Fermi level because $n > n_i$. Similarly, the doping of a semiconductor with acceptors yields a more positive Fermi level, as given by Eq. 8b with $p > p_i$. Of course, since $np = n_i^2$, Eqs. 8a and b can be used interchangeably to solve for $\mathbf{E}_F$ of a doped semiconductor if either n or p is known. Both expressions will yield identical numerical values for $\mathbf{E}_F$.

It is often convenient to refer the Fermi level to reference levels that are close to the band edge energies. If we were to fill up the conduction band with electrons to a value equal to the effective density of states in the conduction band $\mathbf{N}_c$, then the Fermi level would shift until it was exactly equal to the energy of the bottom of the conduction band $\mathbf{E}_{cb}$. Our new reference level would then be the Fermi level at the bottom of the conduction band, that is, $\mathbf{E}_F = \mathbf{E}_{cb}$. In other words,

$$\mathbf{E}_F = \mathbf{E}_{cb} - kT \ln(n/N_c) \tag{9}$$

In essence, this is analogous to shifting the reference level of an aqueous solution to pH $= 0$. Changes in pH could then be calculated relative to the amount of acid in a 1.0 M H^+ solution, as opposed to calculating pH changes relative to a 10^{-7} M H^+ solution for neutral water. The result for the Fermi level position versus electron concentration is, of course, identical no matter which formula is used. It is only a matter of convenience as to which reference level is used in the calculation of $\mathbf{E}_F$. Similarly, we could choose to refer the Fermi level position to the energy of the top of the valence band $\mathbf{E}_{vb}$. In this case, the expression for $\mathbf{E}_F$ is

$$\mathbf{E}_F = \mathbf{E}_{vb} + kT \ln(p/N_v) \tag{10}$$

The forms used in Eqs. 9 and 10 will not be employed extensively in this chapter, but are presented here because they are often found in the photoelectrochemical literature.

Up to this point in our discussion, we have seen that doping is useful for several purposes: it allows the electrical conductivity and the Fermi level position of a semiconductor sample to be controlled readily. The next step in our understanding of semiconductor photoelectrochemistry is to consider the charge flow that occurs when the doped semiconductor phase is brought into contact with an electroactive solution phase. This process is the topic of Section III.

III. EQUILIBRIUM STATE AT A SEMICONDUCTOR/LIQUID JUNCTION

The key feature that enables semiconductor/liquid junctions to separate charge effectively is the presence of an electric field at the interface between the semiconductor and the liquid. The strength of this field can be on the order of 10^5 V cm^{-1} (43), and the field develops spontaneously, merely as a result of the immersion of a semiconductor into a liquid. Because of the high mobility of delocalized charge carriers in most semiconductors, these enormous field strengths accelerate the charges to velocities of over 10^7 cm s^{-1} (75) and lead to charge separation over distances of greater than 1 μm in less than 10 ps! These fields are present at equilibrium in most semiconductor/liquid systems. These fields are also maintained to a large degree even while the interface is collecting photogenerated carriers and producing electrical and/or stored chemical energy. To understand this behavior, we need to consider the mechanism by which this electric field is established when a semiconductor is placed into contact with a liquid.

In its simplest terms, the charge transfer from a solid to a liquid is no different from the charge transfer between atoms to form an ionic bond. For example, chemists realize that a neutral sodium atom will transfer charge when it encounters a neutral chlorine atom, because Na has a low electronegativity and Cl has a high electronegativity. The bond formation between these atoms results in an equilibrium state in which the compound NaCl is best represented with an ionic bond, that is, Na^+Cl^-. It is also obvious to chemists that the difference in electronegativities of the atoms will determine the degree of charge transfer in the molecule, with HCl having a much more covalent bond than NaCl.

The charge-transfer reaction between two phases is governed by identical principles. However, the controlling factor is the electrochemical potential, not the electronegativity. Whenever two phases of different electrochemical potentials are brought into contact, the phase that has the more negative electrochemical potential will tend to lose electrons to the phase with the more positive electrochemical potential. Charge transfer between the two phases will occur until an equilibrium situation is established. At equilibrium, one phase will have an excess of positive charge, and the other phase will have an excess of negative charge. In our specific examples of concern, the semiconducting solid will be one of the phases that is undergoing charge transfer, and the liquid contact, with its redox couple present to accept or donate the charge, will be the other phase. The difference in electrochemical potentials between the two phases will determine the degree of charge transfer across the phase boundary, much as the difference in electronegativity indicates the degree of bond ionicity in molecules formed from neutral atoms. The only conceptual difference between the molecular case and the interfacial case is that the physical junction between the solid

and the liquid provides an obvious dividing line to separate the phase that will lose electrons from the phase that will gain them.

A. Depletion

1. *Qualitative Description of Interfacial Charge Equilibration*

The simplest case to consider is the situation that describes the contact between an n-type semiconductor and a solution containing the redox pair A/A^-. The electrochemical potential of the isolated semiconductor ($\mathbf{E}_F$) is assumed to be more negative than the electrochemical potential ($\mathbf{E}(A/A^-)$) of the isolated solution phase (Fig. 10*a*). A similar situation could be considered for a p-type semiconductor in contact with a liquid, but the two systems are so closely related conceptually that we will use the n-type semiconductor/liquid interface in most of our examples in this chapter.

The electrochemical potential of the n-type semiconductor is given by the value of its Fermi level ($\mathbf{E}_F$). For the solution phase, the electrochemical potential ($\mathbf{E}(A/A^-)$) can be related to the solution redox potential ($E(A/A^-)$) as follows: $\mathbf{E}(A/A^-) = qE(A/A^-)$. The initial difference in the electrochemical potentials of the two phases indicates that, after contact, charge must flow between the phases in order to reach equilibrium. Under our specific conditions, charge will leave the solid phase, because it has the more negative initial electrochemical potential [$\mathbf{E}_F < \mathbf{E}(A/A^-)$]. This charge will be accepted by the liquid phase, which has a more positive electrochemical potential.

As a result of this initial difference in electrochemical potential, the transfer of electrons across the solid/liquid junction disrupts the original charge neutrality of the semiconductor and of the solution. This interfacial charge-transfer process produces an excess of positive charges in the semiconductor and an excess of negative charges in the solution (Fig. 10*b*). In essence, a capacitor is charged during this process, and the components of the capacitor are the ions in the liquid phase and the charges in the solid phase. This charging process will continue until the initial difference in electrochemical potentials is neutralized, that is, until the capacitor is sufficiently charged that no further net charge transfer is possible thermodynamically. At this point, the junction will have reached charge-transfer equilibrium. After equilibrium is reached, electric fields and electric potential gradients are present in both the solid and liquid phases, because neither phase is electrically neutral. This charge-transfer process, and the establishment of an electric field at a semiconductor/liquid interface, can thus be understood qualitatively based on familiar, simple, chemical concepts.

The charge-transfer process stops only when the electrochemical potentials of both phases are equal, that is, when equilibrium has been reached. In general, the addition of excess negative charges to the liquid phase will tend to decrease the value of its electrochemical potential. This phenomenon can be rationalized

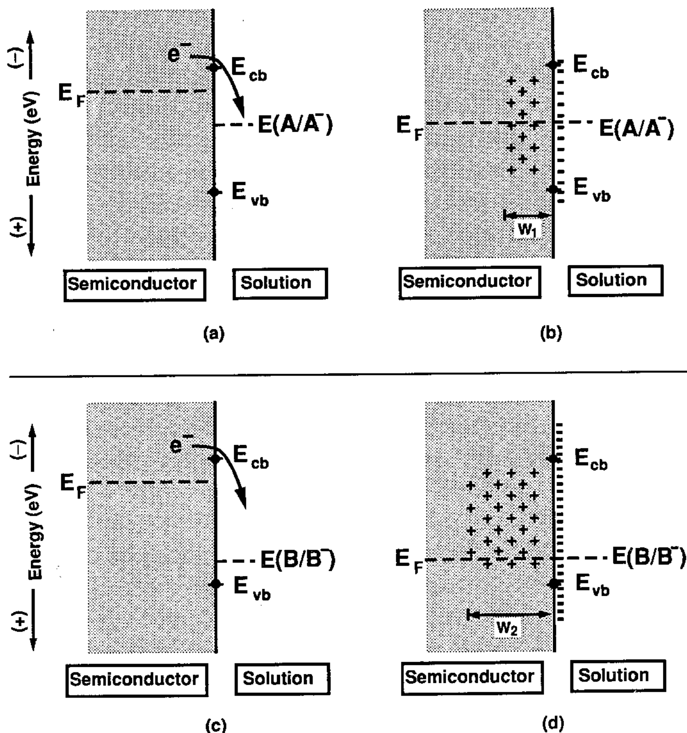

Figure 10. Charge-transfer equilibration processes at semiconductor/liquid junctions. The electrochemical potential of the solution A/A^- ($E(A/A^-)$) is more negative than the electrochemical potential of the solution B/B^- ($E(B/B^-)$). For convenience, the reference energy has been shifted from the vacuum level to an arbitrary value on the electrochemical potential scale. (*a*) Before equilibrium is established, the entire semiconductor is neutral. (*b*) At equilibrium, a positively charged region of width W_1 is present in the semiconductor. (*c*) Similar to (*a*), except that the redox couple (B/B^-) in the solution has a more oxidizing electrochemical potential than A/A^-. (*d*) Similar to (*b*), but the charged region extends deeper into the semiconductor ($W_2 > W_1$), because the number of charges that must cross the semiconductor/liquid interface is greater. In both (*b*) and (*d*), the positions of the conduction and valence band edges are unchanged by the charge equilibration processes.

because it is easier to ionize a phase with excess negative charges than one without such an excess. Similarly, the loss of negative charge from the semiconductor will tend to increase the value of its electrochemical potential. Thus, net charge will continue to flow across the junction until these electrochemical potentials equilibrate at the same level.

For two arbitrary phases, it is not always possible to predict a priori whether the Fermi level of the semiconductor will move more or less than that of the contacting phase. However, for semiconductor/liquid contacts, it is possible to predict what will occur. Even in solutions that contain dilute ($< 10\ \mu M$) con-

centrations of redox species, the number of available states per unit energy in the solution far exceeds the number present in a semiconductor, since the solid has essentially no available states in its band gap region. Thus, during the equilibration process, there is little negative movement of the electrochemical potential of the solution. The Fermi level of the n-type semiconductor, however, becomes more positive until it reaches the value of the solution electrochemical potential. In chemical terms, the solution acts as an excellent "buffer" of energy with respect to excess charge. This situation is analogous to aqueous buffers that resist changes in pH when mixed with nonbuffered solutions that contain small amounts of H^+.

The equilibrium positions of the Fermi level for both the semiconductor and liquid phases are therefore essentially equal to the initial value of the solution electrochemical potential ($\mathbf{E}(A/A^-)$). When sufficient charge has transferred across the interface to produce this change in $\mathbf{E}_F$, equilibrium is reached, and no further net flow across the solid/liquid boundary will occur for this particular combination of solid and liquid phases.

a. Depletion Width. An important quantity, the depletion width, can also be understood using these qualitative concepts. For a doped semiconductor, charge-transfer equilibration removes carriers from the sites that are most easily ionized. Thus, if possible, charge is removed from the dopant atoms, as opposed to being removed from atoms of the semiconductor material. For example, for phosphorus-doped n-type Si, charge-transfer equilibration would be accomplished by the transfer of the fifth valence electron on the P dopant atoms, as opposed to the transfer of electrons arising from the ionization of the Si lattice atoms. In order to reach charge-transfer equilibrium, a certain number of charges must be pulled out of the semiconductor phase. The number of charges that need to be transferred is generally far larger than the number of dopant atoms that are present in one atomic layer of the solid. Thus, as depicted in Fig. 10*b* and *d*, greater degrees of charge transfer require that we "reach further into" the bulk of the semiconductor to obtain the proper number of ionizable charges from the solid.

The depth over which dopants are ionized can be readily calculated. For an n-type semiconductor of majority carrier density (N_d), a good first approximation is that charge transfer produces a fixed concentration of charged dopant atoms for a depth W. Within this depth, essentially all of the electrons donated by the available dopants have been removed from the solid. The ionized dopant atoms are thus left in this region as positive charges. However, beyond this depth, essentially no electrons have been removed, and the ionized dopants are surrounded by electrons. This approximation is called the *depletion approximation* (76), and the quantity W is called the *depletion width*. In the semiconductor, the charged region of width W is called the *depletion region*.

With this approximation, W is readily calculated if the amount of charge

transferred per unit area (Q) is known. The parameter W is then simply Q/N_d. When a higher dopant density is available for donating electrons to the solution, one needs to "reach in" less deeply into the solid to achieve a given degree of charge transfer. The value of W thus becomes smaller as the dopant density increases. The depletion width will be an important quantity to understand when considering the effects of various chemical modifications on the behavior of semiconductor/liquid interfaces. As discussed above, its accurate calculation using the depletion approximation depends only on a prediction of the amount of charge per unit area (Q) that must be transferred to equilibrate the desired semiconductor/liquid interface.

Without any additional quantitative information, some important chemical trends in junction behavior can be clearly understood. In a molecule, a large difference in electronegativity between bonded atoms should lead to a large degree of ionicity in the bond. At the solid/liquid interface, a greater initial difference in the electrochemical potentials of the isolated solid and liquid phases should produce a greater propensity for interfacial charge transfer at the solid/liquid junction. Using our example of an n-type semiconductor, solutions with more positive redox potentials on the electrochemical scale will produce greater initial contact potentials to a given semiconductor surface. These solutions would thus be expected to produce larger degrees of interfacial charge transfer than solutions with less positive redox potentials (Fig. 10). Similarly, semiconductors with more negative Fermi levels, that is, either more highly doped samples of a given material, or materials with lower electron affinities at similar doping levels, would be expected to produce a greater degree of charge transfer when placed in contact with a solution of a given redox potential. This chemical control over the strength of the interfacial electric field is one of the key experimental features of semiconductor/liquid junctions.

2. *Quantitative Description of Interfacial Charge Equilibration*

a. Electric Field and Electric Potential. It is also important to understand quantitatively the strength of the electric field, and the values of the electric potential, that are produced as a result of this charge-transfer equilibration process. Simple electrostatic considerations suggest that an electric field and an electric potential will be present in the solid, because the interfacial charge transfer has removed negative charges from an initially neutral phase to produce a net charge density in the semiconductor portion of the junction (77). Our goal now is to understand how to describe the electric field and electric potential that result from this process.

The relationship between the charge density and the electric field strength is simply obtained from electrostatics. Consider a negative test charge that we will bring through the semiconductor and towards the solid/liquid interface. At points within the bulk of the semiconductor, the negative charges on the liquid side of

the interface are offset (i.e., screened) by an approximately equal number of positive charges in the depletion region of the semiconductor. Thus, negligible electric fields are experienced by this test charge. This region is called the *quasi-neutral region* of the semiconductor, as a negative test charge at these positions in the solid is not influenced by the presence or absence of charge transfer at the solid/liquid interface.

As we proceed to move our negative test charge closer to the semiconductor/liquid interface, it will start to penetrate into the depletion region. This negative test charge will be repelled from the interface, because it will experience the repulsion of all of the negative charges in the liquid phase, while being screened by only a portion of the positive charges in the semiconductor phase. Another way of thinking about this situation is that there is now a net dipole acting on the test charge that pushes the charge away from the interface. This net dipole arises from the excess of negative charges that is sensed by the test charge.

Under these conditions, work is required to push this negative test charge towards the interface. We can quantitatively express this work either in terms of the electric field strength at each position in the solid, or in terms of the electric potential at each position of the system. According to electrostatics, the electric field is simply the integral of any excess charge density along the path of interest (77). Thus, using the depletion approximation, which states that the charge density is simply the dopant density for all values of x up to the depletion width, we calculate that

$$\mathscr{E}(x) = \left(\frac{qN_d}{\varepsilon_s}\right) x \quad (0 \leq x \leq W) \tag{11}$$

where $\mathscr{E}(x)$ is the electric field strength at position x in the solid, ε_s is the static dielectric constant of the semiconductor, and N_d is the dopant density of the semiconductor. In Eq. 11, the origin of the x-axis has been defined as the position that separates the depletion region from the quasi-neutral region; therefore, the semiconductor/liquid interface is at a distance $W (W > 0)$ from the origin (Fig. 11*a* and *b*).

As given in Eq. 11, since the depletion approximation ensures that the charge density in the depletion region is independent of distance, the electric field strength in this region increases linearly as the solid/liquid junction is approached. The maximum electric field strength in the semiconductor ($\mathscr{E}_{max}$) is obtained at the position $x = W$.

$$\mathscr{E}_{max} = \left(\frac{qN_d}{\varepsilon_s}\right) W \tag{12}$$

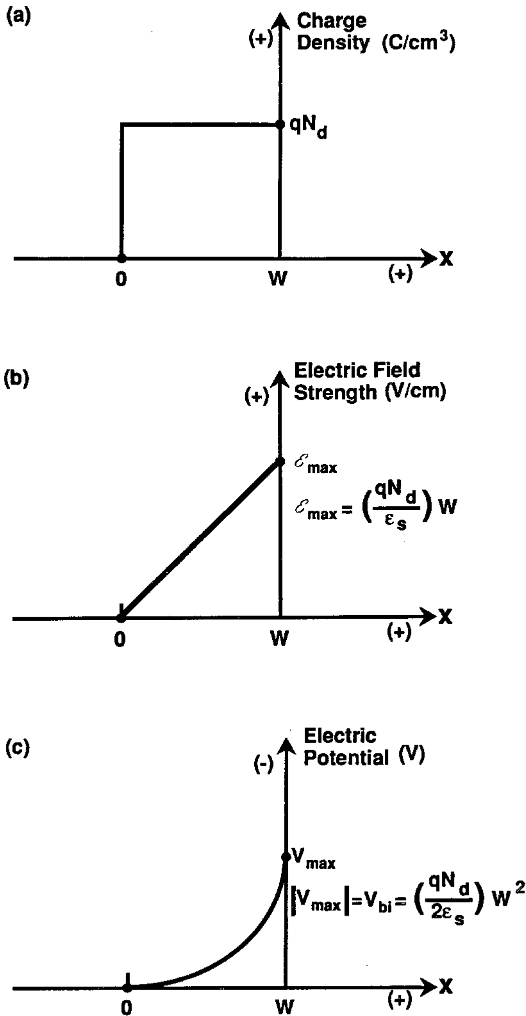

Figure 11. The spatial dependence of the charge density, the electric field, and the electric potential in the semiconductor at equilibrium. The origin of the x-axis (the distance axis) is chosen for convenience as the point where the net charge density in the semiconductor becomes zero. (*a*) The distance dependence of the charge density under the depletion approximation. (*b*) The electric field strength as a function of distance. Note that the maximum electric field strength occurs at the semiconductor/liquid interface. (*c*) The distance dependence of the electric potential in the semiconductor. The electric potential in the bulk of the semiconductor has been defined to be zero. Because the sign of the electric field strength is positive, the electric potential at the interface is more negative than it is in the bulk.

Thus, the maximum electric field strength in a semiconductor/liquid junction is located at the interface. This is an important feature for constructing efficient energy conversion devices using semiconductor/liquid junctions, because the maximum ability for charge separation by the electric field occurs at the solid/liquid interface.

An alternative and convenient method of expressing the work required to push our negative test charge towards the interface is given by the electric potential at each point in the semiconductor. Electrostatics states that the electric potential is equal to the negative integral of the electric field over the path of interest (77). Thus, integrating the linear electric field (Eq. 11) from the bulk of the semiconductor towards the semiconductor/liquid interface yields a quadratic expression for the electric potential in the semiconductor phase.

$$V(x) = -\left(\frac{qN_d}{2\,\varepsilon_s}\right)x^2 \quad (0 \leq x \leq W) \tag{13}$$

The electric potential of an electron near the interface is thus more negative than in the bulk. The negative sign in Eq. 13 merely indicates that the electric potential at the interface is more negative than that in the bulk, that is, the electric potential at the interface is closer to the vacuum level than in the bulk. This makes sense, because work was required to push the negative test charge towards the interface. The difference in electric potential between the quasi-neutral region and any other position is a quantitative measure of the work required to move this test charge in the solid.

Figure 11 contains plots of the charge density, electric field strength and electric potential versus distance for a semiconductor/liquid junction. Because these diagrams are all related to each other, only one type of diagram is often depicted when a particular semiconductor/liquid interface is discussed. The most convenient diagram is that of the electric potential energy versus distance, because the electric potential energy can be directly related to the potential energy of an electron at any point in the system. The potential energy of an electron at each position in the solid can be obtained by multiplying the electric potential by the charge on an electron.

A schematic of the potential energy versus distance relationship for a semiconductor/liquid junction is depicted in Fig. 12. These potential energy versus distance diagrams are often called *band bending diagrams*. The electric potential gradient leads to a quadratic increase in the potential energy of an electron in the solid as it approaches the surface of the semiconductor. Both the conduction and valence bands are shown bent because the electric field acts equally well on test charges that are in either band. Note also that on these diagrams, the distance between the bottom of the conduction band and the top of the valence band always remains constant. This situation results because the pres-

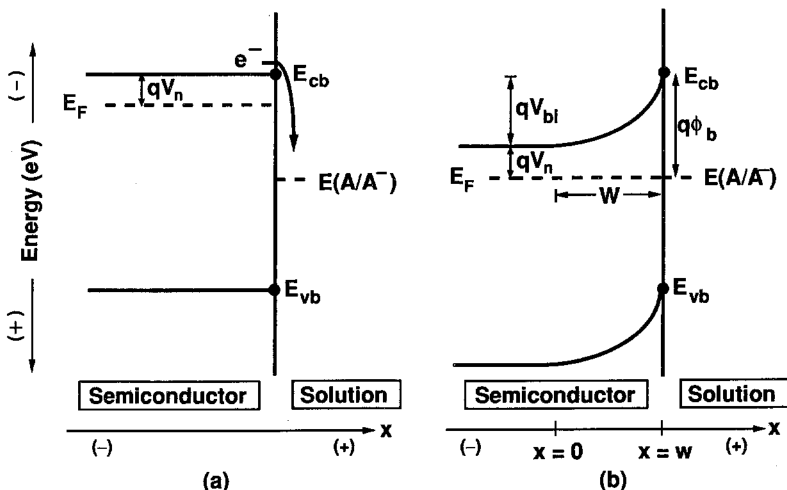

Figure 12. An energy diagram of an n-type semiconductor/liquid junction at equilibrium. (*a*) Before charge equilibration occurs, the energy levels of the semiconductor conduction and valence bands are uniform at all points along the x-axis. (*b*) After charge equilibration has occurred, a depletion layer is formed in the semiconductor. As shown, the electric potential energy levels of $\mathbf{E}_{cb}$ and $\mathbf{E}_{vb}$ are dependent on distance in the depletion region. However, at equilibrium, the electrochemical potential is the same in the solution and at all points in the semiconductor [i.e., $E(A/A^-) = \mathbf{E}_F$]. The parameter qV_n is defined as the difference between $\mathbf{E}_F$ and $\mathbf{E}_{cb}$ in the bulk semiconductor, and V_{bi} is the built-in voltage of the junction. The parameter ϕ_b, the barrier height, is defined as $\phi_b = V_n + V_{bi}$.

ence of an electric field has a negligible effect on the value of the band gap for most semiconductors.

Another chemical analogy will be useful in elucidating the meaning of band bending diagrams. Chemists are quite comfortable with reaction coordinate diagrams, in which the free energy of the system is plotted versus some (typically unknown) reaction coordinate for a chemical reaction. A similar interpretation is possible for band bending diagrams (Fig. 12*b*). These diagrams can be interpreted as representing the activation energy required to move a negative charge along a reaction coordinate towards the interface. This movement will require energy, because of the repulsion due to the unscreened negative charges on the liquid side of the semiconductor/liquid junction. The difference between the common chemical reaction coordinate diagram and a band bending diagram is that if the amount of charge is known, the electric potential (Eq. 13) and, therefore, the electric potential energy of the system, can be calculated precisely at each point along the reaction coordinate. In contrast, typical chemical reaction coordinates are only schematic in both energy and in direction along the bond coordinates. Thus, the same interpretation applies to band bending and

reaction coordinate diagrams. However, more quantitative information is available from a band bending diagram, because the electrostatic equations allow calculation of the potential energy along each position of the reaction coordinate.

b. Built-in Voltage. A few quantitative values are worth deriving in order to complete the diagrams of Figs. 11 and 12. According to Eq. 13, the absolute value of the electric potential reaches its maximum at the interface ($x = W$). The absolute value of this potential difference between the interface and the semiconductor bulk is called the *built-in voltage* (V_{bi}). The built-in voltage is a direct result of the initial electrochemical potential difference between the semiconductor and the solution, with $V_{bi} = |\mathbf{E}_F - \mathbf{E}(A/A^-)|/_q$ (Fig. 12). The parameter V_{bi} represents the amount of voltage drop that has occurred across the semiconductor phase during the charge-transfer equilibration process. This quantity is the total change in electric potential that would be experienced upon moving a test charge from the back of the semiconductor solid ($x = -\infty$) all the way to the interface between the solid and the liquid ($x = W$). The parameter V_{bi} is called the built-in voltage because this voltage is "built-in" to the semiconductor as a result of equilibration with the solution redox level. The parameter V_{bi} can be related to the amount of charge transferred and, therefore, to the depletion width W, using the equations developed above. From Eq. 13

$$V_{bi} = \left(\frac{qN_d}{2\,\varepsilon_s}\right) W^2 \tag{14a}$$

or

$$W = \sqrt{\frac{2\,\varepsilon_s V_{bi}}{qN_d}} \tag{14b}$$

Another quantity of interest on the band bending diagrams refers to the bulk of the semiconductor. In the semiconductor bulk region where no electric fields are present, the difference between the Fermi level and the energy of the bottom of the conduction band remains the same as it was in the neutral semiconductor before equilibration with the liquid. Thus, we can define $V_n \equiv (\mathbf{E}_F - \mathbf{E}_{cb})/q$ as the potential difference between the Fermi level and the conduction band energy in the semiconductor bulk, as shown on the band bending diagram in Fig. 12.

The difference between the equilibrium Fermi level and the energy of the bottom of the conduction band at the semiconductor/liquid interface is also an important quantity often mentioned in the literature. This difference is called the *barrier height energy* of the junction. This parameter is generally abbrevi-

ated as $q\phi_b$, where ϕ_b is the barrier height in volts and $q\phi_b$ is the barrier height energy in electron volts. From Fig. 12*b* and from the definitions of V_{bi} and V_n, it can be seen that $\phi_b = V_n + V_{bi}$. It is generally convenient to use ϕ_b to characterize the barrier height of semiconductor/liquid contacts, because unlike V_n and V_{bi}, ϕ_b is independent of the doping level of the semiconductor. In fact, the magnitude of ϕ_b depends only on the initial position of the semiconductor conduction band edge ($\mathbf{E}_{cb}$) and on the initial electrochemical potential of the solution ($\mathbf{E}(A/A^-)$) with $q\phi_b = \mathbf{E}_F - \mathbf{E}_{cb}$ (at the electrode surface).

The values of V_{bi} and ϕ_b are key experimental quantities that are used to characterize the physical properties of semiconductor/liquid interfaces. If V_{bi} or ϕ_b can be determined, then W, Q, $\mathscr{E}(x)$, and most of the other important thermodynamic quantities that are relevant to energy conversion can be readily calculated using the simple equations that have been presented above. Methods to determine these important parameters will be discussed in more detail later in this chapter. However, it would be useful at this point in the discussion to consider what values of ϕ_b and V_{bi} are theoretically expected for a given semiconductor/liquid interface. By definition, $\phi_b = [\mathbf{E}(A/A^-) - \mathbf{E}_{cb}]/q$ at the electrode surface (Fig. 12*b*). Thus, in principle, the barrier height can be predicted if the energies of the semiconductor band edges and the electrochemical potential of the solution can be determined with respect to a common reference energy.

A problem with this approach involves the relationship between the electrochemical potential of the solution and the electrochemical potential of the solid. Like most electronic energy levels for molecules, the Fermi level of the semiconductor is usually calculated relative to the vacuum level. Experimental measurements to determine $\mathbf{E}_F$ for semiconductors (generally through determination of the semiconductor work function and dopant density) also yield values that can be related to the energy of an electron in vacuum. However, Nernst potentials of liquid phases can only be measured as potential differences between the test solution and a solution that is used as a reference (78). Since it is not possible to measure directly the energy of an individual electrochemical solution relative to the vacuum level, it is not possible to determine directly the desired relationship between the energy levels on the solid side of the junction and those on the liquid side.

Typically, the reference level for solution redox potentials is chosen to be the normal hydrogen electrode (NHE). Some tabulations use the saturated calomel electrode (SCE) as the reference level, but the difference between these two scales is well known to be NHE = −0.24 V versus SCE (79). The fundamental problem is the determination of the absolute energy of the NHE relative to vacuum. Although a method to determine directly the absolute electrochemical potential of a NHE has not yet been conceived, a recent indirect measurements has indicated that it is approximately 4.43 eV below the vacuum

level (80). This value is often used to relate the electrochemical potential scale to the vacuum level scale. It provides the best approximation that is presently available to calculate the values of ϕ_b and V_{bi}, based only on the values of $\mathbf{E}_{cb}$ and $E(A/A^-)$. Figure 13 shows the approximate positions of some common redox potentials relative to the energy band positions of various semiconductors.

c. Surface Concentration of Electrons. A final quantitative aspect of these band bending diagrams concerns the equilibrium concentration of electrons at different positions in the semiconductor. Before contact with the solution phase, the carrier concentration was equal at all points in the semiconductor. For a moderately doped solid with completely ionized dopants, this carrier concentration is simply given by the value of N_d. For a depleted n-type semi-

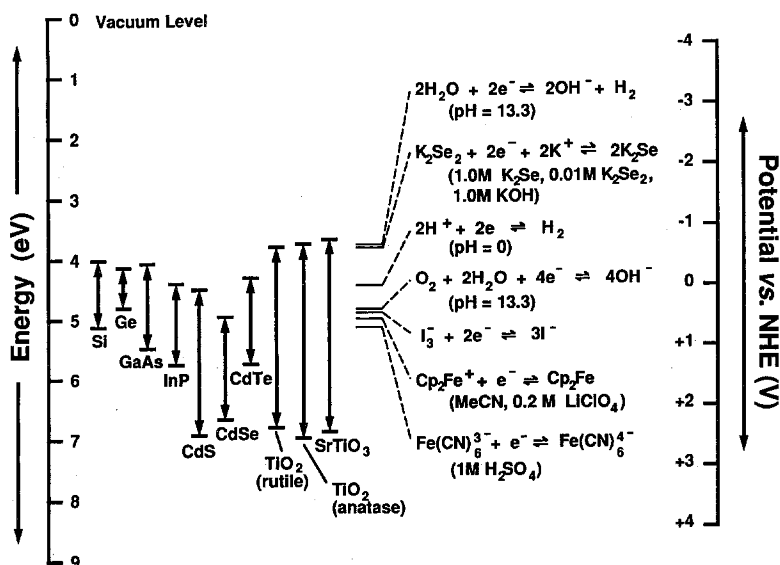

Figure 13. The positions of the conduction and valence band edges of various semiconductors and the redox potentials of selected solutions. The semiconductor conduction band edge positions are determined from electron affinity measurements, and are referenced against the vacuum level (45, 56, 81). The solution redox potentials are measured against the NHE in V (78, 82) and can be converted to energies (eV) by multiplying by q. The electrochemical potential of the normal hydrogen electrode (NHE) is taken to be 4.43 eV below the vacuum level (80). It should be noted that the band edge positions of TiO_2 and $SrTiO_3$ depend on the pH of the contacting solution. The positions illustrated here are for these semiconductors when in contact with solutions of pH = 13.3 (56, 82). The potentials for the reduction of H_2O to $H_2(g)$, and for the oxidation of H_2O to $O_2(g)$, are also given for pH = 13.3. From the figure, it is obvious that TiO_2 (rutile) cannot reduce water, while TiO_2 (anatase) and $SrTiO_3$ can split water to $H_2(g)$ and $O_2(g)$ under standard conditions.

conductor, however, the presence of unshielded negative charge on the liquid side of the interface will make it energetically difficult to support negatively charged electrons in the semiconductor depletion region. Because the screening of interfacial charge is a function of distance away from the solid/liquid junction, the actual majority carrier concentration in a depleted semiconductor is expected to be a function of distance from the solid/liquid interface.

To obtain an expression for this carrier concentration versus distance relationship, we need to consider the potential energy difference between various points in the semiconducting solid. The relationship between the bulk carrier concentration (n_b) and the carrier concentration at any other position in the solid can be obtained simply by using the Boltzmann equation

$$n(x) = n_b \exp\left[\frac{qV(x)}{kT}\right] \tag{15}$$

where $V(x)$ is the electric potential difference between the bulk semiconductor and any other position of interest (Fig. 11*c*). The concentration of electrons in the bulk is the same as that in the neutral material, so $n_b = N_d$. The parameter $V(x)$ is negative with respect to the potential of the conduction band in the semiconductor's quasi-neutral region (Fig. 11*c* and Eq. 13). Therefore, as the solid/liquid interface is approached, $n(x)$ decreases exponentially from the bulk electron concentration.

From Eq. 15, it can be seen that $n(x)$ reaches a minimum at the semiconductor surface. The concentration of electrons at the surface (n_s) is given by

$$n_s = n_b \exp\left(-\frac{qV_{bi}}{kT}\right) \tag{16}$$

where V_{bi} is the absolute value of $V(x)$ at $x = W$.

This expression clearly shows that V_{bi} represents the total electric potential barrier for electrons to move from the bulk of the semiconductor to the solution. As will be discussed in Section IV, the surface concentration of electrons is an important factor that controls the charge-transfer events between the semiconductor and the solution. Thus, V_{bi} directly affects the current–voltage properties of a semiconductor/liquid junction.

B. Accumulation

We have described above the relevant physics and electrostatics for a depleted semiconductor/liquid contact. It is also possible, however, that the initial electrochemical potential of the solution will be more negative than the Fermi level of the semiconductor. During the approach to equilibrium, charge will

then tend to flow into the semiconductor from the solution phase. This flow of electrons into the semiconductor leads to a qualitatively different energetic situation than the one that has been described for depletion. We briefly discuss the properties of these types of contacts in Section III.B.

When electrons from the solution phase are transferred into the semiconductor, these electrons are not confined to dopant atom sites. Instead, the majority carriers exist as delocalized charges in the conduction band. The spatial region in the semiconductor where the negative charges accumulate is called the *accumulation region* (Fig. 14). The most important difference between the cases of depletion and of accumulation is that the carriers are removed from the immobile dopant atom sites under depletion conditions. In contrast, in accumulation the charges enter orbitals that are a part of the conduction band. Because these excess majority carriers need not reside on dopant atoms, but can also reside on lattice atoms of the semiconductor, the charge density that can be supported in accumulation is not limited by the dopant density. Instead, it is more closely approximated by the atom density in the crystal lattice. The thickness of an accumulation region is therefore far smaller than that of a depletion region, at least for the same material and same amount of charge transferred across the interface. The width of an accumulation layer is typically less than 100 Å (83), while the width of the depletion region is usually on the order of micrometers.

Experimentally, the thin width of an accumulation layer implies that charge separation will not be effective for such semiconductor/liquid interfaces. Both

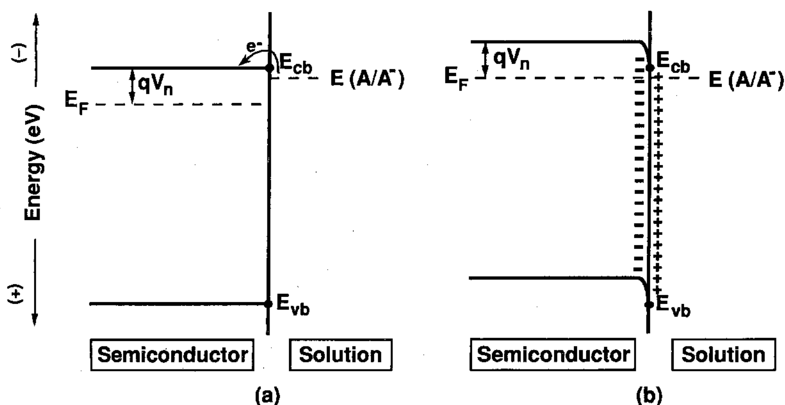

Figure 14. An energy diagram of a semiconductor/liquid junction in accumulation. (*a*) Before charge equilibration occurs, the Fermi level of the semiconductor (E_F) is more positive than the solution electrochemical potential [$E(A/A^-)$], and electrons will flow from the solution into the semiconductor. (*b*) After charge equilibration has occurred, an accumulation layer containing negative charges is formed in the semiconductor.

electrons and holes can tunnel through the thin electric potential barrier in the accumulation region, so the charge separating ability of the electric field is greatly reduced relative to that in depletion. In addition, the spatial extent of the electric field gradient in accumulation is reduced relative to the field width in depletion. Only charge carriers created very near to the semiconductor/liquid interface will sense the excess charges in the liquid phase and will be separated by the field when accumulation conditions are established. Semiconductor/liquid interfaces in accumulation are useful for investigating the electrostatics of junction formation, but are not useful in the formation of efficient solar energy conversion devices.

C. Fermi Level Pinning

In discussing the behavior of semiconductor/liquid junctions in depletion, we have assumed that if the energy of the conduction band edge $\mathbf{E}_{cb}$ and the electrochemical potential of the solution ($\mathbf{E}(A/A^-)$) were known, their difference would yield a quantitative prediction of the barrier height for a given interface (Fig. 12). Furthermore, even if the absolute magnitude of ϕ_b is not known, it should still be the case that a change in the redox potential of the solution should yield a defined change in the barrier height, and also in the built-in voltage, of the resulting semiconductor/liquid contact. The scenario in which these conditions apply is often called the ''ideal'' behavior of a semiconductor/liquid contact. However, for many semiconductor/liquid contacts, this ideal behavior is not observed experimentally. In fact, in some systems, changes in the solution redox potential do not change the properties of the semiconductor/liquid junction. In the remainder of this section, we describe how this important class of exceptions to ideal behavior can be understood, and we describe the implications of this nonideal junction behavior with respect to energy conversion.

The key experimental observation is that the built-in voltage in the semiconductor (V_{bi}) often does not change despite large variations in the redox potential of the solution (84, 85). Attaining equilibrium between two phases requires that different degrees of interfacial charge transfer must occur when the initial electrochemical potential difference between these phases is changed. The experimental observation therefore indicates that another source or sink for charge must exist in the real interfacial system. These sources and sinks for charge are often referred to as *surface states*, and their ability to ''buffer'' the semiconductor from changes in the electrochemical potential of the contacting phase is referred to as *Fermi level pinning*.

Surface states can arise simply because the atomic bonding at a semiconductor surface is necessarily different from that in the bulk. For example, in a Si lattice, the bonds at the Si surface are not fully coordinatively saturated. To

relieve this unsaturation, either a surface reconstruction will occur and/or bonds to solvent, oxygen, or some other species will be formed. This distinct type of surface bonding results in a localized electronic structure for the surface that is different from that in the bulk. The energies of these localized surface orbitals are not restricted to reside in the bands of the bulk material, and can often be located at energies that are more negative than the top of the valence band or more positive than the bottom of the conduction band, that is, inside the band gap of the semiconductor. Orbitals that reside in this forbidden gap region are particularly important, because they will require modifications of our ideal model of charge equilibration at semiconductor/liquid interfaces.

To understand Fermi level pinning, we need to reconsider the charge equilibration process when the semiconductor/liquid junction has a high density of surface states. As an example, we will consider a situation in which the surface states are half-filled when in equilibrium with a given solution and a semiconductor. The relevant question in this example concerns the change in V_{bi} when the solution redox potential is made more positive. In the ideal model, the required charge had to be transferred by removing electrons from dopant atoms further into the semiconductor (Fig. 10). As described above, this process requires increases in both W and V_{bi}.

However, due to the presence of occupied surface states, another source of charge is available in our nonideal example. If the charge required to equilibrate the junction is extracted from the surface states, and if the surface state density is sufficiently high to supply the required charges, then the junction can come to equilibrium without producing any change in V_{bi}. This can occur because no additional charges have been removed from the semiconductor. Instead, the additional charge was provided by the surface state levels. This situation is called Fermi level pinning. This terminology is used when the position of the semiconductor Fermi level is controlled by the occupancy of the surface states, as opposed to being controlled by the solution redox energy (43).

Quantitative calculations of the number of surface states that are needed to achieve Fermi level pinning will not be described here (84). However, such calculations show that even surface state densities as low as 1% of a monolayer (10^{13} states cm^{-2}) can provide sufficient charge to induce complete Fermi level pinning at semiconductor/liquid contacts (84). In other words, for a 1–2 V change in the solution redox potential, this density of surface states is sufficient that the value of W or V_{bi} will not change.

Lower surface state densities will, of course, produce less of a Fermi level pinning effect. This will result in an increased sensitivity of V_{bi} to changes in $E(A/A^-)$. In fact, a quantitative measure of the degree of ideality of a junction can be obtained by plotting changes in V_{bi} (or ϕ_b) as a function of changes in $E(A/A^-)$. When the slope of a plot of V_{bi} versus $E(A/A^-)$ is 1.0, the ideal situation is attained. When the slope of such plots is approximately equal to zero, complete Fermi level pinning is present. Intermediate situations, with

$0 < \text{slope} < 1.0$, or nonlinear behavior of V_{bi} versus $E(A/A^-)$, are often referred to as *partial Fermi level pinning*. All of these different situations have been observed experimentally (cf. Sections V.B.2 and V.B.4).

Fermi level pinning is generally an undesirable feature of semiconductor/liquid contacts. Its presence implies that there is a lack of chemical control over the electric field strength in the semiconductor. Only if the density of surface states is sufficiently low can the maximum possible electric field strength, and therefore the maximum possible charge separating ability, be attained for a given semiconductor/liquid contact. Some reports have appeared in the literature describing the preparations of semiconductor surfaces with acceptably low levels of deleterious surface states. In others, surface modification procedures have been explored with the aim of forming bonds to the defect states. Some of these examples are discussed in Section V. Such efforts are extremely important, as the problems of Fermi level pinning remain a key challenge to the chemist interested in manipulating the properties of photoelectrochemical cells.

IV. CHARGE TRANSFER AT A SEMICONDUCTOR/LIQUID JUNCTION

Up to this point, we have considered the charge flow that occurs to produce the equilibrium state between a semiconductor and a liquid. This type of charge flow is a prerequisite for the use of semiconductor/liquid junctions as energy conversion devices. This charge flow is not sufficient, however, to describe how photoelectrochemical cells store energy. To convert solar energy to electrical and/or chemical energy, a sustained, nonequilibrium current must flow across the semiconductor/liquid junction. Our goal in Section IV is to establish a framework for describing this current flow. We will then have all of the basic information necessary to understand the process of photoelectrochemical energy conversion.

A. Current–Voltage Behavior for a Semiconductor/Liquid Interface

A balanced chemical equation that represents the interfacial charge transfer at a semiconductor electrode is

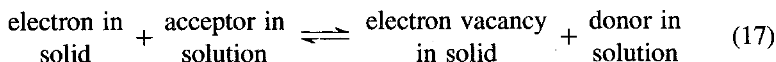

$$\begin{matrix}\text{electron in} \\ \text{solid}\end{matrix} + \begin{matrix}\text{acceptor in} \\ \text{solution}\end{matrix} \rightleftharpoons \begin{matrix}\text{electron vacancy} \\ \text{in solid}\end{matrix} + \begin{matrix}\text{donor in} \\ \text{solution}\end{matrix} \qquad (17)$$

In Eq. 17, the forward reaction represents the reduction of the acceptors in the solution, and the reverse reaction represents the oxidation reaction of the donors. The goal of Section IV.A is to use this equation, in combination with a

simple kinetic model, to obtain an expression for the current–voltage properties of a semiconductor electrode. We will use an n-type semiconductor as our example, although an analogous treatment can be readily performed for p-type semiconductors.

In any chemical system, no net formation of products or net destruction of reactants occurs at equilibrium. There is, however, always some rate of conversion of an individual set of reactant molecules into a set of product molecules, and vice versa. At equilibrium, these rates cancel each other exactly. An analogous situation holds for charge transfer at a semiconductor/liquid interface: at equilibrium, the rate of electrons flowing from the semiconductor into the solution must exactly equal the rate at which electrons flow into the semiconductor from the solution (Fig. 15). Away from equilibrium, the rate constants for these processes will remain fixed for the interface of interest. However, the concentrations of the reactants and products will differ from their equilibrium values, and a net current can therefore be sustained through the interface. Our strategy in describing current flow is to describe the currents at equilibrium in accord with Eq. 17, and then to modify this treatment to include nonequilibrium conditions.

1. Charge Transfer at Equilibrium

The simplest model of electron transfer across a semiconductor/liquid interface assumes that bimolecular kinetics can be applied to the charge-transfer reaction. In this model, the current depends linearly on the concentration of electrons near the semiconductor surface (n_s) and on the concentration of ac-

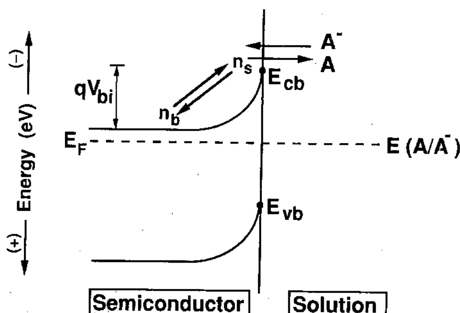

Figure 15. An energy diagram of the equilibrium charge-transfer process at a semiconductor/liquid interface. The surface concentration of electrons (n_s) is determined by the concentration of electrons in the bulk (n_b) and the built-in voltage at equilibrium (V_{bi}). The forward reaction represents the reduction of the acceptors (A) in the solution through the transfer of electrons from the semiconductor surface to the solution. The reverse reaction represents the oxidation of the donors (A^-) in solution by the injection of electrons into the semiconductor conduction band. At equilibrium, the forward rate equals the reverse rate and no net current flows across the interface.

ceptor ions that are available to capture charges at the semiconductor surface (Fig. 15). This assumption is reasonable, provided that the concentration of either electrons or acceptors is not so high that the reaction order saturates and the rate becomes independent of the concentration of either reactant.

In a solution containing a redox couple A/A^-, the rate of direct electron transfer from an n-type semiconductor to the acceptor species (A) can therefore be expressed as

$$\text{rate of electron injection into the solution} = k_{et} n_s [A]_s \tag{18}$$

where k_{et} is the rate constant for the electron transfer and $[A]_s$ is the concentration of acceptors at the surface of the semiconductor. The units of k_{et} are $cm^4\ s^{-1}$, because the rate of charge flow represents a flux of charges crossing the interface, with units of $cm^{-2}\ s^{-1}$, and the concentrations n_s and $[A]_s$ are expressed in units of cm^{-3}. Referring to Eq. 17, this expression represents the rate law for the forward chemical rate, that is, it represents the rate of formation of products for the chemical reaction in Eq. 17.

There also must be a current in the opposite direction that opposes this forward rate, that is, electrons must also be able to leave the redox donors (A^-) and enter the semiconductor conduction band. Because the electrons enter the empty states of the solid, the concentration of these empty states can be taken as a constant. This leads to the expression

$$\text{rate of electron transfer from the solution} = k_{et}^{-1}\ [A^-]_s \tag{19}$$

In Eq. 19, k_{et}^{-1} is the reverse reaction rate constant, and $[A^-]_s$ is the concentration of the donors at the electrode surface. The concentration of states in the semiconductor has been incorporated into the value of k_{et}^{-1}. This rate will be called the reverse rate, because it represents the formation of the species on the left-hand side of the reaction represented in Eq. 17.

At equilibrium, these rates must be equal to each other. Denoting the equilibrium electron concentration at the semiconductor surface by the quantity n_{so}, we then obtain

$$k_{et} n_{so}\ [A]_s = k_{et}^{-1} [A^-]_s \tag{20}$$

This equality can now be used to describe the rate of charge transfer both at, and away from, equilibrium. The net rate of electron transfer into solution $(-dn/dt)$ is always simply the forward rate minus the reverse rate. From Eqs. 18–20, we then obtain the general relationship

$$-\frac{dn}{dt} = k_{et}\ [A]_s\ n_s - k_{et}^{-1}\ [A^-]_s \tag{21}$$

or

$$-\frac{dn}{dt} = k_{et}\,[A]_s\,(n_s - n_{so}) \tag{22}$$

Equations 21 and 22 were obtained merely by treating charge transfer across a semiconductor/liquid interface as we would treat any other simple chemical kinetics problem. It states that the net rate at which charge crosses the semiconductor/liquid interface is the rate of product formation minus the rate of reactant formation. Although Eq. 22 is exactly equivalent to Eq. 21, the form that we have adopted for Eq. 22 will be extremely useful in deriving concise expressions for the current–voltage relationship of a semiconductor photoelectrode. This results because Eq. 22 expresses the net rate of charge transfer relative to the situation at equilibrium, where no current flows across the interface. According to Eq. 22, $-dn/dt = 0$ at equilibrium (as must be the case, because $n_s = n_{so}$ by definition). Away from equilibrium, $n_s \neq n_{so}$, so charge will cross the interface, and thus $-dn/dt \neq 0$.

2. *The Dark Current–Voltage Characteristics of a Junction*

It is now a simple task to describe the interfacial current using Eq. 22. Since the current is merely the electron-transfer rate multiplied by the charge on an electron and by the area of the electrode (A), the interfacial electron-transfer current can be written

$$I = -qA\left(-\frac{dn}{dt}\right) = -C(n_s - n_{so}) \tag{23}$$

where the constant C equals $qAk_{et}\,[A]_s$.

In this notation, the current I is defined to be negative when a reduction occurs at the electrode surface. Therefore, when $n_s > n_{so}$, a negative (reduction) current will flow, because the electrode will tend to donate electrons to the solution. Likewise, when $n_s < n_{so}$, a positive (oxidation) current will flow, because the solution will donate electrons to the semiconductor. A useful form of this equation is

$$I = -Cn_{so}\left(\frac{n_s}{n_{so}} - 1\right) \tag{24}$$

Neither of these two last equations are sufficient to describe explicitly the current–voltage properties of a semiconductor/liquid interface. For example, in Eq. 24, the voltage dependence is implicit in the ratio n_s/n_{so}. To obtain this

voltage dependence explicitly, we need to remember that the electron concentration at the surface of a semiconductor is related to the electron concentration in the bulk. As given in Eq. 16, the surface electron concentration at equilibrium is given by

$$n_{so} = n_b \exp\left(-\frac{qV_{bi}}{kT}\right) \tag{25}$$

Similarly, when a voltage V is applied to the semiconductor, the total voltage drop in the semiconductor depletion region is $V_{bi} + V$, so we obtain an analogous Boltzmann relationship away from equilibrium

$$n_s = n_b \exp\left[-\frac{q(V_{bi} + V)}{kT}\right] \tag{26}$$

These equations represent the physical situation that the electron concentration at the semiconductor surface can be either increased or decreased through the use of an additional voltage. This applied voltage controls the surface carrier concentration in the same fashion as the built-in voltage, so the same Boltzmann relationship applies.

These Boltzmann relationships (Eqs. 25 and 26) lead to a simple expression for the variation in the surface electron concentration as a function of the applied voltage (Eq. 27).

$$\frac{n_s}{n_{so}} = \exp\left(-\frac{qV}{kT}\right) \tag{27}$$

This makes sense, because any change in the voltage dropped across the solid should exponentially change the electron concentration at the semiconductor surface relative to its value at equilibrium.

Substituting Eq. 27 into Eq. 24, we obtain the desired relationship between the current and the voltage of a semiconductor/liquid junction.

$$I = -Cn_{so}\left[\exp\left(-\frac{qV}{kT}\right) - 1\right] \tag{28}$$

This equation is merely the simple rate equation, Eq. 24, which has been rewritten to emphasize the explicit dependence of the current on V.

We are now in a position to examine the properties of the current–voltage (I–V) behavior of a semiconductor electrode in detail. Equation 28 predicts that the current is exponentially dependent on the voltage for $V < 0$, but is essen-

tially independent of voltage, and of opposite sign, when $V > 0$. This prediction can be understood qualitatively by reference to the elementary rate processes that are described by from Eqs. 21 and 22. The net current across the solid/liquid interface is always given by the difference of the forward and reverse interfacial charge-transfer rates, that is, by the rate of the reaction going to the right minus the rate going to the left, as written in Eq. 21. For voltages that reduce the surface electron concentration below its equilibrium value, LeChatelier's principle implies that the reaction should proceed to the left as written in Eq. 17. Physically, a value of $V > 0$ will yield a larger electric potential drop in the semiconductor, which will exponentially reduce the surface concentration of electrons. This lower surface electron concentration will reduce the rate of electrons leaving the semiconductor (Fig. 16*a*). However, the rate of electrons entering the semiconductor, that is, the rate of reactant formation, will remain unchanged. Therefore, for this direction of voltage change, the net current will be independent of voltage. This direction of the applied voltage is called *reverse bias*. In reverse bias, the reaction proceeds to the left

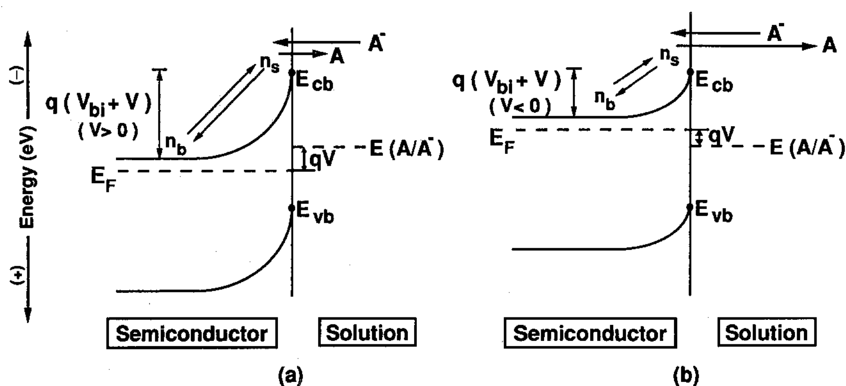

Figure 16. An energy diagram of the equilibrium charge-transfer process at an n-type semiconductor/liquid interface when an external potential (V) is applied to the semiconductor electrode. This potential will change the electric potential difference between the semiconductor surface and the bulk region; therefore, the concentration of electrons at the surface of the semiconductor will change. The equilibrium situation is perturbed and a net current will flow across the semiconductor/liquid interface. The forward reaction represents the reduction of the acceptors (A) in the solution through the transfer of electrons from the semiconductor surface to the solution. The reverse reaction represents the oxidation of the donors (A^-) in solution by the injection of electrons into the semiconductor conduction band. The reverse bias condition for an n-type semiconductor (i.e., where $V > 0$) can be seen in (*a*). The forward reaction rate is reduced relative to its equilibrium value, while the reverse reaction rate remains constant. A net oxidation current exists at the electrode surface. The forward bias condition (i.e., where $V < 0$) can be seen in (*b*). The forward reaction rate has increased compared to its equilibrium value, while the reverse reaction rate remains unaffected. A net reduction current exists at the electrode surface.

as written in Eq. 17, and electrons are injected into the semiconductor from the solution.

For voltages that increase the surface electron concentration above its equilibrium value ($V < 0$), the sign of the current will be opposite to that of the current obtained at reverse bias. In this situation, more electrons will be leaving the solid than entering it. LeChatelier's principle now implies that the reaction will go to the right as written in Eq. 17, so there will be a net transfer of electrons to acceptors in the solution phase. Through the Boltzmann relationship, in *forward bias* ($V < 0$ for our n-type semiconductor example) the surface concentration of electrons increases exponentially with increased bias. This increased concentration of reactants results in an exponential increase in the forward rate of interfacial charge transfer, but has no effect on the reverse rate of charge transfer (Fig. 16*b*). Because the rate of electrons leaving the solid at high forward bias dominates the rate at which they enter it, the net current will depend exponentially on the applied voltage (specifically, when $\exp(-qV/kT) >> 1$), as indicated by Eq. 28.

Equation 28 is often written with only one constant, as follows

$$I = -I_0 \left[\exp\left(-\frac{qV}{kT} \right) - 1 \right] \tag{29}$$

where $I_0 = Cn_{so}$. The parameter I_0 is called the exchange current, because it is the value of the current that is present at equilibrium. The parameter I_0 is responsible for transforming reactants into products, and vice versa, at a semiconductor/liquid interface at equilibrium. For convenience, I_0 is defined as a positive quantity. The parameter I_0 is clearly dependent on the value of the equilibrium surface electron concentration, because a smaller exchange current should flow at equilibrium if there are fewer electrons available to exchange with a particular solution.

The current–voltage characteristic described by Eqs. 28 and 29, where the current can flow predominately in only one direction under an applied potential, is called *rectification*. The rectification characteristic is typical of electrical diodes. Equations that have the form of Eqs. 28 and 29 are therefore generally called *diode equations*. We have shown that a semiconductor/liquid interface is expected to obey the diode equation when interfacial electron transfer is the rate determining step for charge movement. In this situation, the applied voltage changes the electron concentration at the surface of the semiconductor, and this is directly reflected in the current versus voltage relationship of a semiconductor/liquid interface (Fig. 17). This behavior is a direct result of the Boltzmann relationships of Eqs. 25 and 26. This diode I–V behavior would not have occurred for metal electrodes or other surfaces where the surface electron concentration is independent of the applied voltage.

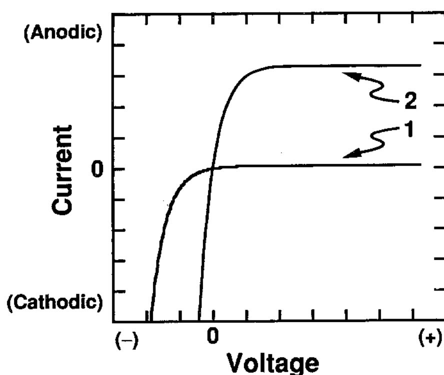

Figure 17. The current–voltage (I–V) behavior of an n-type semiconductor/liquid junction in the dark. The shape of the I–V curve is described by the diode equation (Eq. 29); thus, such a curve is referred to as a diode curve. The difference between curves 1 and 2 is that the equilibrium exchange current I_0 is greater for curve 2.

Up to this point, there has been no explicit discussion of the role of the liquid phase in the current–voltage behavior. Obviously, changing the concentrations of acceptors and/or donors will affect the interfacial current, as expressed in the Eqs. 18–22. These variations in initial conditions should therefore change the value of I_0. Another important role of the liquid phase is in the determination of the equilibrium value of the Fermi level. As described in Section III.A, after charge equilibration at a semiconductor/liquid interface, $\mathbf{E}_F$ will equal $\mathbf{E}(A/A^-)$. The position of $\mathbf{E}_F$ at equilibrium will affect V_{bi} (Fig. 12), which will, in turn, determine n_{so} through the Boltzmann relationship of Eq. 25.

Physically, a more positive solution redox potential will produce a larger built-in voltage at an n-type semiconductor/liquid interface (Figs. 10 and 12). This increased band bending will decrease the equilibrium electron concentration at the surface (n_{so}), and will lead to a smaller exchange current for this semiconductor/liquid junction. The dependence of the current on n_{so} is an important property of the current–voltage relationship of a semiconductor/liquid interface.

In fact, this dependence of the charge-transfer rate on the solution redox potential is perhaps the most important experimental property of semiconductor electrodes. Regardless of the value of the redox potential of the solution ($E(A/A^-)$), the diode behavior of Eq. 29 will be obeyed. Changes in $E(A/A^-)$, however, will produce different values of I_0, because I_0 depends on n_{so}. These different exchange currents will produce a measurable change in the I–V behavior of the semiconductor/liquid contacts.

For an n-type semiconductor, more positive redox potentials will yield smaller values of I_0, and will produce highly rectifying diode behavior. In contrast, more negative redox potentials will yield larger values of I_0, and will produce poorly rectifying diode behavior (Fig. 17). For p-type semiconductors,

the opposite behavior is expected. Negative redox potentials should produce highly rectifying contacts, while positive redox potentials should produce poorly rectifying contacts. In Section IV.B, we will see that rectifying I–V behavior is required for efficient photoelectrochemical devices that use either n-type or p-type semiconductors. Thus, one goal in constructing semiconductor/liquid junctions is to insure that chemical control is maintained over the I–V properties of semiconductor/liquid junctions. Changes in the solution redox potential are therefore one of the most important methods of manipulating the I–V properties of semiconductor/liquid interfaces.

The equilibrium exchange current (I_0) cannot only be broken down into a constant multiplied by the value of n_{so}, but can also be broken down further. The parameter I_0 contains the intrinsic electron-transfer rate constant (k_{et}). The electron-transfer rate constant is a very important parameter in the kinetics of electron transfer at a semiconductor/liquid junction, and k_{et} appears in most of the equations that utilize kinetic models for I_0. Although we have not described k_{et} in detail, theoretical expressions for k_{et} have been derived by Morrison (83) and by Gerischer (86, 87). These treatments have been reviewed extensively in the literature and are primarily based on the Marcus theory for electron transfer at metal electrodes (88, 89).

The value of k_{et} is one of the elusive experimental parameters of a semiconductor/liquid interface, and little definitive work is available to allow comparison between theory and experiment for this parameter (30, 90). Fortunately, we will not need to calculate or determine k_{et} precisely in order to evaluate the energy conversion properties of most photoelectrochemical cells. Thus, for the remainder of our discussion, we will treat k_{et} as a known experimental parameter of a given semiconductor/liquid junction, much as rate constants for chemical reactions can, at some level, be understood without comparison to theoretical calculations of transition state energies. The value of I_0 will be of primary interest to us, as will its dependence on the solution redox potential.

Although we have derived the diode behavior of a semiconductor/liquid junction by assuming that electron transfer is the important charge flow process across the interface, the diode equation is generally applicable to semiconductor/liquid devices even when other processes are rate limiting. A similar derivation can be performed for other possible charge flow mechanisms, such as recombination of carriers at the surface and/or in the bulk of the semiconductor. It can be shown that the I–V relationships for these mechanisms almost all adopt the form of Eq. 29 (45). The major difference between the various mechanisms is the value of I_0 for each system. Mechanistic studies of semiconductor/liquid junctions therefore reduce generally to investigations of the factors that control I_0. Such studies also involve quantitative comparisons of the magnitude of I_0 with the value expected for a specific charge transport mechanism. These types

of investigations have yielded a detailed level of understanding of many semiconductor/liquid interfaces. Recent reviews, describing more details of this work, have been written by Koval and Howard (30) and by Lewis (90).

B. Current–Voltage Characteristics of a Semiconductor Electrode Under Illumination

1. Basic I–V Equations for Illuminated Semiconductor/Liquid Junctions

We have now described the electron-transfer processes at a semiconductor/liquid interface under equilibrium and nonequilibrium conditions. For energy conversion applications, the last major effect to consider is the role of light-generated charge carriers. Fortunately, the effects of illumination are relatively simple to incorporate into our I–V treatment. This final step in understanding the I–V behavior of semiconductor/liquid junctions is the topic of Section IV.B.1.

To accomplish this task, it is convenient to partition the current into two separate components: one that originates from majority carriers and one from minority carriers. Absorption of photons creates both majority carriers and minority carriers; therefore, an increase in each of the two current components is expected under illumination.

We will first address light-induced changes in the majority carrier current. The key point is that the concentration of majority carriers generated by absorption of sunlight is usually small compared to that present from the thermal ionization of dopant atoms. This implies that illumination does not significantly perturb the majority carrier behavior either in the semiconductor or at the semiconductor/liquid interface. Because the majority carrier concentrations are essentially unchanged, the rate equations that govern majority carrier charge flow also are unchanged. Majority carriers should thus exhibit an I–V characteristic that is well described by the diode equation, regardless of whether the semiconductor is in the dark or is exposed to moderate levels of illumination.

The remaining goal is to obtain a description of the minority carrier component of the photocurrent at a semiconductor electrode. As mentioned in Section II.B.3.b, unlike the situation for majority carriers, illumination generally effects a substantial change in the concentration of minority carriers. Calculation of the minority carrier current is greatly simplified by the presence of the electric field at the semiconductor/liquid junction. As pointed out in the introduction, the electric field in a semiconductor separates the photogenerated minority carriers from the photogenerated majority carriers. This field also drives the minority carriers towards the solid/liquid interface. For most semiconductor/liquid junctions in depletion, the electric field is so strong that essentially all of the photogenerated minority carriers are separated and then collected.

Using this approximation, the photogenerated minority carrier current I_{ph} is simply equal to the photon flux absorbed by the semiconductor multiplied by the charge on an electron q.

The current–voltage characteristics of an illuminated semiconductor electrode can now be obtained by adding together, with the appropriate sign, the majority and minority carrier components of the current. The majority carrier current obeys the diode equation, while the minority carrier photocurrent is related to the absorbed light intensity.

$$I = I_{ph} - I_0\left[\exp\left(-\frac{qV}{kT}\right) - 1\right] \tag{30}$$

The sign of the minority carrier current (photocurrent) is opposite to that of the majority carrier current, because holes crossing the interface lead to an oxidation current, while electrons crossing the interface lead to a reduction current. Equation 30 is obviously just the diode curve of Eq. 29, offset by a constant amount I_{ph} over the voltage range of interest (Fig. 18).

2. *Energy Conversion Properties*

This simple I–V relationship (Eq. 30) is our general description of the photocurrent–voltage properties of a semiconductor/liquid interface. It is useful in understanding essentially all of the experimental behavior of a photoelectrode, and is essential in quantifying the energy conversion properties of a photoelectrochemical cell. In the introduction, we mentioned that there were three properties of a photoelectrochemical cell that were relevant to energy conversion

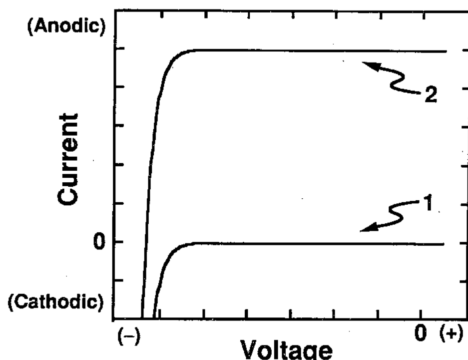

Figure 18. The current-voltage (I–V) behavior of a semiconductor/liquid junction, both in the dark (1) and under illumination (2). The light curve is offset by a constant amount, namely, the photocurrent (I_{ph}), from the dark curve.

applications: the open circuit voltage, the short circuit current, and the fill factor. Now that we have developed Eq. 30, these important quantities can be understood in a simple, quantitative fashion.

We first examine the open circuit voltage, V_{oc}. This voltage represents the maximum free energy that can be extracted from an illuminated semiconductor/liquid interface. Note that for $I_{ph} > I_0$, as is generally the case, the "1" in Eq. 30 can be neglected. We then obtain

$$I \cong I_{ph} - I_0 \exp\left(-\frac{qV}{kT}\right) \tag{31}$$

By definition, at open circuit, the net current I is zero. We then define $V_{oc} \equiv |V\,(\text{at } I = 0)|$, and obtain

$$V_{oc} = \frac{kT}{q} \ln\left(\frac{I_{ph}}{I_0}\right) \tag{32}$$

This equation brings out several important features of the open circuit voltage. First, V_{oc} increases logarithmically with the light intensity, because I_{ph} is linearly proportional to the absorbed photon flux. Second, the open circuit voltage of a system increases (logarithmically) as I_0 decreases. Chemically, such behavior is reasonable, because I_0 represents the tendency for the system to return to charge-transfer equilibrium. Smaller values of I_0 imply a slower rate of interfacial equilibration, so it is easier to obtain a large photovoltage with a small value of I_0. Third, Eq. 32 emphasizes that a mechanistic understanding of I_0 is crucial to controlling V_{oc}. Only through changes in I_0 can systematic, chemical control of V_{oc} be established for different types of semiconductor/liquid junctions.

The second quantity of concern for energy conversion applications is the *short circuit current density* (J_{sc}). Short circuit conditions imply $V = 0$. From Eq. 30, the net current at short circuit (I_{sc}) equals I_{ph}. The short circuit current density (J_{sc}) is simply I_{ph}/A, where A is the projected area of the electrode. The short circuit current density provides a measure of the collection efficiency of photogenerated carriers in a particular photoelectrochemical cell.

Several factors can influence the value of J_{sc}. Incident light may be absorbed by the solution, or it might be reflected at the various interfaces in the cell, or it may be absorbed by the semiconductor and then converted into photocurrent. Two quantities are often measured to describe the photocurrent collection efficiency of a semiconductor/liquid junction: the *internal quantum yield* and the *external quantum yield*. The *internal quantum yield* is the quantity familiar to chemists. It measures the yield of collected charges based on the number of photons that are actually absorbed by the photochemically active species, that

is, the semiconductor. The internal quantum yield for a semiconductor/liquid interface is simply J_{sc}/q divided by the flux of photons that is *absorbed* by the semiconductor. For many semiconductor/liquid junctions, recombination losses of minority carriers are negligible at short circuit, so the internal quantum yield approaches unity for photons of energy greater than $\mathbf{E}_g$.

The *external quantum yield* is J_{sc}/q divided by the flux of photons that is *incident* onto the photoelectrochemical cell. Due to reflective losses and optical transmission losses in any real system, the number of photons absorbed by the semiconductor is only a fraction of the total photons incident onto the cell. Thus, the external quantum yield is always less than the internal quantum yield. The external quantum yield obviously depends on the design of a specific photoelectrochemical cell, while the internal quantum yield depends only on the intrinsic photoelectrochemical properties of the semiconductor/liquid junction. Both quantities are valuable in assessing the photochemical response of an actual energy conversion system.

Quantum yields are sometimes called quantum efficiencies in the literature. Furthermore, to add to the confusion, quantum efficiencies are often quoted on a percentage scale, with a 0.3 quantum yield being considered synonymous with a 30% quantum efficiency. We strongly discourage the use of this latter terminology. To avoid any possibility of confusion between quantum yields and energy conversion efficiencies, quantum yields should be quoted on a scale of zero to unity.

To relate a quantum yield to an energy conversion efficiency, the energy stored in each collected charge carrier must be included into the calculation. No power is produced by a photoelectrochemical cell at either open circuit (V = 0) or short circuit (I = 0), because the power (P) equals IV. In general, however, the I–V characteristic of Eq. 31 results in nonzero power outputs for voltages between short circuit and open circuit. The point where the IV product is maximized is called the *maximum power point* [$(IV)_{max}$] of the photoelectrochemical cell (Fig. 2). For convenience, the maximum power is taken to be a positive quantity regardless of the actual sign of the photovoltage or photocurrent in any given convention. The maximum energy conversion efficiency of a semiconductor/liquid junction can then be expressed as

$$\text{Efficiency } \% = \frac{(IV)_{max}}{P_{in}} \times 100 \tag{33}$$

where P_{in} is the incident solar power on the semiconductor electrode.

The ratio of $(IV)_{max}$ divided by $I_{sc}V_{oc}$ is called the *fill factor* (f) of the cell. The fill factor quantifies how well the actual power curve fills the maximum possible rectangle (defined by I_{sc} and V_{oc}) for a particular semiconductor/liquid interface. The fill factor has a typical value of 0.7–0.8 for an I–V relationship described by Eq. 30 (9). Often, however, resistive losses or recombination losses

lower this value in actual operating systems. Another expression for the cell efficiency is therefore

$$\text{Efficiency } \% = \frac{(I_{sc} V_{oc}) f}{P_{in}} \times 100 \tag{34}$$

From Eq. 34, we realize that the energy conversion efficiencies of semiconductor/liquid junctions are functions of three factors: V_{oc}, I_{sc}, and f. The parameter I_{sc} can be maximized by reducing recombination losses of the carriers in the system. For systems with an internal quantum yield of 1, I_{sc} is limited by the number of photons in the solar spectrum that have energies greater than the semiconductor band gap. The parameter V_{oc} can be maximized by reducing the equilibrium exchange current (I_0). From Eqs. 23–26, I_0 can be reduced by increasing V_{bi} or by reducing the value of k_{et}. The fill factor can be maximized through reduction of cell resistance losses and of other recombination losses for the photogenerated carriers. Therefore, the choice of redox couples, solution electrolytes, and of semiconductors will be based on maximizing these three factors in order to obtain the maximum energy conversion efficiency from the system.

C. Photoelectrosynthetic and Photocatalytic Cells

In operation, the simplest type of photoelectrochemical cell is one that results in no net chemical change in the electrolyte, and only produces electrical power. These types of photoelectrochemical cells are called *regenerative cells*. As shown in Eqs. 33 and 34, efficiency measurements are straightforward for a regenerative cell: the overall energy conversion efficiency is simply the total maximum output electrical power divided by the total input solar power. In making such an efficiency measurement, the spectral distribution of the illumination source should be as close to the solar spectrum as possible. Otherwise, even if the laboratory source is adjusted to contain the same total integrated power as the terrestrial solar spectrum, substantial overestimates of the energy conversion efficiency can be introduced if the source provides more photons with energies greater than $\mathbf{E}_g$ than are contained in the solar spectrum.

Efficiency calculations are less straightforward for cells that produce chemical fuels. The first distinction to be made is whether the chemical transformation from reactants to products stores free energy in the fuels or releases it. When the molar Gibbs free energy for the chemical reaction in the cell is positive ($\Delta G > 0$), the system is called a *photoelectrosynthetic cell*. In this situation, light energy has been partially stored in the chemical conversion process. An example of a photoelectrosynthetic cell would be the n-$SrTiO_3$/H_2O/Pt cell (91), which can sustain the light-induced electrolysis of water to H_2(g) and

O_2(g). When $\Delta G < 0$ for the chemical reaction in the cell, the overall process will proceed spontaneously without illumination, and the presence of light then only acts to catalyze a thermodynamically favorable process. These types of cells are called *photocatalytic cells*. Photocatalytic cells do not lead to useful energy conversion devices, but can be of commercial interest when specific chemicals are formed as a result of photoelectrochemical operation (25).

Efficiency calculations for photoelectrosynthetic cells are less straightforward than those for regenerative cells (12). The most rigorous thermodynamic definition of the cell efficiency is obtained by dividing the sum of the output electrical power and the stored chemical energy by the total incident photon power (P_{in}).

$$\text{Efficiency } \% = \frac{\left(\Delta G \frac{d\xi}{dt} + IV_R\right)}{P_{in}} \times 100 \tag{35}$$

In this equation, $d\xi/dt$ is the amount of products produced in moles per unit time, V_R is the voltage drop at an external resistor (R), and I is the current flowing through the circuit. This calculation can be related to the efficiency calculation of a regenerative cell by realizing that $\Delta G = -n_e \mathfrak{F} E_{cell}$, where $\mathfrak{F}$ is Faraday's constant, and E_{cell} is the Nernstian potential difference between the oxidation and reduction half reactions in the system. For a regenerative cell $\Delta G = 0$, so Eq. 35 reduces to Eq. 33 for the proper choice of V_R.

The current (I) passing through the external circuit equals the number of charges passed during the reaction per unit time [$I = n_e \mathfrak{F}(d\xi/dt)$]. Therefore, Eq. 35 can also be expressed as

$$\text{Efficiency } \% = \frac{(-E_{cell} + V_R)I}{P_{in}} \times 100 \tag{36}$$

This form is extremely useful, because both the electrical power and stored free energy are treated with respect to their electrochemical potentials. Essentially, the production of chemical fuel can be considered as an added load to the regenerative cell, and the fuels therefore contain some of the energy that would otherwise be collected as electrical power in the external circuit.

In certain cells, the photogenerated electrons contribute some energy towards fuel production, but are not sufficient to provide the total energy necessary to drive the chemical reaction in the cell. An external electrical bias is then required to supply the remaining free energy in the system. Equation 36 can still be used in this case as well, except that the term V_R will be negative when electrical power must be supplied to the system.

Other definitions of efficiency are sometimes used in the literature, but they are not as fundamentally useful as the free energy expressions given in Eqs. 35 and 36. For instance, it is sometimes useful to consider the power available from the chemical fuels that have been produced photoelectrochemically. This fuel will eventually have to be converted back to the starting materials in order to extract energy from the photochemical system. Of course, these subsequent processes also have efficiency losses. Another definition of power conversion efficiency, therefore, is the power recoverable in an operating system divided by the total incident photon power on the semiconductor. This efficiency will always be lower than the maximum thermodynamic efficiency calculated from Eq. 35 or 36. One drawback of this definition is that different recovery systems will have their own inherent efficiencies. Therefore, the calculated efficiency will depend not only on the efficiency of the semiconductor/liquid junction, but also on the efficiency of the particular recovery system used. Using this definition, a poor recovery system will result in a low solar efficiency even if the semiconductor photoelectrode is highly efficient at storing energy. This recovery-based definition of efficiency would be quite useful in making comparisons between practical systems for design engineering and production purposes. However, it is not the best method for assessing the relative energy storing capabilities of semiconductor/liquid junctions.

We have now dealt with the fundamental principles of operating photoelectrochemical cells as energy conversion devices. With this background, it is now possible to evaluate the relative merits of different combinations of semiconductors and electrolytes, and to critically discuss trends in photoelectrochemical cell behavior for various experimental systems. Specific examples that have been chosen with a historical perspective are discussed in Section V.

V. STRATEGIES FOR THE DESIGN OF SEMICONDUCTOR/ LIQUID JUNCTIONS FOR ENERGY CONVERSION

In the remainder of this chapter, we will summarize the main experimental observations in the field of photoelectrochemical energy conversion. In many ways, the ideal photoelectrochemical cell would be one that utilizes a semiconductor in contact with an innocuous aqueous solution, operates indefinitely with high efficiency, and converts water into H_2(g) and O_2(g). Unfortunately, no such system yet exists. There are presently many obstacles that impede the development of such an energy conversion device, including the constraint placed on any system by the energy distribution of sunlight.

At present, a double paradox exists in this field. Some large band gap semiconductors, such as $SrTiO_3$, are stable in water and can sustain the unassisted photoelectrolysis of water to H_2(g) and O_2(g). The band gaps of such semicon-

ductors are so large, however, that these photoelectrochemical cells are not capable of providing high solar energy conversion efficiencies. As discussed earlier, semiconductors with band gaps of 1.1–1.7 eV are ideally suited for the efficient conversion of solar energy. However, semiconductors with these band gaps exhibit either facile corrosion or passivation processes in aqueous solutions. Thus, semiconductor materials that are inherently efficient for harvesting the energy from sunlight have, to date, been unable to provide stable photoelectrolytic devices, whereas large band gap semiconductors, which are stable under solar illumination, are inherently inefficient at harvesting the energy in the terrestrial solar spectrum. This key problem is not a thermodynamic limitation of the semiconductor. Rather, it is a kinetic stability issue which can, in principle, be overcome with proper choice of the material. This problem has not yet been solved despite over 15 years of work in this field, and remains as arguably the most important single challenge in the discipline.

To deal with this drawback several alternate strategies are being pursued to both understand and develop stable, efficient photoelectrochemical cells. One method is to search for redox reagents that can kinetically compete with photocorrosion and photopassivation processes. Such reagents, when present in an aqueous electrolyte in sufficient concentration, can minimize electrode corrosion. This method might enable the construction of stable, efficient photoelectrochemical energy conversion devices from small band gap semiconductors. Because the reaction products of the stabilizing reagents are not usually in themselves useful fuels, the solution reagents must be recycled in the cell. These types of cells are therefore constrained to provide only electrical power.

Another approach is to remove the corrosive liquid entirely and to use nonaqueous solutions as the electrolytes. This strategy also results in cells that can only provide electrical power. It does have experimental advantages, because a wide variety of semiconductors, liquids, and redox couples provide stable cell operation. Recent work has shown that these systems can display relatively high energy conversion efficiencies. These types of cells also allow detailed comparison to theoretical expectations for the current–voltage behavior of semiconductor/liquid interfaces. Nonaqueous-based semiconductor/liquid junctions are thus very useful in exploring the fundamental principles of semiconductor/liquid interfaces as energy storage systems.

A third approach is to modify the surfaces of semiconductors. The primary goal of this approach is to improve photoelectrode stability in aqueous electrolytes. The surface modification can either be designed to increase the rate of charge transfer to the redox species, or to decrease the rate of surface passivation. Both outer- and inner-sphere coordination to the surface have been shown to be effective in achieving improved electrode stability. The surface coordination chemistry of these inorganic materials often has direct analogies to the coordination chemistry of transition metal complexes, and the chemistry of mo-

lecular species often serves as a guide to new developments in this area. This approach also has the advantage that molecular-based catalysts for fuel-forming reactions can, in principle, be attached to the appropriate semiconductor surface. This type of attachment could simultaneously induce electrode stability, efficient solar energy conversion, and effective fuel formation from aqueous-based semiconductor/liquid junctions.

The fourth general line of attack is to coat the surface of large band gap semiconductors with dyes. The purpose of the dye is to extend the wavelength response of the semiconductor into the visible region of the solar spectrum. In this scheme, the dye acts as the initial light absorber, and it creates the initial excited state of the system. The interfacial electric field at the semiconductor/liquid interface then acts to separate the charge. Unfortunately, most dye photosensitization schemes exhibit low energy conversion efficiencies. Monolayers of dyes often have high internal quantum yields for photocurrent production, but a monolayer of dye does not generally absorb a significant fraction of the incident light. Thus, the external quantum yields of these systems, based on the photon flux input into the device, are generally relatively low. Increased thicknesses of dye can lead to increased light absorption, but charge separation is usually not effective in dye molecules that are removed spatially from the semiconductor/dye interface. A significant finding in this area is a recent report of solar energy conversion efficiencies of 7% using very rough, high-surface–area, dye-coated TiO_2 electrodes (92). This finding has produced new excitement concerning the potential usefulness of dye sensitization as a practical energy conversion method. It has also induced a reinvestigation of the properties of metal oxides as useful materials in semiconductor/liquid junctions.

In Section V, we will deal with each strategy separately. We will attempt to maintain some historical perspective on the developments in the field, and will deal with the topics roughly in order of their emphasis in the literature. First, we will examine efforts to use large band gap semiconductors to perform the unassisted photoelectrolysis of water. Then we will describe attempts to stabilize small band gap semiconductors in aqueous solutions. This topic will be followed by a discussion of the use of nonaqueous solvents for photoelectrochemical energy conversion, which will provide a natural link to a discussion of chemical modification of semiconductor surfaces. Finally, we will review current efforts to exploit dye sensitization in photoelectrochemical energy conversion.

A. Photoelectrochemical Cells Employing Large Band Gap Semiconductors

Although the properties of semiconductor electrodes have been carefully studied since 1955, with notable contributions by Gerischer (93), Memming

(94), Morrison (83), and others (95–98), perhaps the single most important contribution to the area was the report by Fujishima and Honda in 1971 (99). In this paper, these researchers described the successful electrolysis of water upon illumination of a rutile TiO_2 electrode (99, 100). The use of a rutile TiO_2 electrode in the electrolysis of water had previously been reported by Boddy (101); however, Fujishima and Honda were the first to report the possible application of light-assisted water electrolysis to solar energy conversion (98). Given the energy crisis of the early 1970s, and the advances in solid state physics, semiconductor technology, and photovoltaic technology during the 1960s and 1970s, Fujishima and Honda's recognition of this potential use of semiconductor/liquid junctions created a huge surge of interest in the use of semiconductor/liquid interfaces for energy conversion.

In their experiment, Fujishima and Honda used a single-crystal TiO_2 anode in contact with a buffered, pH 4.7 aqueous solution (99, 100). They observed that the anode evolved dioxygen upon illumination with light of energy $h\nu > \mathbf{E}_g$ for TiO_2. They also reported that current flowed through an external resistive load that was connected between the TiO_2 anode and a Pt counter electrode. Thus, Fujishima and Honda concluded that they had converted energy from the light into stored energy, specifically into chemical fuels in the form of H_2(g) and O_2(g) (cf. Fig. 1). The H_2(g) could, in principle, be burned or used in a fuel cell at a later date to supply energy on demand. The complete process might then provide a path to an abundant, clean, transportable energy source. These results spurred immediate interest in examining the properties of TiO_2/liquid junctions, and in extending this behavior to other semiconductor materials.

Further work confirmed that TiO_2 was stable in aqueous solution and oxidized water to O_2(g), as claimed by Fujishima and Honda. However, the current flowing through the circuit probably did not effect the reduction of H_2O to H_2(g). It is now believed that this current simply resulted in the reduction of impurities in solution (102) or in the reduction of O_2(g) at the Pt electrode (103, 104). Attempts to induce TiO_2 electrodes to produce significant amounts of H_2(g) under standard (1 atm) conditions (with no added electrical bias) have generally failed, and such behavior is now understood to result from the unfavorable positions of the band edges of rutile TiO_2 (81).

Of course, the use of conventional metal electrodes to electrolyze water according to Eq. 37 requires at least 1.23 V under standard conditions.

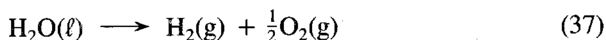

$$H_2O(\ell) \longrightarrow H_2(g) + \tfrac{1}{2}O_2(g) \tag{37}$$

Although the band gap of rutile TiO_2 (3.0 eV) provides a greater amount of energy than the 1.23 eV required to split water under standard conditions, the positions of the band edges at TiO_2/H_2O interfaces are not optimally situated for the H_2O photoelectrolytic process. The position of the valence band edge is

more positive than the O_2/H_2O electrochemical potential, so there is a large driving force for the oxidation of H_2O to O_2 using photogenerated holes. The ejected electrons do not, however, have a sufficiently negative electrochemical potential to reduce H_2O to $H_2(g)$. Despite the fact that TiO_2 anodes do not actually lead to the unassisted "water splitting," or photoelectrolysis, reaction, these early experiments of Fujishima and Honda were extremely important, because they demonstrated that TiO_2 was a stable material that could be used to produce $O_2(g)$. Furthermore, it has been confirmed that TiO_2 anodes do store energy, in that they can promote the assisted photoelectrolysis of H_2O. In other words, even though 1.23 V is the minimum voltage that is required in a conventional electrolytic apparatus to sustain the electrolysis of H_2O [under 1 atm of $H_2(g)$ and $O_2(g)$], when TiO_2 anodes are used, some of this voltage can be obtained from the incident light. Therefore, applied voltages of less than 1.23 V are sufficient to effect the same chemical transformation in a TiO_2/Pt photoelectrolytic cell (99, 100) (cf. Section IV.C).

An obvious approach to producing a better match between the H_2O/H_2 electrochemical potential and the energy of electrons in the TiO_2 conduction band is to change the pH of the solution. The Nernst equation indicates that the H_2O/H_2 potential will shift negative by 59 mV per increased pH unit, so the use of basic solutions should produce a larger driving force for reduction of H_2O by electrons in the conduction band of TiO_2. Unfortunately, changes in pH do not significantly affect the energetics of H_2O photoelectrolysis for TiO_2/H_2O junctions. Instead, the pH affects the composition of $Ti{-}O^-$ and Ti—OH groups that exist on the surface of TiO_2. These surface groups undergo an acid–base equilibrium, with basic solutions leading to deprotonation of surface hydroxyl groups. It can be shown that the electric potential energy due to this change in the surface charge exactly offsets any pH-induced change in the electrochemical potential of the H_2/H_2O system; thus, the energetics for production of H_2 by photogenerated electrons in TiO_2 remain unfavorable at all pH values (54).

The failure of rutile TiO_2 to reproducibly sustain the unassisted photoelectrolysis of H_2O prompted the investigation of other metal oxide semiconductors for this purpose. Both $SrTiO_3$ (91) and $BaTiO_3$ (105, 106), among others (98), provided examples of materials that effected the stable, unassisted photoelectrolysis of H_2O. The band gap of $SrTiO_3$ (3.2 eV) is not significantly larger than that of rutile TiO_2 (3.0 eV), but the band edge positions for $SrTiO_3$ are more favorably located for the photoelectrolysis of H_2O. As shown in Fig. 13, $\mathbf{E}_{cb}$ for $SrTiO_3$ is more negative than $\mathbf{E}(H_2O/H_2)$, while $\mathbf{E}_{vb}$ is much more positive than $\mathbf{E}(O_2/H_2O)$.

As noted in the introduction to Section V, the main drawback of the $SrTiO_3$ system is its inefficient use of the solar spectrum. The $SrTiO_3/H_2O$ junction is relatively efficient at converting absorbed photon energy into stored chemical energy; in fact, the calculated efficiency of the $SrTiO_3/H_2O$/Pt cell for 3.76 eV

(330 nm) photons is approximately 20% (91). The overall solar energy conversion efficiency, however, can be calculated to be less than 1% for $SrTiO_3$/H_2O–KOH junctions, because of the low percentage of photons in the solar spectrum that are absorbed by the $SrTiO_3$ electrode.

The solar energy conversion limitations of $SrTiO_3$ underscore the need to use smaller band gap materials in the photoelectrolysis of H_2O. Unfortunately, no small band gap metal oxide electrode investigated to date has been reported to effect the unassisted photoelectrolysis of H_2O. Studies of a number of metal oxide photoanodes have shown that the valence band edge energies are roughly constant in these materials (52). This general trend has been rationalized because the valence band in metal oxides is generally oxygen 2*p* in character (52) (cf. Section II.B.1). Thus, changes in the band gap primarily reflect changes in the position of the conduction band edge (52), as predicted by the common anion rule (cf. Section II.B.1). This situation is unfortunate, because it implies that smaller band gap metal oxides, which provide enhanced wavelength response to the solar spectrum, will not be thermodynamically capable of sustaining the reduction of H_2O to H_2(g) under standard conditions. For example, Fe_2O_3 has a band gap energy of 2.2 eV, which is one of the smallest band gap energies for any metal oxide that has been used as a photoanode. Although Fe_2O_3 is stable in aqueous solutions under some conditions, its conduction band edge is greater than 0.5 V more positive than the potential required for H_2(g) evolution at 1 atm and 298 K (107). Unless a new class of metal oxides with different band edge positions is developed, this drawback will remain a major hurdle for the exploitation of metal oxides in the photoelectrolysis of water.

A related problem with the metal oxides is that their valence band energies are too positive relative to the O_2/H_2O electrochemical potential. A large change in potential energy occurs when holes are transferred from the top of the semiconductor valence band to produce O_2(g); therefore, this process results in a waste of free energy for the system as a whole. The most efficient semiconductor for the electrolysis of H_2O would be one in which the band gap straddled both electrochemical potentials necessary to electrolyze water, $E(O_2/H_2O)$ and $E(H_2O/H_2)$. This constraint places a minimum of 1.23 eV on the band gap energy for a semiconductor to be used in H_2O photoelectrolysis. Although only 1.23 eV is necessary to drive the electrolysis of H_2O under standard conditions, any real system must provide a higher amount of free energy in order to store fuels under such conditions. This excess energy is required to maintain some band bending in the semiconductor, which will maintain favorable charge separation at the semiconductor/liquid interface (54, 91). In addition, cell resistances and kinetic requirements must be overcome in any operating electrolytic cell (54, 91). It has been calculated that a band gap of 2.0–2.6 eV is necessary to overcome these kinetic requirements in a practical system (108). The efficiency of an ideal photoelectrochemical cell with a band gap of 2.0 eV would

only be about 17% [calculated from (68)], due to poor overlap with the solar spectrum and wasted energy relative to the fuel content of the $H_2(g)$ and $O_2(g)$ that are produced. These restrictions, combined with the general lack of control over the valence band edge energies in the metal oxides, have led researchers to pursue alternative strategies to exploit metal oxide electrodes in photoelectrolytic reactions.

Several investigators have attempted to create a *false valence band* by using high concentrations of dopant ions in TiO_2 and $SrTiO_3$ (32). The goal of this approach is to extend the wavelength response of large band gap semiconductors, while also maintaining some of the favorable stability properties of these materials. If one can introduce a sufficient concentration of dopants into the crystal lattice, then a new set of delocalized MOs will be produced. This new set of orbitals can result in a new valence band, which might be at a more negative energy (i.e., closer to the vacuum level) than the one arising from the original lattice constituents of the solid (Fig. 19). Control over the dopant could, in principle, offer some control over the energy of the valence band (32). The

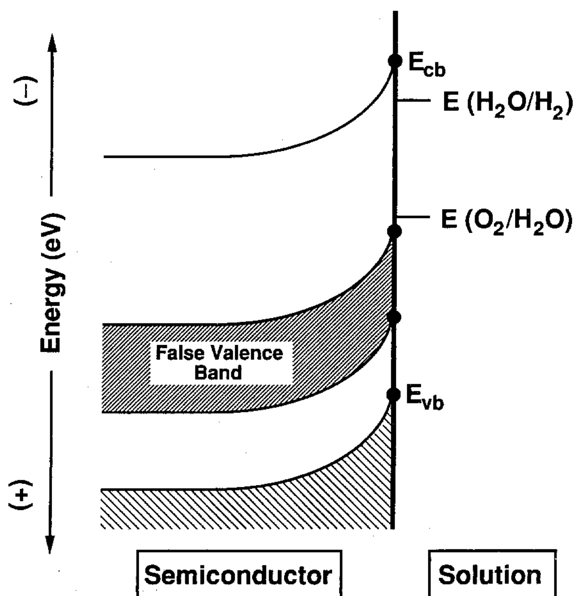

Figure 19. The generation of a "false valence band." A false valence band is created through the introduction of transition metal cations into the crystal lattice of a metal oxide semiconductor. The transition metal *d* orbitals overlap to form a new filled band that is closer to the water oxidation potential. A new smaller band gap also results for the material, being the separation between the new false valence band and the original metal oxide-derived conduction band.

electronic absorption energy from this new valence band to the original, lattice-derived conduction band could therefore shift the band gap of this modified semiconductor into the visible region of the spectrum.

Because the substitution of anions into the lattice of metal oxides was observed to reduce the stability of photoelectrodes in aqueous solutions, the preferred method for controlling the band gap was thought to involve doping the semiconductor with metal cations (108). The "false" valence band would then be created through overlap of the *d* orbitals of these dopant atoms. To this end, many different metal cations have been incorporated into both TiO_2 and $SrTiO_3$ lattices [for a more complete listing, see (32, 54, 109)].

Although some contradictions exist between various reports, doping metal oxides with transition metal cations, such as Co, Cu, Ru, and Pt, has been claimed to increase the response of these semiconductors to visible light (32). In all cases, the doping process resulted in a significant reduction in the internal quantum yield in the high-energy region of the spectrum (32). The cationic dopants generally introduced energy levels in the middle of the semiconductor band gap, but these levels increased the rate of carrier recombination in the semiconductor. To explain this result, Goodenough et al. (110) have postulated that the holes introduced into these localized mid-gap states should have an extremely low mobility. According to these authors, this decreased mobility should contribute to increased recombination and should produce low quantum yields for charge collection (110). Thus, although the strategy of introducing a false valence band was once popular, such experiments have been largely abandoned as of this time.

Other experiments have utilized nontransition metal cations, such as Al^{3+} (111, 112) or Y^{3+} (112) [or see (32) for a more complete listing], in metal oxide lattices. For example, Al^{3+}-doped single-crystal TiO_2 electrodes yielded solar conversion efficiencies of 1.3% in the electrically-assisted photoelectrolysis of H_2O (111). This value represented a significant improvement from the approximate 0.4% efficiency that was observed for an undoped TiO_2 electrode (111). Although these metal ions have been found to increase the internal quantum yield of the semiconductor/liquid interface in the UV region, the doping process did not produce any significant shifts in the threshold energy for light absorption (111, 112). While the mechanism of this increased yield is not known, two possibilities have been suggested (32). One hypothesis is that the doping of TiO_2 with Al^{3+} ions may act to passivate recombination traps (111). In addition to decreasing recombination, it has been proposed that this doping may also provide surface states that enable more efficient oxidation of OH^- to occur (111).

In general, efficient photoelectrolysis of H_2O using metal oxide electrodes remains an intriguing, but unrealized, approach to solar energy conversion. Further advances in this area must either await a new class of materials with more

optimal electronic properties, or will depend on modification of existing semiconductor surfaces. Efforts in both areas are continuing at present, although they are generally of reduced emphasis when compared to other approaches under consideration.

B. Advances in Semiconductor/Liquid Junctions Employing Small Band Gap Semiconductors

1. Strategies for the Generation of Stable Aqueous Photoelectrochemical Cells

As described above, metal oxide semiconductors generally have band gaps that are too large for optimal light absorption from the terrestrial solar spectrum. Semiconductors with smaller band gaps are better suited for this purpose. However, most contacts between aqueous electrolytes and small band gap semiconductors result in photocorrosion or photopassivation of the semiconductor surface. One strategy to mitigate this problem is to add a redox reagent that can compete kinetically with the undesired decomposition reaction. The electroactive species in the solution might scavenge the photogenerated carriers before they could induce decomposition of the semiconductor surface, thereby extending the operating lifetime of the electrode.

This approach has proven to be extremely useful in stabilizing various semiconductors and has led to numerous efficient photoelectrochemical energy conversion devices. The drawback associated with this method is that generally only electrical energy can be usefully obtained from these types of systems. In such electrolytes, the chemical products produced by the photoanode usually are not, in themselves, of substantial fuel value [unlike H_2(g) and O_2(g) from the photoelectrolysis of H_2O]. The products must therefore be recycled in the electrochemical cell to avoid a requirement for a continuous supply of chemical feedstocks into the system. Examples of semiconductor/liquid junctions that have been stabilized by kinetic methods are discussed in Section V.B.1.

Early attempts to stabilize small band gap semiconductors in contact with aqueous solutions employed n-CdS or n-CdSe electrodes. Typical redox species included the highly corrosive $Ce^{4+/3+}$(aq) and $Fe^{3+/2+}$(aq) systems, as well as more benign redox species, such as $[Fe(CN)_6]^{3-/4-}$(aq) and I_3^-/I^-(aq) (113, 114). In these studies, limited photoelectrode stability over the time scale of a few hours was observed for some systems; however, photocorrosion processes were not entirely eliminated in any of these electrolytes (115, 116). This observation is not surprising, given the extraordinary kinetic requirements that must be met to compete effectively with photocorrosion reactions. For example, prevention of dissolution of a 1-μm thick layer of CdSe over a 24-h time period at a current density of 20 mA/cm^2 would require that more than 99.97% of the

photogenerated holes be involved in the desired redox stabilizing reaction. Similarly, the passivation of Si electrodes only requires formation of 10–20 Å of SiO_2, so even 1 h of stable operation at a current density of 20 mA/cm^2 requires that more than 99.99% of the holes are directed into the desired charge-transfer process. Due to these severe kinetic constraints, as of 1975, no photoelectrochemical cell that was based on a small band gap semiconductor had been reported to be stable for extended periods.

a. Cadmium Chalcogenides and Chalcogenide Redox Couples. A key development in this area occurred in 1976, when three research groups independently reported that the chalcogenide redox couples (X_2^{2-}/X^{2-}; X = S, Se, and Te) in basic aqueous electrolytes prevented the photocorrosion of n-CdS and n-CdSe (117–119). These semiconductor/liquid junctions used small band gap materials, yet effected the sustained conversion of solar energy into electrical power. The reasoning that led to this discovery was straightforward: the photocorrosion reactions of CdS and CdSe involve oxidation of lattice S^{2-} or Se^{2-}, respectively, so addition of sufficient S^{2-} or Se^{2-} to the solution might possibly suppress lattice oxidation and lead to oxidation of the solution species (Eq. 38; X = S or Se).

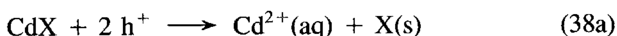

$$CdX + 2\,h^+ \longrightarrow Cd^{2+}(aq) + X(s) \tag{38a}$$

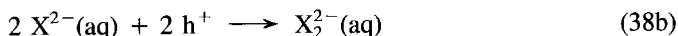

$$2\,X^{2-}(aq) + 2\,h^+ \longrightarrow X_2^{2-}(aq) \tag{38b}$$

This strategy worked remarkably well, even when high concentrations of $[Fe(CN)_6]^{4-}$ and I^- had been shown not to be effective in yielding electrode stability (113).

In these systems, the band gaps for CdS (2.4 eV) and CdSe (1.7 eV) are above the optimal value desired for solar energy conversion, and the solar efficiencies of the initial CdX/X_2^{2-}–$X^{2-}(aq)$ cells were extremely low. However, the important result clearly was that small band gap semiconductors could be stabilized in aqueous solutions through proper choice of the redox couple. This finding rapidly diverted attention from the metal oxide materials. It also channeled effort into understanding the factors that were responsible for stable, efficient photoelectrochemical energy conversion using small band gap semiconductor/liquid junctions.

Subsequent work on these interfaces emphasized controlling the surface defect density, optimizing the electroactive components of the solution, controlling the surface etching process, controlling the bulk properties of the semiconductors, and controlling other system variables. These studies resulted in substantial improvements in the energy conversion efficiency of these systems and also produced substantial advances in our understanding of semiconductor/liquid junction behavior. At present, typical values of 6–13% have been ob-

tained for the solar energy conversion efficiencies of n-CdSe/and n-$CdSe_xTe_{1-x}$/ liquid junctions (120–124), illustrating the progress that can be made with sustained effort towards optimizing a particular semiconductor/liquid interface.

To obtain semiconductor/liquid junctions with a better match to the solar spectrum, this kinetic approach to photoelectrode stabilization was then extended to other semiconductors with smaller band gaps. In an important study, Wrighton and co-workers (125) examined the stability of n-CdTe photoelectrodes ($\mathbf{E}_g$ = 1.56 eV) in contact with aqueous X_2^{2-}/X^{2-}(aq) solutions. They found that n-CdTe was unstable when the S_2^{2-}/S^{2-} redox couple was used, but that the electrode was stable in the presence of Te_2^{2-}/Te^{2-}(aq) (125). In general, it has been found that CdX semiconductors are stabilized by aqueous chalcogenide solutions, provided that the solution chalcogenide is either identical to the lattice species or is in a lower row of the periodic table than the lattice chalcogenide (126).

This trend can be explained by the observation that lattice chalcogenide atoms near the semiconductor surface have been found to undergo facile exchange with dissolved chalcogenide atoms in the solution (127, 128). For example, exposure of CdTe or CdSe anodes to aqueous solutions of the S_2^{2-}/S^{2-} redox couple resulted in the formation of a thin film of CdS on the electrode surface. Because CdS has a larger band gap than CdSe or CdTe, growth of CdS on these electrode surfaces presents a barrier to interfacial charge transfer. As this CdS layer grows in thickness, it becomes more difficult for holes to reach the solution; thus, the photocurrent decays with time. In contrast, operation of n-CdS or n-CdSe electrodes in contact with Te_2^{2-}/Te^{2-}(aq) results in the formation of a layer of CdTe on the semiconductor surface. The band gap of CdTe is lower than that of CdS or CdSe, so photogenerated holes can move freely from the CdS or CdSe into the solution. Thus, the formation of a layer of CdTe is not deleterious to the operation of these photoelectrochemical cells, and electrode stability is observed.

b. Cadmium Chalcogenides and Other Redox Couples. Other redox couples have also been used to stabilize CdX semiconductors in aqueous solution. A motivation for using other redox systems is to avoid the air-sensitivity and high toxicity of aqueous S^{2-}, Se^{2-}, and Te^{2-} solutions. Licht and Peramunage (4) recently reported the stable operation of an n-CdSe/ $[KFe(CN)_6]^{2-/3-}$–KCN(aq) photoelectrochemical cell that has a conversion efficiency of 16.4%. The operation of n-CdX/$[Fe(CN)_6]^{3-/4-}$(aq) junctions results in the formation of an overlayer of $[CdFe(CN)_6]^{-/2-}$ on the CdX surface (116, 129, 130). This layer has been postulated to stabilize the CdSe photoelectrode by attenuating its photoanodic dissolution (116, 129, 130). However, the presence of this overlayer, and the high energy conversion efficiency of this cell, have both been debated in the recent literature (131–135).

Wrighton and co-workers (136–138) recently reported that n-CdS and n-CdSe

photoelectrodes are stable in aqueous solutions containing organic thiolates or dithiocarbamates. These anionic sulfur donors appear to adsorb onto the Cd sites of the CdX surface, and thereby act to capture photogenerated holes faster than photocorrosion can occur (136, 138). An advantage of these reagents is that they did not undergo facile exchange with the lattice chalcogenide atoms (136) and, therefore, these reagents did not affect the optical or electronic properties of the semiconductor crystal. Although these junctions are interesting from a fundamental standpoint, they should not be considered as useful energy conversion devices. In this system, the oxidation process of the stabilizing reagent is chemically irreversible, and the products of this oxidation, disulfides, are not useful fuels because they are lower in free energy than the parent stabilizing reagents.

c. Other Semiconductors and Chalcogenide Redox Couples. The approach of using high concentrations of chalcogenides to compete with electrode decomposition has been successful even with semiconductors that do not contain chalcogenide atoms in their crystal lattice. Although this might seem surprising, several studies have shown that aqueous basic chalcogenide solutions produce adlayers of chalcogenides on the surfaces of most semiconductor electrodes (139–141). As in the case of the dithiocarbamates on II–VI surfaces (137), the presence of this layer of adsorbed donors serves to scavenge the photogenerated holes rapidly, and thereby competes with photocorrosion.

For example, the use of the chalcogenide redox couples Se_2^{2-}/Se^{2-}(aq) and Te_2^{2-}/Te^{2-}(aq) has proven effective in stabilizing three other small band gap semiconductors, n-GaAs (142, 143), n-GaP (142), and n-InP (144). In the latter case, only Te_2^{2-}/Te^{2-}(aq) was observed to stabilize the semiconductor (144). This approach is also useful for enhancing the stability of the related ternary semiconductor systems n-$GaAs_xP_{1-x}$ (145–148) and n-$Al_xGa_{1-x}As$ (149).

The experiments with GaAs are especially noteworthy, because they initiated a series of important electrochemical investigations into the surface properties of GaAs and other III–V semiconductors. These investigations underscored the advantages of using liquid contacts as a novel method of obtaining information and control over the surface chemistry of important semiconductor materials. Although the initial energy conversion efficiencies of these GaAs/liquid junctions were a respectable 8–9% (143), subsequent surface treatments and optimization of other cell parameters resulted in solar conversion efficiencies in excess of 16% for the n-GaAs/KOH–Se_2^{2-}–Se^{2-} system (3). As a result of these detailed studies, the n-GaAs/KOH–Se_2^{2-}–Se^{2-} interface is one of the most understood and efficient semiconductor/liquid junctions known to date.

d. High Salt Concentrations. When typical concentrations of redox reagents do not produce effective stabilization of a specific semiconductor, another approach is to use extremely high concentrations of supporting electrolyte.

The high salt concentration will diminish the activity of the water in the cell, and will thereby lower the rate of the corrosion reaction. This strategy should be even more effective if the supporting electrolyte is also an active redox donor, because the high donor concentration will also increase the rate of interfacial hole capture.

Examples of this approach are the n-MoX_2 (X = S or Se)/Y_2–Y^- (Y = Cl or Br) junctions, which are unstable at typical electrolyte concentrations of less than or equal to 1 *M* but are stable in 12 *M* LiCl(aq) and in 15 *M* LiBr(aq), respectively (150). Concentrated aqueous iodide solutions have also been shown to stabilize n-CdS (151), n-InP (151), and n-GaAs surfaces (152). In these solutions, the halide ion serves both to accept holes from the semiconductor and to diminish the activity of water. These studies are significant because all of these semiconductors have been found to corrode rapidly in solutions that contain lower concentrations of the aqueous halide ions.

Stable photoelectrochemical cells have also been constructed using high concentrations of salt solely to lessen the activity of water. In this approach, a separate redox-active reagent is required in order to collect holes from the illuminated semiconductor. For example, while the n-InP/$Cu^{2+/+}$(aq) junction loses photoactivity within a few minutes of operation when the cell contains 0.5 *M* $CaCl_2$, significantly higher concentrations of $CaCl_2$ (~5.6 *M*) resulted in stable cell operation for more than 20 h (153). In both electrolytes, the Cl^- ions are spectators for interfacial charge transfer and are not oxidized by holes. A similar approach has been used to stabilize n-Si surfaces that are coated with polypyrrole (154). Such electrodes showed some photocurrent stability when in contact with $Fe^{3+/2+}$(aq) solutions, but exhibited increased stability in the presence of 11 *M* LiCl(aq).

e. Layer-type Semiconductors. Another strategy to obtain stable aqueous photoelectrochemical cells is to use layer-type semiconductors. In 1977, Tributsch (66, 67) proposed that the unique electronic properties of such materials, which exhibit *d–d* transitions from the valence band to the conduction band, should afford a general approach to more stable photoelectrode surfaces. These compounds are especially promising because a number of transition metal chalcogenides—MX_2: M = Mo (155), W (155, 156), Pt (155), Zr (155), Hf (155), Re (157), Ru (158); X = S, Se, Te—have band gap energies in the range of 1.1–1.7 eV.

These photoelectrode materials have indeed proven to be remarkably stable in contact with a variety of aqueous electrolytes (159). For example, greater than 6×10^5 C cm^{-2} of photogenerated charge have been passed through n-FeS_2 (E_g = 0.9 eV)/I_3^-–I^- ($E^{\circ\prime}$ = 0.53 V vs. NHE) interfaces without any evidence of corrosion (160). While other redox couples, such as Br_2/Br^- ($E^{\circ\prime}$ = 1.08 V vs. NHE) and Cl_2/Cl^- ($E^{\circ\prime}$ = 1.36 V vs. NHE) resulted in only partial photo-

electrode stability (161), the ability of the n-FeS_2 to evolve Br_2 or Cl_2 over 4 days of operation, with less than a 50% loss in current density, further demonstrated the unusual stability of this class of semiconductors.

The native stability of this class of semiconductors has also been demonstrated for a variety of other layer-type photoanodes, including n-MoX_2 (150, 162, 163) and n-WX_2 (156, 163–168) (X = S or Se). In fact, the most impressive combination of efficiency and stability in any photoelectrochemical cell has been obtained in the n-WSe_2/I_3^-–I^-(aq) system. Stable operation of the electrode was observed for over 400,000 C cm^{-2} of charge passed through the semiconductor/liquid interface. This amount of charge is equivalent to over 3 years of operation in sunlight (166, 167). During this remarkable stability demonstration, the cell displayed a solar energy conversion efficiency of 10% for the duration of the experiment.

f. p-Type Semiconductors. Stable semiconductor/liquid contacts using aqueous electrolytes have also been constructed from p-type semiconductors. The strategic elements for the design of efficient, stable photoelectrochemical cells that employ p-type semiconductors are related to those for n-type semiconductors. The semiconductor should have a band gap of about 1.4 ± 0.3 eV, and the redox couple should rapidly collect minority carriers, while rejecting majority carriers. Stable semiconductor/liquid junctions using p-type materials should be easier to construct, in theory, than those employing n-type materials. For n-type materials, holes are driven to the surface by the electric field, and this increased hole concentration accelerates oxidative corrosion at the electrode surface. In contrast, the presence of excess electrons at the surface of a p-type photocathode should afford protection from oxidative corrosion processes. Therefore, a wide variety of redox couples should allow stable cell operation when p-type semiconductors are used as photoelectrodes.

This advantage was only fully realized in 1978, almost 20 years after the development of the first modern photoelectrochemical cell. However, it was rapidly exploited to construct a variety of stable p-type semiconductor/liquid interfaces. By 1978, stable semiconductor/liquid junctions had been constructed from p-MoS_2, p-CdTe, p-GaAs, and p-GaP with aqueous solutions of $Fe^{3+/2+}$, I_3^-/I^-, or S_2^{2-}/S^{2-} (67, 169–172). In general, stability is not a major problem for p-type electrodes in contact with aqueous solutions.

However, as described in Section V.B.2, the problem with these systems was not electrode stability, but rather low solar energy conversion efficiency. Although p-type semiconductors did not corrode in aqueous solution, the negative potentials at the semiconductor surface led to plating of impurities, changes in the surface stoichiometry, and other undesirable changes in the properties of the semiconductor/liquid interface. Unless these changes could be avoided or controlled, aqueous p-type semiconductor/liquid interfaces would not be useful

for solar energy conversion. The lack of initial success in this area discouraged many researchers, and other strategies for stable, efficient photoelectrochemical energy conversion devices were pursued instead.

2. *Energetics of Aqueous Photoelectrochemical Cells: Fermi Level Pinning*

Experiments with p-type photoelectrodes played an important role in the development of a somewhat controversial aspect of the theory of semiconductor/liquid junctions. In 1980, Bard et al. (84) postulated that semiconductor/liquid junctions using Si or GaAs electrodes exhibited complete Fermi level pinning. Experiments with p-type semiconductors formed the basis for this hypothesis, because nonideal behavior was observed initially for aqueous p-Si and p-GaAs junctions (85, 173).

For these systems, the open circuit voltage (V_{oc}) of the semiconductor/liquid junction was observed to be essentially independent of the redox potential of the contacting phase. For example, p-GaAs cathodes exhibited V_{oc} values of 0.40 ± 0.10 V when contacted with a series of aqueous solutions, even though the redox potential of the solution had been varied by about 1.0 V (from 0.53 V vs. NHE in the I_3^-/I^- system to -0.43 V vs. NHE in the $Eu^{3+/2+}$ system) (85). According to the formalism presented in Section III.A and Figs. 10 and 12, changes in the redox potential of the contacting phase should induce different amounts of band bending in the semiconductor. In an ideal system, such changes should result in a different value of V_{oc} for each semiconductor/liquid interface. The fact that V_{oc} was independent of the redox potential of the liquid phase implied that some of the potential difference between the two phases was not being dropped across the semiconductor. This nonideal behavior was ascribed to the presence of surface states in the semiconductor band gap (cf. Section III.C).

The suggestion that Fermi level pinning occurred at semiconductor/liquid junctions was not encouraging. One of the major attractions of semiconductor/liquid contacts, as opposed to semiconductor/metal or semiconductor/semiconductor contacts, was the potential for exerting direct chemical control over the electrical properties of the junction. For semiconductor/liquid contacts, this control can be exerted merely by changing the constituents of the liquid phase. If complete Fermi level pinning were present for common semiconductors, this advantage would not be realizable. In fact, there would be no means to exert chemical control over the potential drop in the semiconductor phase through changes in the properties of the liquid contact. A second implication of Fermi level pinning is relevant to device construction, because semiconductor/metal contacts had been well documented to exhibit Fermi level pinning with a variety of common semiconductors (174, 175). If this behavior were also observed for semiconductor/liquid contacts, there would be no practical advantage in using

semiconductor/liquid contacts for energy conversion. Instead, semiconductor/metal junctions could be used to provide the same solar energy conversion capabilities, with no concern about photocorrosion of the semiconductor.

So another dilemma seemed to be present: the problems involving photoanode stability in aqueous solutions had been largely overcome through the use of photocathodes, yet these photocathodes apparently could not be used to construct efficient energy conversion devices. As of 1980, Fermi level pinning appeared to exist on the surfaces of most small band gap semiconductors. Fortunately, several photocathode systems were subsequently discovered that did not display Fermi level pinning over a wide range of voltages. Chemical control over electrical properties of the junction was thus recovered, and these systems were eventually developed into efficient devices for solar energy conversion.

The first experiments to exhibit ideal junction behavior involved p-Si and p-InP photocathodes. Aqueous HCl solutions that contained vanadium ions were advantageous for such studies, because the redox potential could be varied over a wide range through use of the stable V^{V}, V^{IV}, V^{III}, and V^{II} oxidation states. For p-Si/HCl–$V^{5+/4+/3+/2+}$ (176) and p-InP/HCl–$V^{5+/4+/3+/2+}$ interfaces (177), variations in the redox potential of the solution were found to produce the expected ideal changes in the open circuit voltages of these semiconductor/liquid junctions. This variation clearly demonstrated that the redox potential of the solution affected the performance of these semiconductor/liquid junctions. It also demonstrated that Fermi level pinning could be avoided through proper choice of the contacting phase, even for common semiconductors such as Si and InP.

By choosing a redox potential in the HCl–$V^{5+/4+/3+/2+}$ system that maximized V_{bi}, it was possible to optimize the open circuit voltage and efficiency of p-InP photocathodes. This strategy led to the development of the p-type InP/HCl–$V^{3+/2+}$ photoelectrochemical cell, which has a solar energy conversion efficiency of 11.5% (177). This system is currently the most efficient aqueous p-type semiconductor/liquid junction (177, 178). Similar stability and high open circuit voltages have been observed for p-Si surfaces in contact with the HCl–$V^{3+/2+}$ (aq) electrolyte, although the energy conversion efficiency was only about 3% (176).

Surprisingly, only a few other p-type semiconductors have been extensively studied in contact with aqueous electrolytes: p-GaAs (85), p-RuS_2 (158), p-WX_2 (165, 168), and p-ReX_2 (157) (X = S or Se). Baglio et al. (168) observed that p-WS_2 exhibited ideal junction behavior for a range of aqueous redox couples, whereas related studies using p-GaAs concluded that Fermi level pinning limits the efficiency of p-GaAs/aqueous junctions (85). Thus, more work is required before concluding that highly efficient cells can be routinely obtained by the use of photocathodes in contact with aqueous solutions. A related problem is that the potential for reduction of water to H_2(g) establishes a negative limit on

the accessible value of any redox potential in aqueous solution. For some semiconductors, the position of the conduction band edge is more negative than this value, so the maximum electric field cannot be obtained from any available, stable redox reagent in aqueous solution. For these reasons, nonaqueous solvents provide very attractive media for the study of semiconductor/liquid interfaces (cf. Section V.B.4).

3. Photoelectrochemical Generation of Fuels Using Small Band Gap Semiconductors

Given that various strategies have been developed for obtaining stable, efficient semiconductor/liquid interfaces, it should be possible to use these methods to construct photoelectrochemical cells that produce chemical fuels. One of the most attractive features of semiconductor/liquid junctions is the ability to generate fuel directly from sunlight. As discussed previously, small band gap semiconductors generally cannot provide enough photovoltage to sustain H_2O electrolysis under standard conditions. However, small band gap photoelectrodes can decrease the amount of electrical power that is required to generate fuels in an electrolytic cell. These semiconductors can also be used to form fuels that do not require as much free energy as the decomposition of H_2O into $H_2(g)$ and $O_2(g)$. Studies that have been directed towards these goals are the topic of Section V.B.3.

a. Photoassisted Generation of $H_2(g)$. Photocathodes have been used to construct the most efficient photoelectrochemical cells that can electrolyze H_2O. The high efficiency of regenerative cells based on p-InP made it the obvious material to exploit in the photoelectrochemical production of $H_2(g)$. However, the native InP surface was found to be a poor catalyst for the 2 e^- reduction of H_2O to $H_2(g)$ (179). The slow interfacial electron transfer rate yielded a slow rate of $H_2(g)$ evolution, and led to low solar energy conversion efficiencies for p-InP/H_2O junctions.

A catalyst was clearly required to accelerate the rate of $H_2(g)$ formation at the photocathode surface. The deposition of continuous thin metal films did not produce the desired result, because Fermi level pinning at the semiconductor/metal interface limited the open circuit voltage of p-InP/metal photovoltaics (9). The key to reducing the overvoltage in the semiconductor/liquid system, while still maintaining a high-energy conversion efficiency, was the clever deposition of optically transparent islands of noble metals (179). These islands acted as electron-transfer catalysts but did not lead to deleterious semiconductor/metal junctions on the photocathode surface. The metal islands also did not absorb or reflect a substantial fraction of the incident light. The photons could then reach the InP surface and be absorbed by the semiconductor, so the external quantum

yields in such cells were very high. Using this approach, deposition of Pt, Rh, Re, or Ru onto p-InP surfaces has resulted in solar energy conversion efficiencies of 12–16% for the light-assisted generation of H_2(g) (1, 180, 181).

This system differs from the unassisted photoelectrolytic cells that were discussed above in the context of metal oxide photoelectrochemistry. The band gap of InP is sufficiently small (1.35 eV) that the open circuit voltage of p-InP/HCl(aq) junctions is only about 0.65 V, and the voltage at maximum power in the photoelectrolytic cells is only about 0.45 V (1, 181). These types of cells therefore provide very efficient energy storage with respect to the reduction in Gibbs free energy for the electrolysis of H_2O. However, an additional applied voltage is required in order to obtain any net electrolytic current under standard conditions. Nevertheless, the solar energy conversion efficiencies of these devices are extremely impressive, and exceed those of any other known chemical systems for the generation of stored fuels from water.

b. Light-Assisted Reduction of CO_2. The reduction of CO_2 to other carbon-containing molecules is a reaction of practical importance. The possible C_1 products (formic acid, formaldehyde, methanol, and methane) are commodity chemicals, and these species are potential feedstocks for fuel cells. Photocathodes offer the possibility of producing these feedstocks using sunlight as the energy source. The reduction of CO_2 has been examined primarily with p-type semiconductors [GaP (182, 183), Si (184, 185), CdTe (186), GaAs (187, 188), and InP (188)] that have band gaps near those required for optimal energy conversion.

Unfortunately, due to the high overpotential for the 1 e^- reduction of CO_2, the conduction band electrons from these materials are not sufficiently reducing to obtain high rates of CO_2 reduction. Instead, a bias of −1 to −2 V must be applied to assist the reduction of CO_2. In these reactions, the photoassisted reduction of CO_2 produced mixtures of formic acid, formaldehyde, and methanol. Energy conversion efficiencies were rather low (~0.5–4%), because these semiconductor surfaces were not able to catalyze the multielectron-transfer reactions that are required for energy-efficient CO_2 reduction. This scientific problem is the key obstacle that needs to be overcome in order to achieve efficient photoelectrochemical reduction of CO_2 (189). Recently, coating p-GaP (183) or p-Si (185) with thin layers of Pb has been reported to stabilize these electrodes during the photoassisted reduction of CO_2 and to yield increased current densities over those of the bare electrodes. This latter improvement is postulated to result from a catalysis of the reduction of CO_2 on these electrodes by the Pb film (185).

In an intriguing use of a semiconductor/liquid junction, Parkinson and Weaver (190) reduced CO_2 to formic acid enzymatically using an illuminated p-InP electrode as the electron source. In their photoelectrochemical cell (Fig.

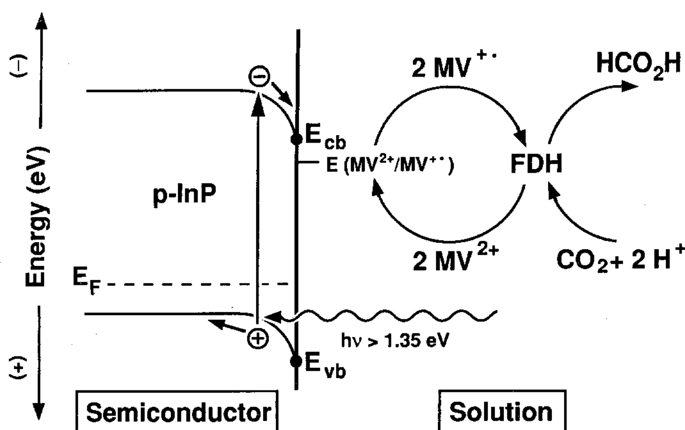

Figure 20. A schematic illustration of the photoelectrochemical enzymatic reduction of CO_2 (190). Photogenerated electrons from p-InP are supplied to formate dehydrogenase (FDH) in solution, which performs the 2 e^- reduction of CO_2 to formic acid. The electron transfer between p-InP and the enzyme is mediated by methyl viologen ($MV^{2+/+\cdot}$) in solution.

20), methyl viologen ($MV^{2+/+\cdot}$) was employed as a mediator between the electrode and solution-phase formate dehydrogenase (FDH). The mediator provided two 1 e^- transfers to the enzyme and FDH then catalyzed the reaction given in Eq. 39.

$$CO_2 + 2H^+ + 2\,e^- \xrightarrow{\text{FDH}} HCO_2H \tag{39}$$

The catalytic nature of the conversion was confirmed by noting that the enzyme underwent about 21,000 turnovers during the length of the experiment. Interestingly, the limitation on this system for reducing CO_2 is not the stability of the semiconductor/liquid junction, but rather the denaturation of the FDH.

The key to the success of this system is the FDH enzyme, because the FDH catalyzes the multielectron reduction of CO_2 in an energy efficient fashion. Thus, the $MV^{+\cdot}$—FDH combination can produce formate from CO_2 without a significant loss of free energy. For CO_2 to be a useful feedstock in photoelectrochemical energy conversion, similar catalytic properties must be developed from a simple, stable, molecular catalyst or metallic thin film that can be attached to a photoelectrode surface. At present, unfortunately, no such systems are available.

4. *Semiconductor/Liquid Junctions in Nonaqueous Solvents*

As mentioned previously, for some small band gap photoanodes, notably Si, no aqueous redox species has yet been identified that can compete effectively

with pathways for corrosion or passivation of the semiconductor. A logical alternative is to use nonaqueous solvents to form the semiconductor/liquid junction (191–193). Because water is intimately involved in most corrosion and passivation reactions of semiconductor electrodes, these undesirable processes can generally be minimized merely by eliminating one of the reactants in the corrosion reaction.

a. **Photoelectrode Stability.** Among the first stable nonaqueous semiconductor/liquid junctions was the n-Si/C_2H_5OH–ferrocene$^{+/0}$ interface (194). In this photoelectrochemical cell, the ferrocenium/ferrocene (Fc^+/Fc) system proved to be extremely effective in preventing oxidation of the n-Si surface. Photooxidation of the Si was suppressed because the ferrocene reacted with holes faster than they could be used in photocorrosive processes. The relatively low concentration of H_2O in the C_2H_5OH also served to minimize the rate of oxidation of the semiconductor surface.

The C_2H_5OH–$Fc^{+/0}$ system was used soon thereafter to construct the first stable n-Ge/liquid interface (195). These early photoelectrochemical cells had solar conversion efficiencies that were low (~1%) (194, 195), but the observation of long-term anode stability with n-Si or n-Ge was the most important finding of these reports. During this period, Tsubomura and co-workers (196) reported the stable operation of an n-CdS/liquid junction formed with 0.2 *M* solutions of NaI in CH_3CN.

Given these promising results, the use of nonaqueous solutions was rapidly adopted by a number of research groups as a strategy for generating new, stable photoelectrochemical cells. This strategy has been extended to a variety of photoanodes, including n-InP (197), n-GaAs (198, 199), n-GaP (200), n-$GaAs_{1-x}P_x$ ($0 \leq x \leq 1$) (147, 148, 201), n-$Al_xGa_{1-x}As$ ($0 \leq x \leq 1$) (149), n-CdTe (202), n-MoS_2 (203, 204), n-WSe_2 (204, 205), and others (162, 204, 206). The wide range of materials that have been stabilized in nonaqueous electrolytes clearly illustrates the generality of this important method of corrosion suppression.

As of 1981, despite improved stability in contact with nonaqueous solvents, no efficient semiconductor/liquid junctions had been developed using this approach. For example, the Si/C_2H_5OH–[*n*-Bu_4N][ClO_4]–$Fc^{+/0}$ interface only exhibited quantum yields at short circuit of 0.4 and solar energy conversion efficiencies of about 1% (194). Given that the band gaps of these materials were in the optimal range for solar energy conversion, the low efficiencies that had been obtained in all of these cells were troubling. In a number of papers, Fermi level pinning and surface state recombination were suggested to be responsible for the low efficiencies. So another dilemma had appeared: now a general method for enhancing the stability of photoanodes had been developed, yet fundamental limitations on efficiency due to surface state recombination would again prevent the formation of efficient solar energy conversion devices.

Again researchers rebounded and devised a solution to the problem. The low efficiencies were shown to be due primarily to losses from the high resistance of the electrolyte used in these cells, and not to inherent limitations in the electrical quality of the semiconductor/liquid contacts (207). By increasing the electrolyte concentration in the organic phase (thereby lessening the solution resistance), using more soluble redox couples and a more conductive solvent, and by simultaneously optimizing the bulk and surface properties of the semiconductor, n-Si/CH_3OH–$(CH_3)_2Fc^{+/0}$ photoelectrochemical cells operated with solar energy conversion efficiencies as high as 14% under AM 1.5 conditions (2, 208). In this cell, charge transfer across the Si/liquid interface was so efficient that the limiting recombination step was not even associated with the semiconductor/liquid contact, but was instead a property of the semiconductor material itself (208, 209). In fact, the electrical properties of the Si/$(CH_3)_2Fc^{+/0}$–liquid junction are superior to those of all known Si/metal contacts and are better than those of p–n junctions manufactured in the photovoltaic processing industry (9).

Nonaqueous solvents have subsequently been used in the development of efficient photoelectrochemical cells using a variety of n-type semiconductors. For example, in the III–V family, n-GaAs (210), n-$GaAs_{1-x}P_x$ ($0 \leq x \leq 1$) (149, 201), n-$Al_xGa_{1-x}As$ ($0 \leq x \leq 1$) (149), and n-InP (211) all have been shown to be efficient photoanodes in contact with ferrocene-based electrolytes. In fact, it now appears that the use of nonaqueous solvents will allow the construction of efficient photoelectrochemical cells from most semiconductor surfaces, even in cases where efficient photovoltaic devices cannot be obtained using semiconductor/metal contacts (211, 212).

b. Fermi Level Pinning. Nonaqueous solvents have also been important in the evaluation of Fermi level pinning restrictions on semiconductor surfaces. The enhanced stability of semiconductors in nonaqueous solvents allows use of a variety of outer-sphere, 1 e^- redox couples to establish the electrochemical potential of the solution phase. In addition, the potentials for oxidation and reduction of the solvent are further apart in CH_3CN and tetrahydrofuran (THF) than in H_2O. This increased potential window allows access to a wider range of redox potentials than is possible in H_2O. In early work, p-GaAs (84), p-Si (84, 173), and p-InP (213) were thought to exhibit complete Fermi level pinning in contact with CH_3CN solutions, because the open circuit voltages of these semiconductor/liquid junctions did not depend on the value of the redox potential of the solution phase. More recent studies have shown that, under certain conditions, n-Si (214), p-Si (214), n-InP (211), p-InP (215, 216), n-WSe_2 (217), p-$WeSe_2$ (217), and to some extent n-GaAs (212), all show a response to the solution redox potential, and do not display severe Fermi level pinning restrictions in nonaqueous solvents.

A recent example nicely illustrates the differences between semiconductor/metal interfaces, which generally exhibit Fermi level pinning, and certain semiconductor/liquid junctions. Metal contacts to n-InP only yield very low barrier height, nonrectifying diodes. This I–V behavior is obtained because the built-in voltage is limited to 0.3–0.4 V, due to Fermi level pinning of n-InP/metal contacts (218, 219). In contrast, n-InP/CH_3CN junctions have been found to exhibit a variety of different I–V behaviors depending on the redox couple of the solution phase (211). Contacts between n-InP and solutions with negative redox potentials yielded large exchange current densities and behaved as weakly rectifying diodes. In contrast, solutions with positive redox potentials produced small exchange current densities and yielded excellent diode I–V behavior. This behavior is in accord with the ideal model, in which changes in $E(A/A^-)$ affect the value of V_{bi} and, therefore, I_0, for the semiconductor/liquid interface. After evaluating a series of redox couples, the $Fc^{+/0}$ redox system was chosen for energy conversion applications because it produced the maximum electric field at the semiconductor/liquid junction (211). Cells employing n-InP/CH_3CN–$Fc^{+/0}$ interfaces exhibited solar energy conversion efficiencies of about 7%, despite the lack of any photovoltage from n-InP/metal contacts. The energy conversion efficiency for n-InP/$Fc^{+/0}$ contacts could even be improved further if so desired, because neither the surface properties, nor the electrolyte composition, had been optimized in this cell (211).

Subsequent work has shown that Fermi level pinning restrictions can be avoided even for materials such as Si. Lieber et al. (220) obtained a V_{oc} of 0.50 $\pm$ 0.02 V and a solar energy conversion efficiency of more than 10% for the p-Si/CH_3CN–$CoCp_2^{+/0}$ junction. This value of V_{oc} was within 80 mV of the theoretical value and was about 100 mV greater than the maximum possible value predicted by the Fermi level pinning model (84, 173). Furthermore, the open circuit voltages of p-Si/CH_3OH interfaces were found to vary in an ideal fashion as the redox potential of the solution was varied. In related experiments, values of V_{oc} for p-GaAs/CH_3CN–$CoCp_2^{+/0}$ interfaces were more than 100 mV higher than the maximum value suggested by the Fermi level pinning model (214). In addition, recent experiments with p-InP/CH_3CN interfaces have also verified a lack of Fermi level pinning under certain conditions (215, 216). These results are consistent with those in aqueous solution, in which p-InP contacts to $V^{3+/2+}$(aq) (177, 178) or to H_2O/H_2(g) (1, 180, 181) have shown large V_{oc} values and excellent energy conversion efficiencies.

5. *Hot Electrons in Photoelectrochemical Cells*

Nonaqueous solvents have also played an important role in the search for "hot electrons" at semiconductor/liquid contacts. In our discussion of the optimal band gap for utilizing the solar spectrum, it was assumed, as is generally

the case, that any excess excitation energy of photogenerated carriers is rapidly released into the solid (Section II.B.2.a). Thus, only the band gap energy was assumed to be available as potential energy for use in the photoelectrochemical cell. In principle, however, charge transfer across the semiconductor/liquid interface might compete with thermalization of some of the carriers. Minority carriers that are transferred with energies greater than the band gap energy are called *hot carriers* (Fig. 21). If one could extract the excess potential energy present in these hot electrons, it has been postulated that higher photovoltages could be obtained from a particular semiconductor/liquid interface (221, 222). The hot electrons might thereby allow a greater output of power to be harnessed from the cell, and thus might provide an increased solar conversion efficiency for a given band gap material.

Experimentally, the yield of hot electrons in photoelectrochemical cells has been determined by monitoring the rate of reduction of molecules with various redox potentials. Using this strategy, Nozik and co-workers (223) suggested that hot electrons from p-InP and p-GaP could be used to generate significant photocurrents at energies that are more negative than the bottom of the conduction band.

In related experiments, Koval and Segar (224, 225) demonstrated that a chemical product can be produced by hot electrons from a semiconductor/liquid

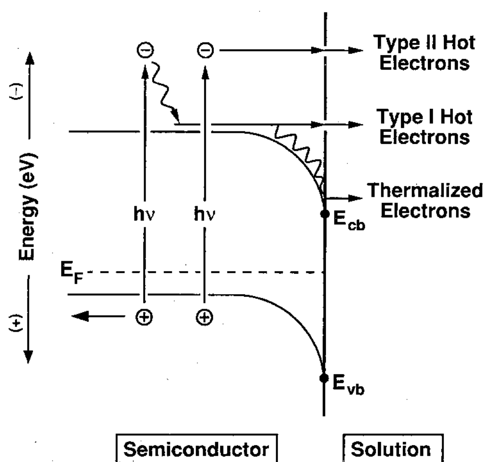

Figure 21. Types of electrons potentially available at a p-type semiconductor/liquid junction. The semiconductor is in depletion, and has been illuminated with light of energy greater than the band gap of the semiconductor ($h\nu > E_g$). The phrase "hot electrons" refers to electrons having potential energies greater than the edge of the conduction band (E_{cb}) at the semiconductor/liquid interface. The "degree" to which a hot electron thermalizes before it transfers to the contacting solution determines its type.

interface. In these experiments, the reduction of a Cu(I) complex in CH_3CN was effected by photogenerated electrons in a p-InP sample. The particular Cu(I) complex was chosen because it could only have been reduced to Cu(0) at potentials that were significantly negative of the conduction band edge at the InP/liquid junction. From these experiments, Koval et al. concluded that the potential energy of these hot electrons was approximately the value of the bottom of the conduction band in the bulk of the semiconductor. In other words, these electrons behaved as "type I" hot carriers (Fig. 21), because they apparently did not thermalize completely in the depletion region of the p-InP/CH_3CN contact prior to their transfer to solution.

Presently, the utility of hot electrons to increase the photovoltage from, and the efficiency of, a semiconductor/liquid junction remains unclear. For example, in the experiment discussed above, the internal quantum yield for the reduction of the Cu(I) complex was only about 0.0025. The possibility of using hot electrons remains a current topic of investigation, but significant advances in the utilization of hot electrons will require methods that maximize the lifetime of the hot carriers within the semiconductor (226, 227). An essential requirement will be the development of suitable redox species that can rapidly remove the hot carriers from the semiconductor. In addition, if such redox species are to harness the excess energy contained in the hot electrons, they must also be slow to equilibrate with other reagents that are simultaneously capturing the thermalized carriers from the semiconductor/liquid junction. Although no system has yet been identified that could meet these requirements, the photoelectrochemistry of hot carriers remains an interesting and current scientific question.

6. *Surface Modification of Small Band Gap Semiconductors*

Another strategy towards obtaining the elusive combination of stability, efficiency, and fuel production from semiconductor/liquid interfaces is to modify the surface of small band gap semiconductors with molecular reagents. Because the surface of the semiconductor plays a crucial role in the energy conversion behavior of a semiconductor/liquid interface, efforts to modify chemically the surface properties can, in principle, lead to dramatic improvements in the performance of most photoelectrochemical cells.

Two basic strategies have been developed for surface modification of semiconductor photoelectrodes. The first strategy involves the coordination of molecular reagents directly to the semiconductor surface. The goal of surface modification in this situation is to make new surface bonds, and to thereby change the electrical recombination properties of the semiconductor. Generally, the nature of both the surface species and the molecular reagent will be changed after this bonding process. If successful, the chemistry that is developed and moni-

tored using semiconductor/liquid interfaces could then be applied to semiconductor surfaces in a variety of applications, including solid state systems, chemical sensors, detectors, and other surface-sensitive devices.

The second strategy involves the attachment of electrochemically active groups to the semiconductor surface. In this approach, a reduction in the rate constant for surface recombination is not specifically the goal. Instead, manipulation of the charge flow across the solid/liquid interface is of prime importance. Generally, reagents used in this approach are designed to retain their electrochemical properties after attachment to the surface. Both strategies draw heavily on the concepts of inorganic chemistry. In Sections V.B.6.a–c, we first describe the coordination chemistry of complexes with electron donors and electron acceptors. This description is followed by a discussion of the modification of semiconductor surfaces using electroactive reagents.

a. Reactions of Electron Donors with Semiconductor Surfaces. It is convenient to divide the discussion of the semiconductor surface chemistry according to the bonding characteristics of the molecular reagent. Generally, the Lewis bases that have been used to modify semiconductor surfaces are organic donors, such as amines, phosphines, or sulfides. These types of reagents generally are expected to bond to electron-deficient sites on the semiconductor surface. A second class of molecular reagents consists of Lewis acids, which are expected to bond to electron-rich sites on the surface of the semiconductor. These reagents usually are complexes of transition metals. The chemistry of Lewis bases is discussed in this section, and Section V.B.6.b emphasizes the surface coordination reactions of Lewis acids.

Layer-Type Semiconductors. The use of Lewis bases to modify the surfaces of semiconductors was employed as early as 1980 in a study of the n-WSe_2/I_3^-/I^-(aq) junction (228). The semiconductor WSe_2 has a layered structure, with atomically flat planes of Se atoms exposed at the surface. In a macroscopic sample, these atomically flat planes are connected by "steps," and the edges of these steps are believed to contain a high concentration of defect sites. Upon treatment with a variety of substituted pyridines, Parkinson et al. (228) observed improvements in the I–V characteristics of the WSe_2/I_3^--I^-(aq) interface. These authors logically ascribed the I–V changes to the coordination of defect sites by the pyridine ligand. This study was extremely important, because it demonstrated that simple acid–base concepts could be applied to manipulate the electrical properties of semiconductor surfaces. Unfortunately, the I–V improvements for this particular semiconductor/liquid interface persisted for only a few hours, until the adsorbate desorbed or degraded on the semiconductor surface.

In related work, Razzini et al. (229) used multidentate adsorbates, such as

ethylenediaminetetraacetic acid (EDTA), on another layer-type semiconductor, n-$MoSe_2$. After exposure of an n-$MoSe_2$ electrode to EDTA, the power output of the electrode more than doubled, with significant improvements in V_{oc}, J_{sc}, and the fill factor of this semiconductor/liquid interface. The long-term stability of the n-$MoSe_2$ electrode was superior to that of pyridine-treated WSe_2/I_3^--I^-(aq) interfaces; however, approximately 50% of the improvement in the n-MoS_2/I_3^--I^-(aq) junction disappeared after 3 days of operation.

In more recent work, Tributsch and co-workers (230) examined the stability of n-FeS_2 in contact with the Br_2/Br^-, $[Fe(phen)_3]^{3+/2+}$(phen = 1,10-phenanthroline), and $[Fe(bpy)_3]^{3+/2+}$ (bpy = 2,2′-bipyridine) ($E°'[Fe(bpy)_3]^{3+/2+}$ = 1.01 V vs. NHE) redox systems. These three redox couples have similar redox potentials, but differ in the sign of the charge on the redox reagents. In this system, only the negatively charged Br^- ions yielded stable photoelectrochemical behavior. This observation suggested that the coordination of an anionic species to the positively charged Fe atoms on the n-FeS_2 surface was required for effective interfacial electron transfer. As further evidence of this requirement, the addition of Cl^- ion to unstable n-$FeS_2/[Fe(phen)_3]^{3+/2+}$ cells was found to yield stable photoelectrode behavior (230). The authors suggested that the Cl^- ions coordinated to the n-FeS_2 surface and acted as a bridge for electron transfer between the semiconductor and the $[Fe(phen)_3]^{3+/2+}$. Although these stability results required some detailed understanding and modification of the semiconductor surface structure, they are quite impressive when compared to the typical behavior for II–VI and III–V materials in contact with typical aqueous electrolytes.

GaAs. The studies described above represent possibly the only documented cases of surface modification acting to passivate defect sites in semiconductor/liquid junctions. For some other semiconductors, beneficial surface chemistry has been documented in contact with gaseous ambients, but the passivation chemistry has not yet been extended to the behavior of photoelectrochemical cells. In this section, the principles of this surface chemistry are briefly described for GaAs, and the next section summarizes results for II–VI semiconductors.

Gallium arsenide is a technologically important semiconductor, and there is great interest in developing chemical methods to control the electrical properties of GaAs surfaces. Yablonovitch and co-workers (231) recently reported that coating GaAs surfaces with thick layers of $Na_2S \cdot 9H_2O$ produced a significant reduction in the surface recombination rate at GaAs/air interfaces (139, 231). These studies were motivated by the favorable current–voltage properties of n-GaAs/KOH–Se_2^{2-}–Se^{2-} junctions, as discussed in Section V.B.1. The initial proposal was that an epixatial, lattice-matched layer of As_2S_3 formed on the GaAs surface, and that this layer terminated the surface bonding in a fashion similar to the bonding in the bulk of the semiconductor.

After extensive spectroscopic studies of this system (140, 232, 233), there is little agreement to date on the mechanism or products of this surface passivation reaction. It has been shown, however, that other sulfur-containing bases, including short-chain thiols, can produce similar changes in surface recombination (233, 234). In nonaqueous solvents, the thiols did not yield detectable amounts of As_2S_3, yet the exposure to these reagents did result in improved surface recombination rates. The details of the chemistry used to modify the semiconductor surface appear to be extremely important in determining the electrical properties of the GaAs interface. For example, the exposure of GaAs to various *n*-alkanethiols at higher temperatures (100 vs. ~25°C) yielded oriented monolayers that consisted of densely packed thiolates (235). Although this procedure generated a highly ordered thiolate layer on the semiconductor surface, it did not result in a significant improvement in the electrical recombination properties of GaAs surfaces (236). Clearly, detailed studies of the surface chemistry are required to understand and control this behavior. Recently, a solution containing both S^{2-} and Se^{2-} has been claimed to yield superior surface recombination properties at GaAs electrodes (141, 237), but the chemistry in this system is even less clear at present.

CdS and CdSe. Another application of surface modification is to introduce a controlled amount of charge onto the semiconductor surface. If negative charge is introduced on the surface of an n-type material, increased positive charges will be created within the semiconductor in order to offset this negative charge. These positive charges will increase the depletion width and the built-in voltage of the semiconductor, and will usually lead to a reduction in the value of the exchange current I_0. Controlled adsorption of charges or dipoles onto the semiconductor can therefore allow deliberate, molecular-based variation in the *I–V* properties of a semiconductor/liquid interface. It can also induce changes in V_{bi} for semiconductor surfaces in contact with gaseous ambients. This type of surface modification has been used extensively to control the chemistry of II–VI semiconductor/liquid interfaces.

To introduce negative charge onto a semiconductor surface, Wrighton and co-workers (136–138) and Uosaki et al. (238) exposed CdS/and CdSe surfaces to various anionic sulfur donors. These reagents included HS^- (238), $[MoS_4]^{2-}$ (138), thiolates (136), and dithiocarbamates (137, 138). These species were found to adsorb strongly onto the Cd-rich face of the semiconductors. As predicted, substantial changes in the *I–V* properties of CdS/and CdSe/liquid interfaces were observed as a result of adsorption. The value of V_{bi} increased significantly after surface modification, with changes in V_{bi} as large as 1 V being observed in the most favorable cases.

This approach has also been used to manipulate the properties of II–VI semiconductors in contact with gaseous ambients. In a series of studies by Ellis and

co-workers, a variety of Lewis acids (239, 240) and Lewis bases (241–245) have been shown to affect the surface recombination rate of CdS and CdSe crystals. A strong correlation was observed between the surface recombination rate and the electron-donating ability of the adsorbate. These studies suggested that the chemical passivation of defect sites was much less important than the donation or withdrawal of electron density into the depletion region of the CdSe crystals. This series of papers represents an impressive example of the deliberate, chemically based manipulation of the electrical properties of semiconductor surfaces.

Colloidal particles of II–VI materials also have been exposed to Lewis bases. Small semiconductor particles are expected to have a high density of defects at their surfaces, so large changes in the rate of surface recombination are expected after chemical modification of the particles (246–248). In a recent example, the treatment of very small semiconductor particles (diameter ≈ 100–300 Å) of CdS and of Cd_3As_2 with $(C_2H_5)_3N$ dramatically decreased the surface recombination rate of the particles (249). Similar changes have also been observed upon treatment of these particles with $(CH_3)_3N$, 1,4-diazabicyclo[2.2.2]octane, and alkanethiols (249). The surfaces of the II–VI particles thus appear to be affected differently than the surfaces of II–VI single crystals, because coordination of Lewis bases to the particles is thought to affect the surface state bonding while coordination to the single crystals is thought to induce changes in the total charge in the depletion layer.

b. Coordination of Lewis Acids to the Surfaces of Semiconductors. The treatment of semiconductor surfaces with Lewis acids, specifically with transition metal ions, has historically been avoided ever since the late 1950s. In early work on solid state junctions, adsorption of trace metal ion impurities, such as Cu ions that had leached from Cu pipes into rinse water, was found to produce high surface recombination rates at Si and Ge. As a result, the elimination of trace metal ion contaminants is one of the goals of the fastidious cleanliness procedures that have been developed for modern semiconductor processing facilities. In 1978, the discovery that adsorption of metal ions could improve the current–voltage properties of the n-GaAs/Se_2^{2-}–Se^{2-} interface (250) provided a stunning counterexample to this long-held notion.

n-GaAs + Metal Ions. While working with n-GaAs/KOH–Se_2^{2-}–Se^{2-}(aq) interfaces, Parkinson, Heller, and Miller (11, 250, 251) observed solar energy conversion efficiencies that varied from 7–10%. They ascribed the differences in the properties of these cells to the presence of trace impurities, and were prompted to examine the effects of various cations on the performance of n-GaAs/KOH–Se_2^{2-}–Se^{2-} junctions. While many cations, including Ca^{2+}, Sr^{2+}, and Ba^{2+}, did not adsorb to the GaAs or had little effect on the perfor-

mance of the cell, treatments with other ions, such as Bi^{3+} and Ru^{3+}, were found to yield reproducible changes in the current–voltage properties (251). The Bi^{3+} ion reduced the cell's performance, and this behavior was not surprising given the previous history of impurity adsorption effects. However, exposure of GaAs surfaces to solutions of 0.01 *M* $RuCl_3$ in 0.10 *M* HCl(aq) improved the photoanode performance to a solar energy conversion efficiency of 12% (250). This value was the highest solar conversion efficiency reported to date for any photoelectrochemical cell. The improved efficiency persisted during more than 20 days of operation, suggesting that Ru^{3+} ions were adsorbed strongly to the GaAs surface (251).

Subsequently, adsorption of other metal ions has been shown to result in even higher energy conversion efficiencies in this system. Group 8 and 9 (VIIIB) metal complexes, including Co(III) and Os(III) species, produced substantial improvements in the energy conversion efficiency of n-GaAs/Se_2^{2-}–Se^{2-}(aq) junctions (252). For example, chemisorption of Os(III) complexes onto n-GaAs anodes produced cells with solar energy conversion efficiencies as high as 15.0 $\pm$ 1.0% (3).

A number of studies investigated the mechanisms by which metal ions improve the *I–V* characteristics of the n-GaAs/Se_2^{2-}–Se^{2-}(aq) interface. The experimental observation is that chemisorption of Ru^{3+} leads to higher photocurrents (at a given applied voltage) than those displayed by untreated GaAs anodes (250). This chemisorption process also produces higher open circuit voltages and a higher fill factor in the cell (Fig. 22). One explanation for this behavior was that the adsorption of metal ions removed surface states that were present on etched n-GaAs anodes. Time-resolved luminescence studies of GaAs/air interfaces supported this interpretation, because such experiments revealed a 30-fold reduction in the rate constant for surface recombination after chemisorption of Ru^{3+} ions (253). However, because no electrolyte solution was present during the luminescence experiments, whether this reduction was the sole, or even the dominant, effect of the metal ion treatment could not be determined unambiguously.

An alternative explanation for the increased *I–V* performance is that the metal ions catalyze the hole transfer between Ru^{3+}-treated n-GaAs and KOH–Se_2^{2-}–Se^{2-}(aq) solutions. Even if the surface recombination rate does not change after chemisorption of metal ions, a larger rate of interfacial hole transfer would result in a higher quantum yield for photocurrent flow. From electrochemical impedance studies of n-GaAs electrodes, Allongue and Cachet (254) concluded that the *I–V* improvements had little to do with recombination losses. Instead, they postulated that the improvements were due primarily to increases in the minority carrier current between the semiconductor and the redox couple. Experiments by Lewis and co-workers (252, 255, 256) subsequently confirmed this conclusion.

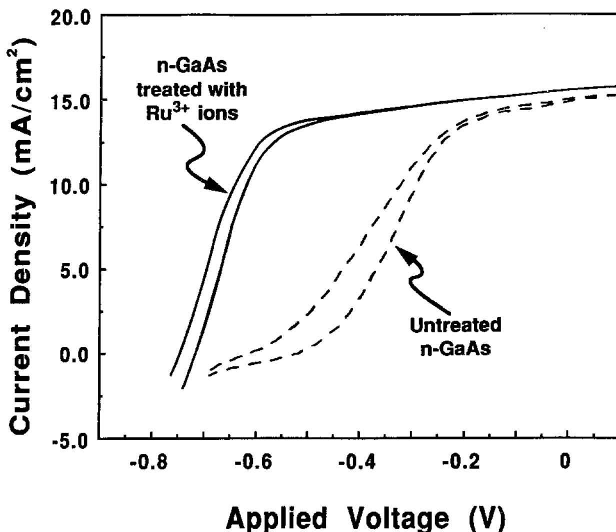

Figure 22. Improvement in the current–voltage characteristics of an n-GaAs electrode after treatment with $RuCl_3 \cdot 3H_2O$. After immersion of the GaAs electrode into 0.10 *M* HCl–0.010 *M* $RuCl_3$(aq), improvements are observed for the open circuit voltage and the fill factor of the cell. Data are for n-GaAs photoanodes in contact with 1.0 *M* KOH–0.8 *M* K_2Se–0.1 *M* K_2Se_2(aq) (252).

Despite the ability of these metal complexes to produce efficient photoelectrochemical energy conversion devices, surprisingly little is known about the chemical structure of the adsorbed metal ions. For example, in the case of the treatment of n-GaAs with Os^{3+} ions, neither the coverage nor the oxidation state of the adsorbed Os^{3+} ions has been reported. The most characterized system to date is the adsorption of Co(III) complexes onto GaAs surfaces. After exposure to a Co(III) complex, Tufts et al. (257) demonstrated that the species on the GaAs surface is a film of $Co(OH)_2$. Upon exposure of this $Co(OH)_2$ film to the Se_2^{2-}/Se^{2-}(aq) electrolyte, the $Co(OH)_2$ reacted to form a new species that was predominantly $CoSe_2$ (257). This latter surface was actually the one that was electrocatalytically active in the n-GaAs/KOH–Se_2^{2-}–Se^{2-}(aq) photoelectrochemical cell. Such observations imply that further work is needed in order to provide a firm basis for controlling and understanding the interfacial chemistry of Lewis acids at III–V surfaces.

p-InP + Ag. The beneficial effects of metal ion chemisorption are not limited to n-GaAs surfaces. For example, the efficiency of p-InP/HCl–VCl_3–VCl_2(aq) interfaces has also been improved by adsorption of metal ions onto the InP surface. Heller and co-workers (258) observed that a brief ($\sim$1 s) ex-

posure of p-InP to 0.1 *M* $KAg(CN)_2$–0.1 *M* KCN(aq) resulted in an increased fill factor and increased V_{oc} for the p-InP/HCl–VCl_3–VCl_2(aq) junction. These improved *I–V* characteristics resulted from the adsorption of submonolayer amounts of silver onto the InP surface. In a subsequent study, using polycrystalline p-InP films as electrodes, Heller and co-workers (258) obtained solar energy conversion efficiencies of 7% using this Ag^+ treatment. This reaction provides another impressive example of the benefits of surface modification of semiconductor/liquid interfaces. Unfortunately, no information is yet available on the mode of binding or on the coordination environment of the Ag atoms that are important in producing this improved photoelectrochemical cell behavior.

c. Attachment of "Outer-Sphere" Systems to the Semiconductor Surface. Another distinct strategy for surface modification involves the attachment of electroactive reagents to the semiconductor surface. In contrast to the "inner-sphere" modifications discussed above, this approach does not attempt to modify the electrical properties of the semiconductor nor to change the electron-transfer properties of the molecule. Instead, the surface-attached molecule is designed to serve as a specific electroactive site through which carriers must flow as they cross the semiconductor/liquid interface. In principle, this approach can lead to chemical control over the electrochemical reactivity of a semiconductor/liquid interface. Experiments that have utilized this approach are the subject of Section V.B.6.c.

This elegant strategy is based on the concept of "mediated" charge transfer (Fig. 23). In this approach, the photogenerated minority carrier is efficiently captured by a molecular reagent that has been attached to the surface of the photoelectrode. The minority carrier then resides on the molecule, and the subsequent fate of this charge depends on the chemical reactivity of this electroac-

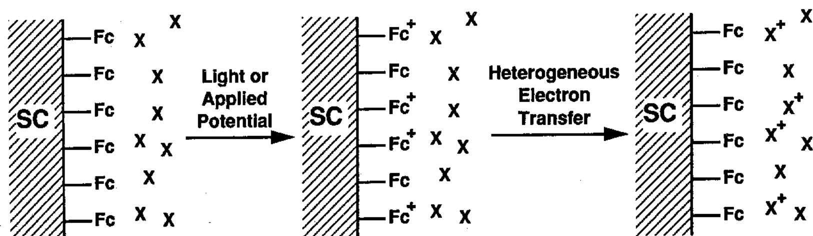

Figure 23. A schematic illustration of the process of heterogeneous electron transfer at a derivatized n-type semiconductor/liquid junction. In the figure, the transfer of holes between the semiconductor (SC) and the solution-phase redox species (X) is mediated by the surface-attached, electroactive species Fc (= ferrocene). The central illustration is drawn to emphasize that the electron-transfer process is mediated, and should not be misconstrued to represent a distinct step whereby the products of hole transfer are solely localized on the semiconductor surface.

tive, surface-bound molecular reagent. The interfacial charge-transfer process is thus "mediated" by the molecular reagent.

This process closely resembles the molecular arrangement in the photosynthetic reaction center. In the reaction center, a series of electron acceptors acts to direct the charge flow through the membrane and into the catalytically active sites. In the semiconductor/liquid junction, the electron acceptor mediates and, therefore, directs the charge flow into the liquid phase. The only conceptual difference is that, in the semiconductor/liquid junction system, the light absorption and initial charge separation take place in the semiconductor, as opposed to taking place in a molecular assembly.

The surface-attached electroactive reagent is desirable in order to control the chemical reactivity of the photogenerated charges. In this fashion, corrosion reactions can be suppressed, or electrocatalytic reagents can be introduced directly onto the surface of the electrode. This result could allow enhanced stability of photoelectrodes in contact with aqueous solution, as well as more efficient means of producing fuels, such as $H_2(g)$.

Pioneering work in this area was performed by Wrighton and co-workers (194, 195, 259). The electroactive reagent was chosen to be a ferrocene group, because ferrocene had been shown to be effective in stabilizing Si, Ge, GaAs, and other small band gap photoanodes in contact with nonaqueous solvents. The goal was to use a surface-attached ferrocene to effectively capture photogenerated holes from these semiconductor surfaces. The ferrocenium formed from this hole capture process would then be used to effect other oxidations in a subsequent, controlled reaction step. If the holes could be completely captured by the surface-attached ferrocene, then in principle, corrosion could be suppressed even in contact with an aqueous solution. Furthermore, mediated electron transfer could be used to direct the photogenerated charges only to the desired chemical reaction pathway at the expense of other possible reaction paths.

To attach ferrocene units to the surfaces of Si, Ge, and GaAs, Wrighton and co-workers (260, 261) reacted (1,1'-ferrocenediyl)dichlorosilane, **I,** with hydroxyl groups that were present on the oxidized surfaces of these semiconduc-

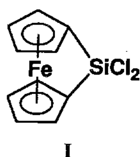

I

tors. Exposure of the hydroxylated surface to **I** led to the covalent attachment of the ferrocene group.

$$\text{Surface—OH} + \text{RSiCl} \longrightarrow \text{Surface—O—SiR} \qquad (40)$$

Using this approach, ferrocene moieties were attached to the surfaces of various semiconductors, including Si (260–263), Ge (195), and GaAs (259). Cyclic voltammetry was then used to prove that the electron transfer was mediated by the surface-bound ferrocene groups. In contact with nonaqueous solvents, these surface-bound ferrocenes reacted extremely rapidly with a variety of electroactive reagents in the solution phase. Even with rotating disk electrodes supplying material rapidly to the electrode, transport of the solution reagent to the surface limited the reaction rate between the surface-bound ferrocenium ions and molecular reagents in the solution (263).

In the most impressive application of this methodology, n-Si electrodes were actually stabilized in contact with aqueous solution (261). The ferrocene groups captured photogenerated holes extremely efficiently from the Si surface, and directed the oxidation of molecular reagents in the solution in competition with oxidation of the Si surface. Silicon photoanodes without a surface-attached layer of ferrocenes exhibited no photocurrent after 5 min in 4 m*M* $[Fe(CN)_6]^{4-}$(aq), but modified Si surfaces showed photocurrent stability for 30 min in these same solutions (261, 262). This stability is even more impressive when considering that formation of a 20-Å layer of oxide would be sufficient to produce passivation, and that such a process would only require about 0.06% of the photogenerated carriers over a 10-min time period at a photocurrent density of 20 mA/cm^2. Even this approach is not sufficient to produce extended stability at high photocurrent densities, however. Thus, further surface modification is required if n-Si/H_2O junctions are to be considered seriously for energy conversion applications.

This surface modification approach has been extended to a variety of other electroactive reagents. Silicon has been functionalized with $(CH_3)_{10}Fc$ derivatives, as well as with viologen reagents. The $(CH_3)_{10}Fc$ derivatives have been used in electron-transfer studies (264), while the viologen reagents have been used in mediated H_2(g) production at p-Si photocathodes (265) and in the reduction of cytochrome *c* at metal and semiconductor surfaces (266). The cytochrome *c* reaction provides a nice example of electrocatalysis that is induced by deliberate surface modification, because cytochrome *c* is not electroactive at unmodified Si surfaces. However, the reduction proceeds extremely efficiently at Pt and p-Si surfaces when the electron transfer is mediated through the surface-attached viologen groups (266).

Gallium arsenide electrodes derivatized with **I** have also been suggested recently for use as chemical sensors (267). As mentioned in Section V.B.6.a, electron-donating and electron-withdrawing groups have been shown to influence the rate of carrier recombination at semiconductor surfaces (239–245). Exposure of ferrocene-modified GaAs surfaces to oxidants led to the production of a surface-attached ferrocenium species, even in the gas phase. The negative charge on the counterion increased the depletion width in the semiconductor

sample in the same fashion as had been observed for electron-withdrawing groups on CdS and CdSe surfaces. This increased depletion width produced an increase in the rate of carrier recombination at the GaAs surface, and led to a decrease in the luminescence from the bulk of the GaAs sample (267). The effect was reversible when the GaAs surface was exposed to reagents that reduced the surface-attached ferrocenium back to the neutral ferrocene state. The use of derivatized semiconductors as sensors is an intriguing one, and represents an additional application of semiconductor surface modification.

As a result of this body of work, it is now possible to envision functionalization of semiconductor surfaces with almost any desired molecular reagent. The ideal surface modification would involve a reagent that reduced the density of electrical traps on the surface of the semiconductor, while also introducing an electroactive reagent to direct the interfacial charge flow in a predetermined reaction path. The reagent would be even more desirable if it catalyzed the multielectron-transfer reactions that are important in fuel formation. Given the recent demonstrations of direct coordination to the surfaces of CdS, CdSe, and GaAs (136–138, 235, 239–245), it should now be possible to realize the benefits of this approach. This method would provide an elegant, molecular-level strategy for the modification of semiconductor surfaces, and would have applications in energy conversion as well as in other aspects of semiconductor technology.

C. Dye Sensitization of Semiconductor Electrodes

The last strategy that has been widely used to construct energy conversion devices from semiconductor/liquid interfaces is dye sensitization. Whereas the studies described above have attempted to obtain improved solar energy conversion efficiencies by altering the bulk or surface properties of the semiconductor, this same goal can, in principle, be achieved through the use of molecular-based light absorbers. This general process is called dye sensitization and studies in this area are the topic of Section V.C.

The goal of dye sensitization is to combine the light absorption and catalytic properties of molecular reagents with the charge separating properties of semiconductor/liquid junctions. Generally, a dye with an excitation wavelength in the visible range is adsorbed onto the surface of a large band gap semiconductor (Fig. 24). The excited state of the dye must have a sufficiently negative redox potential that it can transfer an electron into the conduction band of the semiconductor. The injected electron will experience the force of the electric field in the semiconductor and will then be driven toward the back contact by the field in the semiconductor depletion region. The electron vacancy resides on the oxidized dye, and to complete the process, the dye must be reduced to its original, photoactive form by a donor species in solution. This donor molecule

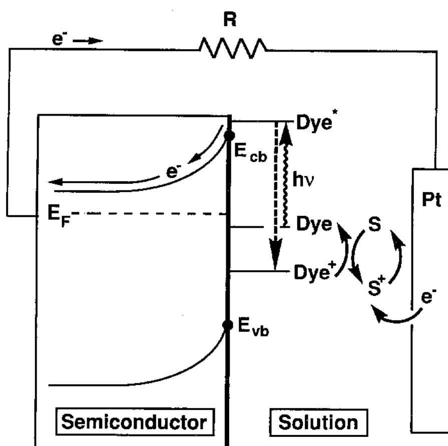

Figure 24. A schematic illustration of a photoelectrochemical cell containing a dye-sensitized semiconductor. Upon illumination, the dye is raised to an excited state (Dye*) and an electron is injected from the excited dye into the conduction band of the semiconductor electrode. To prevent back-reaction of the electron with the dye, a supersensitizer (S) is used in the solution to react with the now-oxidized dye (Dye^+). In this process, the original, photoactive dye is regenerated, and the driving force for recombination is removed. The electron injected into the semiconductor by Dye* is driven through the circuit by the electric field at the semiconductor/dye interface. Work is then performed as the electron travels through an external resistor (R). The cell is then returned to its initial state as the oxidized supersensitizer (S^+) is reduced at the Pt electrode.

is often added to the solution for the sole purpose of providing kinetic competition with recombination between the injected electron and the oxidized dye. In such cases, the donor is referred to as a supersensitizer. Because the dye injects only an electron (i.e., a majority carrier) into the semiconductor, this carrier generation mechanism leads to minimal recombination losses in the semiconductor as compared to direct illumination of the semiconductor.

There are many requirements that must be met for an efficient dye sensitization process (268). Useful dyes must have excited state electrochemical potentials (**E**(Dye^+/Dye*)) that are more negative than the bottom of the conduction band. In addition, the electrochemical potential of the ground state of the dye (**E**(Dye^+/Dye)) should be in the middle of the semiconductor band gap. The rate of electron transfer from the excited dye (Dye*) to the conduction band of the semiconductor must be rapid relative to the intrinsic decay rate of the excited dye. In addition, the oxidized and reduced forms of the dye must both be stable in solution under prolonged illumination. Finally, back electron transfer from the semiconductor conduction band into the oxidized dye should be sufficiently slow that effective charge separation can take place. Due to these various kinetic constraints, only dye molecules adsorbed on the surface of the

semiconductor are generally useful for the injection of electrons. Coverages of greater than a monolayer fail to enhance the solar energy conversion efficiency of these electrodes, because these extra layers of dye tend to filter the incoming light, actually decreasing conversion efficiencies (269). Because dye coverages are limited to a monolayer, or even less, only dyes with high extinction coefficients are useful.

Dye sensitization techniques have long been of significant importance in photography, where adsorbed dyes are used to extend the spectral range of the semiconducting silver halide grains in photographic images (270). Light is used to reduce a tiny fraction of the silver halide grains to Ag metal, forming the latent image that will later be developed to yield a photograph (271). The dyes increase the sensitivity of the film, allowing smaller lens apertures, so that focusing is not as important (271). This increased sensitivity also allows faster shutter times, so that blurring is reduced (271). Maximizing the efficiency of dye sensitization is therefore of great practical interest in photography.

Among dyes, there is a great variance in the efficiency of sensitization. The absolute quantum yield for spectral sensitization of the semiconducting silver halide grains can be measured by monitoring the electrical charge that accumulates during illumination of the dye-modified grains (272). Using such methods, internal quantum yields approaching unity have been observed for the dye-sensitized emulsions (272). Such methods do not offer information about the mechanism of sensitization, however, as it is difficult to control the surface properties of photographic emulsions, and it is essentially impossible to observe the primary process of charge-carrier generation directly (273).

Historically, dye sensitization of semiconductor electrodes was initially explored to elucidate the mechanism of silver halide sensitization (273, 274). Semiconductor electrodes were used to study the mechanism of charge transfer, because they provided a situation in which the flow of charge could be easily detected in the form of current. In general, low internal quantum yields for charge flow were observed for most dye-sensitized semiconductor surfaces. These low quantum yields were thought to result from surface states at the semiconductor/dye interface (275). Surface states are difficult to avoid with semiconductor materials, because the lattice must terminate at each low-index interface (276). In addition, surface states on oxide electrodes, such as ZnO or SnO_2, were in some cases attributed to hydrolyzed surfaces (275). The low quantum yields of such experiments made mechanistic comparisons to the highly efficient dye-sensitized photographic emulsions questionable, at best (270).

Later, as interest increased in the use of large band gap semiconductors in photoelectrochemical cells, dye sensitization experiments were performed with the hope of obtaining improved solar energy conversion efficiencies. Again, initial experiments in this area were not promising, due to low quantum yields. Matsumura et al. (277) and Alonso et al. (278) used rose bengal and rhodamine

B, as well as other dyes, to sensitize sintered ZnO electrodes to visible light. Although the spectral response of the ZnO was extended using this approach, the energy conversion efficiencies remained low (277, 278). A significant problem in these studies was incomplete light absorption, because a monolayer of dye attached to a smooth surface absorbed less than 1% of the incident monochromatic light (92, 279).

More recently, Spitler and Parkinson (275, 276, 280) focused on the use of the layer-type surfaces of layered MX_2 semiconductors (X = S, Se, or Te). These semiconductors were chosen with the hope of minimizing surface state densities at the semiconductor/dye interface. Hydrolyzed surface layers are not present on these materials and the semiconductors do not oxidize or react strongly with solvents (275). It was therefore believed that these systems would provide an abrupt interface between the energy bands of the semiconductor and the electronic states of the absorbed dye (275). Using this approach, Spitler and Parkinson demonstrated internal quantum yields as high as 0.6–0.8 with a variety of materials, including WS_2 (275, 280) (E_g= 1.30 eV), $MoSe_2$ (280) (E_g = 1.06 eV), WSe_2 (275) (E_g = 1.16 eV), and SnS_2 (276) (E_g = 2.2 eV). The most complete study was performed using SnS_2, where a series of dyes, with absorbance maxima varying from 520 to 835 nm, was used to sensitize the semiconductor (276). The high quantum yields were primarily attributed to the lack of bond termination defects, which allowed minimization of the surface state density (276). In some cases yields were believed to be increased through intercalation of the dyes, leading to many semiconductor/dye interfaces (270, 276).

Although the high internal quantum yields of the dichalcogenide electrodes are encouraging, a great deal of research remains before such electrodes can be of practical use. One remaining problem is the need to limit the amount of dye coverage. For example, Eichberger and Willig (281) found that the electron injection efficiency began to decrease when the dye coverage on a SnS_2 electrode reached about 0.1 monolayer. Thus, only limited dye coverages can be used, leading to a typical external quantum yield of only about 0.002 (270). In addition, supersensitizers must be present in solution to maintain high photocurrents (276).

Other researchers have taken a different approach to solving the problem of low solar energy conversion efficiencies from dye-sensitized semiconductors. Grätzel and co-workers (92) recently reported that polycrystalline anatase TiO_2, prepared to maximize its surface area, can yield solar energy conversion efficiencies of greater than 7%. By maximizing the surface area of the semiconductor, the area available for useful dye coverage was increased. The sensitizer with the highest quantum yield was $RuL_2[\mu\text{-}(CN)Ru(CN)bpy_2]_2$ (**II**), where L is bpy-4,4′-dicarboxylic acid (92). Using this dye, the absorbance onset of the semiconductor was shifted from about 450 to 750 nm, with the internal quantum

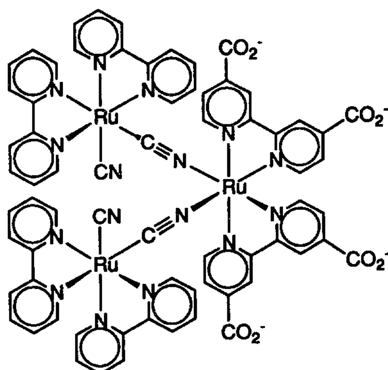

II

yields of the doped semiconductor being about 1.0 for wavelengths less than 550 nm (92).

In this anatase TiO_2 system, a series of dyes has been studied, many of which contain carboxylate groups that are thought to bind directly to the surface titanium atoms (282). The more efficient systems also require the presence of a reducing agent in solution, in order to quench the back-reaction of the oxidized dye with the injected electron. Thus, these regenerative systems can not yet be used for the production of chemical fuels. Experiments to date have generally used supersensitizers with complicated multiple electron redox chemistry, such as iodine (92, 269, 283, 284), bromine (285), hydroquinone (268, 269, 282, 286), and durohydroquinone (268). Parkinson and Spitler (270) showed, however, that the quoted efficiencies of electrodes sensitized with hydroquinone, for example, may be inaccurate due to the complicated redox chemistry of these molecules. Thus, these workers suggested the use of outer-sphere, single-electron reducing agents in future experiments, so that more precise quantum yields might be determined (270).

Once again, the definitions of quoted efficiencies should be carefully noted, as it has become popular in the area of dye sensitization to quote monochromatic light "efficiencies" (92). These numbers are actually monochromatic external quantum yields and should not be confused with energy conversion efficiencies. Although the ability to use dyes to sensitize large band gap semiconductors has vastly increased in recent years, the highest solar efficiency demonstrated thus far is about 7% (92). The corresponding monochromatic "light efficiency," actually an external quantum yield, reported in this same system is over 0.80 (92). The monochromatic quantum yield only gives information regarding the amount of current collected as a function of the number of absorbed photons, whereas the solar conversion efficiency incorporates all of the important quantities that are involved in creating stored power from incident sunlight. What-

ever these yields are named, they clearly represent an encouraging development, and indicate the need for continued efforts in this field.

A major difference between the two dye sensitization approaches outlined above is that, unlike the layer-type dichalcogenide electrodes, which have minimal surface roughness (270), the TiO_2 electrodes used by Grätzel and co-workers (269, 284) have been carefully prepared to maximize roughness. This roughness leads to such high coverages of dye that almost all incident light within the spectral range of the dye can be absorbed (270). The ability to use rough surfaces is also important in the context of surface states, because the quantum yields for dye sensitization on MX_2 semiconductors may be highly dependent on the presence of edges, steps, or other surface defects, which will affect both dye monomer aggregation and surface state formation (276). The anatase TiO_2 system does not suffer from this drawback, and thus appears to be a much more practically useful, but less well-defined, substrate for dye sensitization. In both approaches, substantial progress has been made within the past few years, and dye sensitization is again attracting widespread attention as a viable method of solar energy conversion.

VI. RECENT ADVANCES IN APPLICATIONS OF LARGE BAND GAP SEMICONDUCTOR/LIQUID JUNCTIONS

Throughout most of this chapter, we have concentrated on the use of semiconductor/liquid junction devices for conversion of solar energy to electricity or chemical fuels. While these efforts are extremely important and constitute a large fraction of research in this field, there have also been new developments in other areas of semiconductor photoelectrochemistry. Two particularly timely and important applications of semiconductor/liquid interfaces are toxic waste degradation and novel organic syntheses.

As previously described, the holes formed upon illumination of metal oxide semiconductors are powerful oxidizing agents. For example, in TiO_2, the redox potential of the valence band is about +3 V vs. Hydrogen Electrode Same Solution (HESS), so photogenerated holes in this material can readily oxidize Cl^- to Cl_2, can form OH radicals from water, or can directly oxidize aromatic organic compounds. Wide band gap semiconductors, especially TiO_2, have therefore been exploited to photocatalytically oxidize organic and inorganic compounds for synthetic and waste treatment applications. For these applications, aqueous suspensions of particles, rather than single-crystal electrodes, are often used due to their low cost and high surface area/volume ratio. These systems harness light energy not for generating electricity or chemical fuels, but for catalyzing useful chemical reactions. Solar energy conversion efficiencies, which have been the bane of solar cell researchers, are therefore not an

overriding performance criterion in these applications. Instead, stability of the semiconductor, efficacy of toxic waste amelioration, and ability to catalyze new organic reactions are more critical attributes of a successful system. So although semiconductor/liquid junctions are not yet being used in energy conversion applications, testing of toxic waste degradation systems in practical applications has already begun (287, 288). In Section VI, we discuss recent advances in the use of TiO_2 and other large band gap semiconductors for waste water detoxification and organic synthesis.

A. Photodegradation of Organic Waste Waters with Large Band Gap Semiconductors

Many studies have reported the use of aqueous suspensions of TiO_2 particles to photodegrade organic compounds often found in waste waters. Organic materials that have been shown to undergo degradation include halocarbons (289–292), pesticides (293, 294), and surfactants (295, 296), all of which pose environmental dangers. For many of these systems, the organic compounds are oxidized to CO_2, which can then be more safely released into the environment than the original material. For example, Pruden and Ollis (292) demonstrated the complete degradation of chloroform, an environmental pollutant, in aqueous suspensions of TiO_2.

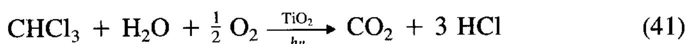

$$CHCl_3 + H_2O + \tfrac{1}{2}\,O_2 \xrightarrow[h\nu]{TiO_2} CO_2 + 3\,HCl \qquad (41)$$

Despite continuing research, the mechanisms for degradation of the organic compounds remain unclear. It appears, however, that both hole and electron-transfer processes are important in the degradation process. One of the major questions yet to be answered is the mechanism by which the organic species is oxidized. In general, two types of mechanisms have been proposed. The first is direct hole transfer to an organic substrate, which would lead to an unstable organic radical cation that could undergo subsequent decomposition reactions to ultimately yield CO_2. In this process, the initial organic substrate might either be adsorbed on the TiO_2 particles or near the particle surface (Fig. 25*a*). The second mechanism involves generation of $\cdot OH$ by the oxidation of hydroxyl groups on the TiO_2 surface (Fig. 25*b*). These radicals could then either remain on the surface or be released into solution prior to their participation in subsequent chemical reactions with the organic substrate. There is evidence from electron spin resonance spectroscopy to support the latter mechanism, because $\cdot OH$ have been detected in aqueous solutions of illuminated TiO_2 particles (296, 297). Hydroxylated intermediates have also been detected when illuminated TiO_2 particles were used to catalyze the oxidation of fluorinated aromatics (289).

It has also been argued, however, that a trapped hole on the TiO_2 surface

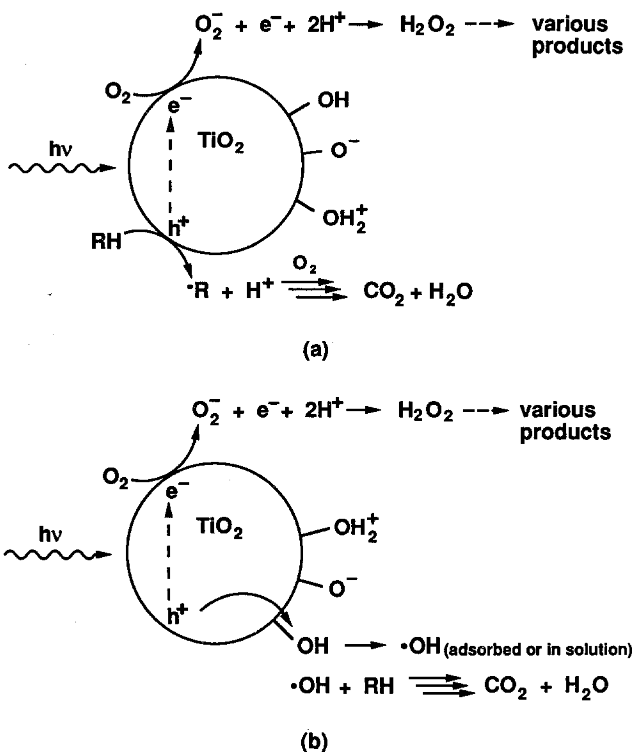

Figure 25. A schematic representation of the two proposed mechanisms of photooxidation of organic compounds on TiO_2 particles. The surface of TiO_2 in aqueous solutions is terminated by either O^-, OH, or OH_2^+ groups, with the relative proportions of each depending on the pH of the solution. The photogenerated electrons can be scavenged by molecular oxygen to form a superoxide anion (O_2^-). The resulting superoxide anion may then react with an organic species in solution, or pick up another electron to form H_2O_2, as shown. The H_2O_2 could then react with species in solution, or scavenge another electron to generate ·OH and anions. (*a*) A direct hole transfer mechanism. The hole reacts directly with an organic substrate, creating a radical intermediate that undergoes further reaction to CO_2. (*b*) Oxidation by ·OH. The photogenerated hole oxidizes an OH group on the surface and forms ·OH, which then reacts with the organic substrate (RH).

and a ·OH adsorbed on the TiO_2 surface are chemically indistinguishable, and therefore the relevant question involves whether or not the subsequent oxidation of the organic molecule occurs at the surface or in the solution (298). One study designed to probe this question found that ·OH that had been generated in solution using pulse radiolysis methods reacted at a diffusion controlled rate with TiO_2 surfaces (298). This reaction yielded species on the TiO_2 particles that were analogous to trapped holes (298). This result also implied that the

photocatalyzed oxidation of organics by $\cdot OH$ in solution was a minor process, because there must have been a large driving force for $\cdot OH$ to remain on the TiO_2 surface (298).

Evidence for the oxidation proceeding by adsorbed $\cdot OH$ was obtained in a recent study of the oxidation of chlorinated ethanes (290). Mao et al. (290) found that the rate of oxidation of a variety of organic substrates correlated with the C—H bond strengths of the organics. This result indicated that H atom abstraction by $\cdot OH$, rather than direct hole transfer, was an important factor in the rate-determining step for degradation. In this work, $C(NO_2)_4$ was also added to suppress the formation of $\cdot OH$ in solution, because the $C(NO_2)_4$ should prevent formation of $\cdot OH$ from reactions between H_2O and either the photogenerated electron or O_2^-. This reagent did not, however, change the yield of oxidation products, suggesting that adsorbed $\cdot OH$ was the active oxidant. When no hydrogen atoms were available for abstraction by $\cdot OH$, however, the authors argued that a direct hole transfer mechanism (photo-Kolbe reaction) was probably operative (290).

In contrast with the evidence presented thus far, one study failed to detect the $\cdot OH$ adducts that would be expected if $\cdot OH$ attack was the mechanism of oxidation. Draper and Fox (299) used diffuse reflectance flash photolysis to study reaction intermediates of 2,4,5-trichlorophenol, *N,N,N′,N′*-tetramethylene-*p*-phenylenediamine, and other organic and inorganic compounds. They observed products of oxidation that were expected to arise from a direct hole transfer mechanism (299). So although there is strong evidence for an $\cdot OH$ mechanism in several cases of importance, the issue remains somewhat controversial, and further work is needed to resolve this issue.

Another important chemical step in the photocatalyzed oxidation of organic substrates might be the reduction of an acceptor by photogenerated electrons in the TiO_2 particles. As previously mentioned, the hole is a powerful oxidizing agent and reacts effectively to oxidize organic species in solution. Unless the photogenerated electrons are also scavenged effectively, however, they will accumulate in the particle. This increased electron concentration will lead to increased recombination with the photogenerated holes and will result in decreased overall quantum yields for the photodegradation of toxic wastes. The electron acceptor most often employed is dioxygen, which is believed to act both as an electron scavenger and as a source of oxygen, so that the organic compounds may be oxidized completely to CO_2. Several investigators have found that degradation reactions do not proceed unless dioxygen is present (290, 291, 300), but the rate of oxidation becomes essentially independent of the concentration of O_2 near (291) or below (301, 302) air saturation.

A model recently proposed by Gerischer and Heller (303, 304), however, suggests that the electron-transfer rate to O_2 may be slow. If this is the case, the resulting accumulation of electrons in the semiconductor would lead to in-

creased recombination of carriers in the particle. This recombination would then limit the yield and rate of oxidative degradation of organic substrates. Gerischer and Heller (303, 304) propose, therefore, that catalysis of oxygen reduction is needed to achieve high conversion efficiencies on TiO_2 particles. Gerischer has suggested that Pt deposits on TiO_2 particles improve electron–hole pair separation and thus reduce losses due to recombination (305). In related work, several investigations have been directed towards the deposition of Pt and of other metals onto the surfaces of TiO_2 particles (306–308). While many of these experiments were directed at improving energy conversion efficiencies for the photoelectrolysis of H_2O, some of these results may also be relevant for use in toxic waste degradation. Although much work must be done before we fully understand the mechanisms involved in toxic waste amelioration, these metal oxide-based devices are an important application of semiconductor photoelectrochemistry, and several systems are currently being tested for use in large scale, low-cost waste water treatment applications (287, 288).

B. Use of Large Band Gap Semiconductors to Catalyze New Synthetic Oxidation Reactions

In waste treatment applications, the goal of oxidative reactions that are mediated by semiconductor surfaces is to mineralize the substrate completely to CO_2. Photocatalytic oxidation can also be utilized more selectively, however, to accomplish specific oxidative reactions. A survey of known reactions can be found in *Photocatalysis: Fundamentals and Applications*, Chapter 13 and references cited therein (309). One of the most important issues in ''photocatalytic'' (overall exoergic) or ''photosynthetic'' (overall endoergic) (25) reactions at semiconductors is selectivity. Clearly, these reactions will only be useful if they impart new or greater selectivity than other known methods of oxidation. When semiconductor particles are the reaction catalysts, selectivity can be obtained by controlling the nature of the semiconductor, solvent, and electron acceptor.

One avenue for controlling reactivity is the choice of the semiconductor itself. Different semiconductors have different valence and conduction band positions and, therefore, have different oxidizing and reducing capabilities. There are also differences in surface properties that may lead to different reactivities. An example of the selectivity imparted by the choice of semiconductor is the photocatalytic reaction of α-hydroxycarboxylic acids (53). Harada et al. (53) found that when the reaction of these compounds was catalyzed by TiO_2 particle suspensions or by TiO_2 electrodes, the majority of organic products resulted from decarboxylation. However, little or no decarboxylation was observed when CdS or ZnS particles were used as the photocatalysts. Instead, oxidation of the α-hydroxy group to form the corresponding keto acids was the major transformation. For example, in the oxidation of lactic acid, acetaldehyde was the ma-

jor product when Pt/TiO_2 particles were used, but pyruvic acid was the main product when Pt/CdS particles were present (Eq. 42).

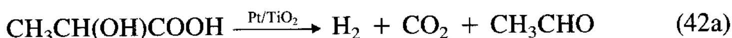

$$CH_3CH(OH)COOH \xrightarrow{Pt/TiO_2} H_2 + CO_2 + CH_3CHO \qquad (42a)$$

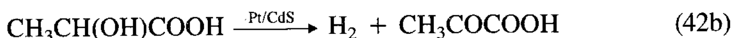

$$CH_3CH(OH)COOH \xrightarrow{Pt/CdS} H_2 + CH_3COCOOH \qquad (42b)$$

Because decarboxylation was also the major reaction observed at glassy carbon electrodes maintained at potentials well negative of the valence band of CdS, this study concluded that the two distinct reaction pathways resulted not from differences in the band edge positions of CdS and TiO_2, but rather from differences in adsorption and surface properties (53). This study illustrates the importance of the choice of semiconductor in photosynthetic applications.

Another potential advantage of using semiconductor particle systems instead of metal electrodes to perform oxidation reactions is the possibility of catalyzing 1 e^- oxidations at particles in cases where only 2 e^- oxidations are seen at metal electrodes (310). At metal electrodes, the oxidizing power is determined by the applied potential, and holes can be continuously supplied to the surface as fast as they are needed by the substrate. Thus, if the second oxidation process of a given substrate has a more negative oxidation potential than the first, the second electron will be removed at potentials where the first oxidation occurs, and the 1 e^- oxidation product will not be observed (310). However, when semiconductor particles are used to perform such oxidations, the flux of holes to the surface can be controlled. At low light intensities, therefore, it is possible to have the 1 e^- oxidation product diffuse away from the particle surface before it encounters another photogenerated hole on the same semiconductor particle (311). An example of this type of interesting process is given by Fox (311), in which the oxidation of vicinal diacids that undergo 2 e^- oxidations at metal electrodes has been shown to produce monodecarboxylated products at irradiated TiO_2 particles (Eq. 43).

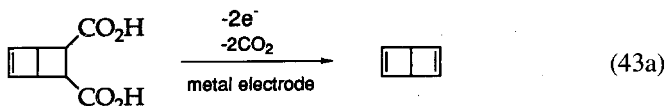

(43a)

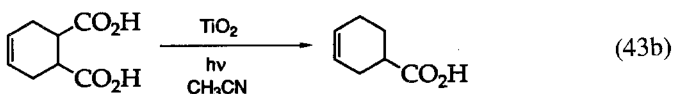

(43b)

In contrast to toxic waste degradation applications, which are generally performed in aqueous solutions, many photosynthetic and/or photocatalytic appli-

cations of TiO_2 are performed in inert organic solvents. Nonaqueous solvents can be used to prevent formation of, and subsequent indiscriminate oxidation by, $\cdot OH$ (25). In general, the mechanism of photooxidation of organic molecules in nonaqueous solvents appears to be direct hole transfer to form radical cations. For example, the photooxidation of toluene yields benzyl alcohol when TiO_2 particles are suspended in liquid toluene, whereas both benzyl alcohol and coupling products are observed when toluene is oxidized by aqueous suspensions of TiO_2 (25). Similarly, the oxidation of benzene using aqueous suspensions of TiO_2 yields some phenol, but the major isolated product is CO_2, which results from complete oxidation of the organic material (25 and references cited therein). Even when nonaqueous solvents are used, selectivity is an important issue, as radical cations are known to be very reactive. Useful chemistry will only result from these organic oxidation processes if the subsequent reactions can be controlled (311).

The choice of the electron acceptor can also be important in photosynthetic applications. As in photocatalyzed degradation processes, molecular oxygen can be used as an electron acceptor in photosynthetic applications. However, if O_2 or O_2^- interferes with the desired transformation, other acceptors, such as methyl viologen, can be employed to scavenge the conduction band electrons and to prevent deleterious electron–hole recombination on the photocatalyst particles (312). An example of this reaction is the Diels–Alder dimerization of 2,4-dimethyl-1,3-pentadiene, which has been accomplished at irradiated TiO_2 particle suspensions with methyl viologen as the electron acceptor (312). In this reaction, the use of O_2 as an electron acceptor would result in unwanted oxygenation side reactions, so the alternative electron acceptor is required to achieve the desired reaction products.

Because both the conduction band electrons and valence band holes generate reactive species at the semiconductor surface, it may be possible, by careful choice of donor and acceptor, to catalyze new transformations that involve the further reaction of these species. Thus, new reactions that are useful in organic synthetic methodology may result from the use of large band gap semiconductors as photocatalysts. To date, this aspect of semiconductor photoelectrochemistry has not been fully exploited, and it is likely that numerous novel applications of metal oxides will be developed as further investigations into their photocatalytic properties are performed.

VII. SUMMARY

During the past 15 years, a great deal of progress has been made in photoelectrochemical energy conversion. There are now numerous methods for obtaining stable cells, and the efficiencies of photoelectrochemical cells are pres-

ently competitive with other types of solar energy conversion systems. In fact, the efficiencies of these systems are sufficiently high that semiconductor/liquid junctions can not be ruled out as viable energy conversion technologies of the future. In this respect, research in this area has been a success.

However, many scientific problems still remain in the construction of stable, efficient photoelectrochemical cells. In aqueous solution, increased stability can be obtained by a variety of methods. Some of these have led to cell efficiencies of 15–16% in simple, stable systems. For other semiconductors, however, no stable, efficient systems have yet been identified in aqueous solution. For still others, such as n-GaAs, stable, efficient photoelectrochemical performance has been observed, but only in contact with very air-sensitive, highly toxic electrolytes, such as the KOH–Se_2^{2-}–Se^{2-} system. Therefore, generalization of any individual stabilization method does not yet appear possible.

Other strategies are maturing as well. Nonaqueous solvents have shown great promise for efficient generation of electrical power and for a fundamental understanding of semiconductor/liquid interfaces. Dye sensitization was once thought to be of limited utility for energy conversion, but recent advances in the field have generated renewed excitement for this type of approach. Other applications of photoelectrochemistry, including chemical sensors, toxic waste treatment, and organic synthesis are also gaining increased attention from researchers worldwide.

Clearly, the field of photoelectrochemistry will be valuable in a number of different areas. Enough of the principles of photoelectrochemistry are now understood to allow advances to be made in a rational, deliberate fashion. Control over surface chemistry is now within the realm of possibility, and new spectroscopic methods have dramatically increased the ability to probe, and manipulate, these interfaces on the molecular level. The combination of inorganic chemistry, solid state chemistry, electrochemistry, and photochemistry that is required to work in the area of photoelectrochemistry makes it a fascinating field in which to do research. Numerous challenges still lie ahead, and completion of our understanding of semiconductor/liquid interfaces will remain at the frontier of inorganic chemistry for years to come.

ABBREVIATIONS

AM	Air mass
aq	Aqueous solution
bcc	Body-centered cubic
bpy	2,2′-Bipyridine
Bu	Butyl
cb	Conduction band

Cp	Cyclopentadienyl
EDTA	Ethylenediaminetetraacetic acid
Fc	Ferrocene
fcc	Face-centered cubic
FDH	Formate dehydrogenase
HOMO	Highest occupied molecular orbital
LUMO	Lowest unoccupied molecular orbital
MO	Molecular orbital
MV	Methyl viologen
NHE	Normal hydrogen electrode
n-type	Doped with donors
phen	1,10-Phenanthroline
p-type	Doped with acceptors
R	Organic group
	External resistor
SCE	Standard calomel electrode
THF	Tetrahydrofuran
UV	Ultraviolet
vb	Valence band

SYMBOLS

A	Acceptor molecule	None
A	Absorbance	None
	Projected area of electrode	cm^2
A^-	Donor molecule	None
[A]	Concentration of acceptor	cm^{-3}
$[A^-]$	Concentration of donor	cm^{-3}
$[A]_s$	Concentration of acceptor at surface	cm^{-3}
$[A^-]_s$	Concentration of donor at surface	cm^{-3}
C	Constant	$A\ cm^3$
c	Concentration of absorbing species	M
Dye	Dye molecule	None
Dye*	Excited dye molecule	None
Dye^+	Oxidized dye molecule	None
E	Energy of incident photon	eV
	Electrochemical potential of the solution	eV
$\mathbf{E}^{o\prime}$	Formal electrochemical potential of the solution	eV
$\mathbf{E}_{cb}$	Conduction band edge energy	eV
$\mathbf{E}_F$	Fermi level energy	eV

$\mathbf{E}_{Fi}$	Intrinsic Fermi level energy	eV
$\mathbf{E}_{g}$	Semiconductor band gap energy	eV
$\mathbf{E}_{vb}$	Valence band edge energy	eV
E	Redox potential of the solution	V
$E^{\circ\prime}$	Formal redox potential of the solution	V
E_{cell}	Redox potential of the cell	V
$\mathcal{E}$	Electric field	V cm^{-1}
$\mathcal{E}_{max}$	Maximum electric field	V cm^{-1}
$\mathfrak{F}$	Faraday's constant	C $equiv^{-1}$
f	Fill factor	None
ΔG	Gibbs free energy change	J mol^{-1} K^{-1}
h	Planck's constant	J s
I	Transmitted light intensity	W cm^{-2}
	Current	A
I_0	Incident light intensity	W cm^{-2}
	Exchange current	A
I_{ph}	Photocurrent	A
I_{sc}	Short circuit current	A
$(IV)_{max}$	Maximum power point	W
J_{sc}	Short circuit current density	A cm^{-2}
K_w	Equilibrium constant for the dissociation of water	M^2
k	Boltzmann constant	eV K^{-1}
k_{et}	Electron-transfer rate constant at a semiconductor	cm^4 s^{-1}
k_{et}^{-1}	Reverse electron-transfer rate constant at a semiconductor	cm s^{-1}
ℓ	Optical path length	cm
N_a	Concentration of acceptor atoms	cm^{-3}
N_c	Effective density of states in the conduction band	cm^{-3}
N_d	Concentration of donor atoms	cm^{-3}
N_v	Effective density of states in the valence band	cm^{-3}
n	Electron concentration	cm^{-3}
n_b	Bulk electron concentration	cm^{-3}
n_e	Electrons per molecule oxidized or reduced	None
n_i	Equilibrium concentration of electrons in an intrinsic semiconductor	cm^{-3}
n_s	Surface electron concentration	cm^{-3}
n_{so}	Equilibrium surface electron concentration	cm^{-3}
P	Power	W
P_{in}	Input power	W

p	Hole concentration	cm^{-3}
p_i	Equilibrium concentration of holes in an intrinsic semiconductor	cm^{-3}
Q	Charge transferred per unit area	$C\ cm^{-2}$
q	Elementary charge	C
$q\phi_b$	Barrier height energy	eV
T	Transmittance	None
	Temperature	K
V	Voltage	V
V_{bi}	Built-in Voltage	V
qV_n	Energy difference between $\mathbf{E}_{cb}$ in the bulk of the semiconductor and $\mathbf{E}_F$	eV
V_{oc}	Open circuit voltage	V
V_R	Voltage drop across a resistor	V
W	Depletion width	cm
x	Distance	cm
α	Absorption coefficient	cm^{-1}
ε	Molar extinction coefficient	$M^{-1}\ cm^{-1}$
ε_s	Static dielectric constant	$\mathfrak{F}\ cm^{-1}$
μ_n	Electron mobility	$cm^2\ V^{-1}\ s^{-1}$
μ_p	Hole mobility	$cm^2\ V^{-1}\ s^{-1}$
ν	Frequency of light	s^{-1}
σ	Conductivity	$\Omega^{-1}\ cm^{-1}$
ϕ_b	Barrier height	V
ξ	Extent of reaction	mole

ACKNOWLEDGMENTS

We thank the National Science Foundation and the Department of Energy, Office of Basic Energy Sciences, for support of work in photoelectrochemistry. JMK acknowledges the National Science Foundation and STN acknowledges the Department of Defense, Office of Army Research for predoctoral graduate fellowships. The authors would like to thank Dr. W. C. A. Wilisch and Dr. R. Blumenthal for assistance, and Dr. B. J. Tufts, T. L. Longin, C. N. Kenyon, and G. A. Shreve for valuable comments on the manuscript. This is contribution 8718 from the Caltech Division of Chemistry and Chemical Engineering.

REFERENCES

1. E. Aharon-Shalom and A. Heller, *J. Electrochem. Soc.*, *129*, 2865 (1982).
2. J. F. Gibbons, G. W. Cogan, C. M. Gronet, and N. S. Lewis, *Appl. Phys. Lett.*, *45*, 1095 (1984).

3. B. J. Tufts, I. L. Abrahams, P. G. Santangelo, G. N. Ryba, L. G. Casagrande, and N. S. Lewis, *Nature (London)*, *326*, 861 (1987).
4. S. Licht and D. Peramunage, *Nature (London)*, *345*, 330 (1990).
5. D. M. Chapin, C. S. Fuller, and G. L. Pearson, *J. Appl. Phys.*, *25*, 676 (1954).
6. A. Cuevas, R. A. Sinton, N. E. Midkiff, and R. M. Swanson, *IEEE Trans. Electron. Devices*, *11*, 6 (1990).
7. P. E. Gruenbaum, J. Y. Gan, and R. M. Swanson, *Appl. Phys. Lett.*, *58*, 945 (1991).
8. J. M. Li, M. Chong, J. C. Zhu, Y. J. Li, J. D. Xu, P. D. Wang, Z. Q. Shang, Z. K. Yang, R. H. Zhu, and X. Cao, *Appl. Phys. Lett.*, *60*, 2240 (1992).
9. R. H. Fahrenbruch and A. L. Bube, *Fundamentals of Solar Cells*, Academic, New York, 1983.
10. H. O. Finklea, *Semiconductor Electrodes*, Elsevier, Amsterdam, 1988.
11. A. Heller, *Acc. Chem. Res.*, *14*, 154 (1981).
12. B. Parkinson, *Acc. Chem. Res.*, *17*, 431 (1984).
13. J. Amesz, in *Photosynthesis*, W. R. Briggs, Ed., from *Plant Biology*, N. S. Allen, Ed., Alan R. Liss, New York, 1989, Vol. 8, pp. 123–133.
14. Govindjee and M. R. Wasielewski, in *Photosynthesis*, W. R. Briggs, Ed., from *Plant Biology*, N. S. Allen, Ed., Alan R. Liss, New York, 1989, Vol. 8, pp. 71–103.
15. R. P. F. Gregory, *Photosynthesis*, Blackie & Son Ltd., Glasgow, Scotland, 1989.
16. P. A. Kohl and F. W. Ostermayer, *Annu. Rev. Mater. Sci.*, *19*, 379 (1989).
17. D. J. Elliott, *Integrated Circuit Fabrication Technology*, McGraw-Hill, New York, 1989.
18. D. G. Hafeman, J. W. Parce, and H. M. McConnell, *Science*, *240*, 1182 (1988).
19. N. F. de Rooij and H. H. van de Vlekkert, in *Chemical Sensor Technology*, N. Yamazoe, Ed., Kodansha, Ltd., Tokyo, Japan, 1991, pp. 213-231.
20. K. Rajeshwar, P. Singh, and J. DuBow, *Electrochim. Acta*, *23*, 1117 (1978).
21. M. S. Wrighton, *Acc. Chem. Res.*, *12*, 303 (1979).
22. A. J. Bard, *J. Photochem.*, *10*, 59 (1979).
23. R. Memming, *Electrochim. Acta*, *25*, 77 (1980).
24. R. Memming, in *Topics in Current Chemistry*, E. Steckhan, Ed., Springer-Verlag, New York, 1988, pp. 79–112.
25. M. A. Fox, *Acc. Chem. Res.*, *16*, 314 (1983).
26. M. A. Fox, in *Topics in Current Chemistry*, E. Steckhan, Ed., Springer-Verlag, New York, 1987, pp. 71–99.
27. H. Gerischer, *Angew. Chem. Int. Ed. Engl.*, *27*, 63 (1988).
28. H. Gerischer, *Electrochim. Acta*, *35*, 1677 (1990).
29. N. S. Lewis, *Acc. Chem. Res.*, *23*, 176 (1990).
30. C. A. Koval and J. N. Howard, *Chem. Rev.*, *92*, 411 (1992).
31. N. S. Lewis and M. Rosenbluth, in *Photocatalysis: Fundamentals and Applications*, N. Serpone and E. Pelizzetti, Eds., Wiley, New York, 1989, pp. 45–98.

32. H. O. Finklea, in *Semiconductor Electrodes*, H. O. Finklea, Ed., Elsevier, Amsterdam, 1988, pp. 43–145.
33. R. Hoffmann, *Angew. Chem. Int. Ed. Engl.*, *26*, 846 (1987).
34. R. Hoffmann, *Solids and Surfaces—A Chemist's View of Bonding in Extended Structures*, VCH Publishers, New York, 1988.
35. R. Hoffmann, *Rev. Mod. Phys.*, *60*, 601 (1988).
36. N. W. Ashcroft and N. D. Mermin, *Solid State Physics*, Holt, Rhinehart, and Winston, New York, 1976.
37. W. A. Harrison, *Solid State Theory*, Dover, New York, 1980.
38. C. Kittel and H. Kroemer, *Thermal Physics*, 2nd ed., W. H. Freeman, New York, 1980.
39. C. Kittel, *Introduction to Solid State Physics*, 6th ed., Wiley, New York, 1986.
40. F. Seitz, *The Modern Theory of Solids*, Dover, New York, 1987.
41. D. R. Goodstein, *States of Matter*, Dover, New York, 1980.
42. J. I. Pankove, *Optical Processes in Semiconductors*, Dover, New York, 1975.
43. S. M. Sze, *The Physics of Semiconductor Devices*, 2nd ed., Wiley, New York, 1981.
44. R. C. Weast, M. J. Astle, and W. H. Bayer, *Handbook of Chemistry and Physics*, 71st ed., CRC Press, Boca Raton, FL, 1991.
45. S. J. Fonash, *Solar Cell Device Physics*, Academic, New York, 1981.
46. S. Munnix and M. Schmeits, *Phys. Rev. Sect. B*, *28*, 7342 (1983).
47. K. Vos, *J. Phys. C: Solid State Phys.*, *10*, 3917 (1977).
48. J. B. Goodenough, *Prog. Solid State Chem.*, *5*, 145 (1971).
49. N. Daude, C. Gout, and C. Jouanim, *Phys. Rev. Sect. B*, *15*, 3229 (1977).
50. T. H. Lowry and K. S. Richardson, *Mechanism and Theory in Organic Chemistry*, 3rd ed., Harper & Row, New York, 1987.
51. J. P. Lowe, *Quantum Chemistry*, Academic, Orlando, FL, 1978.
52. H. H. Kung, H. S. Jarett, A. W. Sleight, and A. Ferretti, *J. Appl. Phys.*, *48*, 2463 (1977).
53. H. Harada, T. Ueda, and T. Sakata, *J. Phys. Chem.*, *93*, 1542 (1989).
54. R. D. Rauh, J. M. Buzby, T. F. Reise, and S. A. Alkaitis, *J. Phys. Chem.*, *83*, 2221 (1979).
55. D. E. Aspnes and A. Heller, *J. Phys. Chem.*, *87*, 4919 (1983).
56. M. A. Butler and D. S. Ginley, *J. Electrochem. Soc.*, *125*, 228 (1978).
57. J. O. McCaldin, T. C. McGill, and C. A. Mead, *J. Vac. Sci. Tech.*, *13*, 802 (1976).
58. M. Aven and C. A. Mead, *Appl. Phys. Lett.*, *7*, 8 (1965).
59. R. K. Swank, *Phys. Rev.*, *153*, 844 (1967).
60. K. Kajiyama, Y. Mizushimo, and S. Sakata, *Appl. Phys. Lett.*, *23*, 458 (1973).
61. J. O. McCaldin, T. C. McGill, and C. A. Mead, *Phys. Rev. Lett.*, *36*, 56 (1976).

62. R. Dingle, W. Wiegman, and C. H. Henry, *Phys. Rev. Lett.*, *33*, 827 (1974).
63. M. A. Butler and D. S. Ginley, *Chem. Phys. Lett.*, *47*, 319 (1977).
64. K. W. Frese, Jr., *J. Vac. Sci. Tech.*, *16*, 1042 (1979).
65. A. H. Nethercot, Jr., *Phys. Rev. Lett.*, *33*, 1088 (1974).
66. H. Tributsch, *Z. Naturforsch.*, *32A*, 972 (1977).
67. H. Tributsch, *Ber. Bunsenges. Phys. Chem.*, *81*, 361 (1977).
68. C. H. Henry, *J. Appl. Phys.*, *51*, 4494 (1980).
69. W. Shockley and H. J. Queisser, *J. Appl. Phys.*, *32*, 510 (1961).
70. APS, *Principal Conclusions of the American Physical Society Study Group on Solar Photovoltaic Energy Conversion*, American Physical Society, New York, 1979.
71. R. F. Pierret, *Semiconductor Fundamentals*, from *Modular Series on Solid State Devices*, Vol. 1, G. W. Neudeck and R. F. Pierret, Eds., 2nd ed., Addison-Wesley, Reading, MA, 1988.
72. H. Ibach and H. Luth, *Solid-State Physics*, Springer-Verlag, Berlin, Germany, 1990.
73. G. I. Roberts and C. R. Crowell, *Solid State Electron.*, *16*, 29 (1973).
74. J. S. Blakemore, *Semiconductor Statistics*, Dover, New York, 1987.
75. K. K. Thornber, *J. Appl. Phys.*, *51*, 2127 (1980).
76. G. W. Neudeck, *The PN Junction Diode*, from *Modular Series on Solid State Devices*, Vol. 2, G. W. Neudeck and R. F. Pierret, Eds., 2nd ed., Addison-Wesley, Reading, MA, 1989.
77. D. Halliday and R. Resnick, *Physics*, Wiley, New York, 1978.
78. A. J. Bard and L. R. Faulkner, *Electrochemical Methods: Fundamentals and Applications*, Wiley, New York, 1980, pp. 1–43.
79. A. J. Bard and L. R. Faulkner, *Electrochemical Methods: Fundamentals and Applications*, Wiley, New York, 1980, pp. 699–702.
80. H. Reiss and A. Heller, *J. Phys. Chem.*, *89*, 4207 (1985).
81. M. V. Rao, K. Rajeshwar, V. R. P. Verneker, and J. DuBow, *J. Phys. Chem.*, *84*, 1987 (1980).
82. S. R. Lunt, L. G. Casagrande, B. J. Tufts, and N. S. Lewis, *J. Phys. Chem.*, *92*, 5766 (1988).
83. S. R. Morrison, *Electrochemistry at Semiconductor and Oxidized Metal Electrodes*, Plenum, New York, 1980.
84. A. J. Bard, A. B. Bocarsly, F.-R. F. Fan, E. G. Walton, and M. S. Wrighton, *J. Am. Chem. Soc.*, *102*, 3671 (1980).
85. F.-R. F. Fan and A. J. Bard, *J. Am. Chem. Soc.*, *102*, 3677 (1980).
86. H. Gerischer, *Z. Phys. Chem. (Frankfurt/Main)*, *26*, 223 (1960).
87. H. Gerischer, *Adv. Electrochem. Electrochem. Engr.*, *1*, 139 (1961).
88. R. A. Marcus, *J. Chem. Phys.*, *43*, 679 (1965).
89. R. A. Marcus and N. Sutin, *Biochim. Biophys. Acta*, *811*, 265 (1985).

90. N. S. Lewis, *Annu. Rev. Phys. Chem.*, *42*, 543 (1991).
91. M. S. Wrighton, A. B. Ellis, P. T. Wolczanski, D. L. Morse, H. B. Abrahamson, and D. S. Ginley, *J. Am. Chem. Soc.*, *98*, 2774 (1976).
92. B. O'Regan and M. Grätzel, *Nature (London)*, *353*, 737 (1991).
93. H. Gerischer, *J. Electroanal. Chem. Interfacial Electrochem.*, *58*, 263 (1975).
94. R. Memming, in *Topics in Surface Chemistry*, E. Kay and P. S. Bagus, Eds., Plenum, New York, 1978, pp. 1–28.
95. W. H. Brattain and C. G. B. Garrett, *Bell Syst. Tech. J.*, *34*, 129 (1955).
96. R. Williams, *J. Chem. Phys.*, *32*, 1505 (1960).
97. D. R. Turner, *J. Electrochem. Soc.*, *103*, 252 (1956).
98. A. J. Nozik, *Annu. Rev. Phys. Chem.*, *29*, 189 (1978).
99. A. Fujishima and K. Honda, *Bull. Chem. Soc. Jpn.*, *44*, 1148 (1971).
100. A. Fujishima and K. Honda, *Nature (London)*, *238*, 37 (1972).
101. P. J. Boddy, *J. Electrochem. Soc.*, *115*, 199 (1968).
102. M. S. Wrighton, D. S. Ginley, P. T. Wolczanski, A. B. Ellis, D. L. Morse, and A. Linz, *Proc. Natl. Acad. Sci. USA*, *72*, 1518 (1975).
103. W. Gissler, P. L. Lensi, and S. Pizzini, *J. Appl. Electrochem.*, *6*, 9 (1976).
104. J. Keeney, D. H. Weinstein, and G. M. Haas, *Nature (London)*, *253*, 719 (1975).
105. R. D. Nasby and R. K. Quinn, *Mater. Res. Bull.*, *11*, 985 (1976).
106. J. H. Kennedy and K. W. Frese, Jr., *J. Electrochem. Soc.*, *123*, 1683 (1976).
107. M. Anderman and J. H. Kennedy, in *Semiconductor Electrodes*, H. O. Finklea, Ed., Elsevier, Amsterdam, The Netherlands, 1988, pp. 147–202.
108. G. Bin-Daar, M. P. Dare-Edwards, J. B. Goodenough, and A. Hamnett, *J. Chem. Soc., Faraday Trans.*, *1*, *79*, 1199 (1983).
109. K. Rajeshwar, *J. Appl. Electrochem.*, *15*, 1 (1985).
110. J. B. Goodenough, A. Hamnett, M. P. Dare-Edwards, G. Campet, and R. D. Wright, *Surf. Sci.*, *101*, 531 (1980).
111. A. K. Ghosh and H. P. Maruska, *J. Electrochem. Soc.*, *124*, 1516 (1977).
112. J. F. Houlihan, D. B. Armitage, T. Hoovler, D. Bonaquist, D. P. Madacsi, and L. N. Mulay, *Mater. Res. Bull.*, *13*, 1205 (1978).
113. H. Gerischer and J. Gobrecht, *Ber. Bunsenges. Phys. Chem.*, *80*, 327 (1976).
114. A. Fujishima, E. Sugiama, and K. Honda, *Bull. Chem. Soc. Jpn.*, *44*, 304 (1971).
115. K. W. Frese, Jr., *Appl. Phys. Lett.*, *40*, 275 (1982).
116. H.-D. Rubin, B. D. Humphrey, and A. B. Bocarsly, *Nature (London)*, *308*, 339 (1984).
117. A. B. Ellis, S. W. Kaiser, and M. S. Wrighton, *J. Am. Chem. Soc.*, *98*, 1635 (1976).
118. G. Hodes, J. Manassen, and D. Cahen, *Nature (London)*, *261*, 403 (1976).
119. B. Miller and A. Heller, *Nature (London)*, *262*, 680 (1976).
120. R. D. Rauh, *Stud. Phys. Theor. Chem.*, *55*, 277 (1988).

121. S. Licht, *J. Phys. Chem.*, *90*, 1096 (1986).
122. G. Hodes, *Nature (London)*, *285*, 29 (1980).
123. S. Licht, R. Tenne, G. Dagan, G. Hodes, J. Manassen, D. Cahen, R. Triboulet, J. Rioux, and C. Levy-Clement, *Appl. Phys. Lett.*, *46*, 608 (1985).
124. S. Licht, G. Hodes, R. Tenne, and J. Manassen, *Nature (London)*, *326*, 863 (1987).
125. A. B. Ellis, S. W. Kaiser, and M. S. Wrighton, *J. Am. Chem. Soc.*, *98*, 6418 (1976).
126. A. B. Ellis, S. W. Kaiser, J. M. Bolts, and M. S. Wrighton, *J. Am. Chem. Soc.*, *99*, 2839 (1977).
127. D. Cahen, G. Hodes, and J. Manassen, *J. Electrochem. Soc.*, *125*, 1623 (1978).
128. A. Heller, G. P. Schwartz, R. G. Vadimsky, S. Menezes, and B. Miller, *J. Electrochem. Soc.*, *125*, 1156 (1978).
129. H.-D. Rubin, D. J. Arent, and A. B. Bocarsly, *J. Electrochem. Soc.*, *132*, 523 (1985).
130. H.-D. Rubin, D. J. Arent, B. D. Humphrey, and A. B. Bocarsly, *J. Electrochem. Soc.*, *134*, 93 (1987).
131. G. Seshadri, J. K. M. Chun, and A. B. Bocarsly, *Nature (London)*, *352*, 508 (1991).
132. S. Licht and D. Peramunage, *Nature (London)*, *354*, 440 (1991).
133. S. Licht and D. Peramunage, *J. Electrochem. Soc.*, *139*, L23 (1992).
134. A. B. Bocarsly, *J. Electrochem. Soc.*, *139*, 1791 (1992).
135. S. Licht and D. Peramunage, *J. Electrochem. Soc.*, *139*, 1792 (1992).
136. M. J. Natan, J. W. Thackeray, and M. S. Wrighton, *J. Phys. Chem.*, *90*, 4089 (1986).
137. J. W. Thackeray, M. J. Natan, P. Ng, and M. S. Wrighton, *J. Am. Chem. Soc.*, *108*, 3570 (1986).
138. J. J. Hickman and M. S. Wrighton, *J. Am. Chem. Soc.*, *113*, 4440 (1991).
139. E. Yablonovitch, C. J. Sandroff, R. Bhat, and T. Gmitter, *Appl. Phys. Lett.*, *51*, 439 (1987).
140. C. J. Sandroff, M. S. Hegde, L. A. Farrow, C. C. Chang, and J. P. Harbison, *Appl. Phys. Lett.*, *54*, 362 (1989).
141. C. J. Sandroff, M. S. Hegde, L. A. Farrow, R. Bhat, J. P. Harbison, and C. C. Chang, *J. Appl. Phys.*, *67*, 586 (1990).
142. A. B. Ellis, J. M. Bolts, S. W. Kaiser, and M. S. Wrighton, *J. Am. Chem. Soc.*, *99*, 2848 (1977).
143. K. C. Chang, A. Heller, B. Schwartz, S. Menezes, and B. Miller, *Science*, *196*, 1097 (1977).
144. A. B. Ellis, J. M. Bolts, and M. S. Wrighton, *J. Electrochem. Soc.*, *124*, 1603 (1977).
145. W. S. Hobson and A. B. Ellis, *Appl. Phys. Lett.*, *41*, 891 (1982).

146. C. M. Gronet and N. S. Lewis, *J. Phys. Chem.*, *99*, 1310 (1984).
147. W. S. Hobson, P. B. Johnson, A. B. Ellis, and R. M. Biefeld, *Appl. Phys. Lett.*, *45*, 150 (1984).
148. P. B. Johnson, A. B. Ellis, R. M. Biefeld, and D. S. Ginley, *Appl. Phys. Lett.*, *47*, 877 (1985).
149. L. G. Casagrande, B. J. Tufts, and N. S. Lewis, *J. Phys. Chem.*, *95*, 1373 (1991).
150. C. P. Kubiak, L. F. Schneemeyer, and M. S. Wrighton, *J. Am. Chem. Soc.*, *102*, 6898 (1980).
151. L. F. Schneemeyer and B. Miller, *J. Electrochem. Soc.*, *129*, 1977 (1982).
152. P. Allongue, P. Cachet, P. Clechet, M. Froment, J. R. Martin, and E. Verney, *J. Electrochem. Soc.*, *134*, 620 (1987).
153. L. F. Schneemeyer, J. M. Rosamilia, and B. Miller, *J. Electrochem. Soc.*, *134*, 2767 (1987).
154. F.-R. F. Fan, B. L. Wheeler, A. J. Bard, and R. N. Noufi, *J. Electrochem. Soc.*, *128*, 2042 (1981).
155. H. Tributsch, *Faraday Discuss. Chem. Soc.*, *70*, 189 (1980).
156. J. Gobrecht, H. Gerischer, and H. Tributsch, *Ber. Bunsenges. Phys. Chem.*, *82*, 1331 (1978).
157. B. L. Wheeler, J. K. Leland, and A. J. Bard, *J. Electrochem. Soc.*, *133*, 358 (1986).
158. S. Piazza, H.-M. Kühne, and H. Tributsch, *J. Electroanal. Chem. Interfacial Electrochem.*, *196*, 53 (1985).
159. W. Jaegermann and H. Tributsch, *Prog. Surf. Sci.*, *29*, 1 (1988).
160. A. Ennaoui, S. Fiechter, W. Jaegermann, and H. Tributsch, *J. Electrochem. Soc.*, *133*, 97 (1986).
161. A. Ennaoui and H. Tributsch, *J. Electroanal. Chem. Interfacial Electrochem.*, *204*, 185 (1986).
162. L. F. Schneemeyer and M. S. Wrighton, *J. Am. Chem. Soc.*, *102*, 6964 (1980).
163. W. Kautek, J. Gorbrecht, and H. Gerischer, *Ber. Bunsenges. Phys. Chem.*, *84*, 1034 (1980).
164. H. J. Lewerenz, A. Heller, and F. J. DiSalvo, *J. Am. Chem. Soc.*, *102*, 1877 (1980).
165. F.-R. F. Fan, H. S. White, B. L. Wheeler, and A. J. Bard, *J. Am. Chem. Soc.*, *102*, 5142 (1980).
166. G. Kline, K. Kam, D. Canfield, and B. A. Parkinson, *Sol. Energy Mater.*, *4*, 301 (1981).
167. G. Kline, K. Kam, R. Ziegler, and B. A. Parkinson, *Sol. Energy Mater.*, *6*, 337 (1982).
168. J. A. Baglio, G. S. Calabrese, D. J. Harrison, E. Kamieniecki, A. J. Ricco, M. S. Wrighton, and G. D. Zoski, *J. Am. Chem. Soc.*, *105*, 2246 (1983).
169. H. Gerischer and I. Mattes, *Z. Phys. Chem. (Frankfurt/Main)*, *49*, 112 (1966).

170. J. M. Bolts, A. B. Ellis, K. D. Legg, and M. S. Wrighton, *J. Am. Chem. Soc.*, *99*, 4826 (1977).
171. M. Tomkiewicz and J. M. Woodall, *Science*, *196*, 990 (1977).
172. K. Ohashi, J. McCann, and J. O. Bockris, *Nature (London)*, *266*, 610 (1977).
173. A. B. Bocarsly, D. C. Bookbinder, R. N. Dominey, N. S. Lewis, and M. S. Wrighton, *J. Am. Chem. Soc.*, *102*, 3683 (1980).
174. J. Bardeen, *Phys. Rev.*, *71*, 717 (1947).
175. C. A. Mead and W. G. Spitzer, *Phys. Rev. Sect. A*, *134*, 713 (1964).
176. A. Heller, H. J. Lewerenz, and B. Miller, *J. Am. Chem. Soc.*, *103*, 200 (1980).
177. A. Heller, B. Miller, and F. A. Thiel, *Appl. Phys. Lett.*, *38*, 282 (1981).
178. A. Heller, B. Miller, H. J. Lewerenz, and K. J. Bachmann, *J. Am. Chem. Soc.*, *102*, 6555 (1980).
179. A. Heller, *Pure Appl. Chem.*, *58*, 1189 (1986).
180. A. Heller and R. G. Vadimsky, *Phys. Rev. Lett.*, *46*, 1153 (1981).
181. A. Heller, E. Aharon-Shalom, W. A. Bonner, and B. Miller, *J. Am. Chem. Soc.*, *104*, 6942 (1982).
182. H. Halmann, *Nature (London)*, *275*, 115 (1978).
183. S. Ikeda, Y. Saito, M. Yoshida, H. Noda, M. Maeda, and K. Ito, *J. Electroanal. Chem. Interfacial Electrochem.*, *260*, 335 (1989).
184. B. Aurian-Blajeni, I. Taniguchi, and J. O. Bockris, *J. Electroanal. Chem. Interfacial Electrochem.*, *149*, 291 (1983).
185. L. Junfu and C. Baozhu, *J. Electroanal. Chem. Interfacial Electrochem.*, *324*, 191 (1992).
186. I. Taniguchi, B. Aurian-Blajeni, and J. O. Bockris, *J. Electroanal. Chem. Interfacial Electrochem.*, *161*, 385 (1984).
187. M. Zafrir, M. Ulman, Y. Zuckerman, and H. Halmann, *J. Electroanal. Chem. Interfacial Electrochem.*, *159*, 373 (1983).
188. D. Canfield and K. W. Frese, Jr., *J. Electrochem. Soc.*, *130*, 1772 (1983).
189. M. H. Schmidt, G. M. Miskelly, and N. S. Lewis, *J. Am. Chem. Soc.*, *112*, 3420 (1990).
190. B. A. Parkinson and P. F. Weaver, *Nature (London)*, *309*, 148 (1984).
191. S. N. Frank and A. J. Bard, *J. Am. Chem. Soc.*, *97*, 7427 (1975).
192. D. Laser and A. J. Bard, *J. Phys. Chem.*, *80*, 459 (1976).
193. A. J. Bard and M. S. Wrighton, *J. Electrochem. Soc.*, *124*, 1706 (1977).
194. K. L. Legg, A. B. Ellis, J. M. Bolts, and M. S. Wrighton, *Proc. Natl. Acad. Sci. USA*, *74*, 4116 (1977).
195. J. M. Bolts and M. S. Wrighton, *J. Am. Chem. Soc.*, *100*, 5257 (1978).
196. K. Nakatani, S. Matsudaira, and H. Tsubomura, *J. Electrochem. Soc.*, *125*, 406 (1978).
197. P. A. Kohl and A. J. Bard, *J. Electrochem. Soc.*, *126*, 598 (1979).

198. P. A. Kohl and A. J. Bard, *J. Electrochem. Soc.*, *126*, 59 (1979).
199. P. A. Kohl and A. J. Bard, *J. Electrochem. Soc.*, *126*, 603 (1979).
200. P. A. Kohl and A. J. Bard, *J. Am. Chem. Soc.*, *99*, 7531 (1977).
201. C. M. Gronet and N. S. Lewis, *Nature (London)*, *300*, 733 (1982).
202. J. S. Curran, *J. Electrochem. Soc.*, *127*, 2023 (1980).
203. L. F. Schneemeyer and M. S. Wrighton, *J. Am. Chem. Soc.*, *101*, 6496 (1979).
204. W. Kautek and H. Gerischer, *Ber. Bunsenges. Phys. Chem.*, *84*, 645 (1980).
205. H. S. White, F.-R. F. Fan, and A. J. Bard, *J. Electrochem. Soc.*, *128*, 1045 (1981).
206. G. Nagasubramanian, B. L. Wheeler, G. A. Hope, and A. J. Bard, *J. Electrochem. Soc.*, *130*, 385 (1983).
207. C. M. Gronet, N. S. Lewis, G. Cogan, and J. Gibbons, *Proc. Natl. Acad. Sci. USA*, *80*, 1152 (1983).
208. M. L. Rosenbluth, C. M. Lieber, and N. S. Lewis, *Appl. Phys. Lett.*, *45*, 423 (1984).
209. M. L. Rosenbluth and N. S. Lewis, *J. Am. Chem. Soc.*, *108*, 4689 (1986).
210. C. M. Gronet and N. S. Lewis, *Appl. Phys. Lett.*, *43*, 115 (1983).
211. M. J. Heben, A. Kumar, C. Zheng, and N. S. Lewis, *Nature (London)*, *340*, 621 (1989).
212. L. G. Casagrande and N. S. Lewis, *J. Am. Chem. Soc.*, *107*, 5793 (1985).
213. R. N. Dominey, N. S. Lewis, and M. S. Wrighton, *J. Am. Chem. Soc.*, *103*, 1261 (1981).
214. N. S. Lewis, *J. Electrochem. Soc.*, *131*, 2496 (1984).
215. P. R. Segar and C. A. Koval, *J. Electrochem. Soc.*, *135*, 2655 (1988).
216. P. R. Segar, C. A. Koval, B. E. Koel, and S. C. Gebhard, *J. Electrochem. Soc.*, *137*, 544 (1990).
217. C. A. Koval and J. B. Olson, *J. Phys. Chem.*, *92*, 6726 (1988).
218. T. Kendelewicz, W. G. Pietro, I. Lindau, and W. E. Spicer, *Appl. Phys. Lett.*, *44*, 1066 (1984).
219. N. Newman, T. Kendelewicz, L. Bowman, and W. E. Spicer, *Appl. Phys. Lett.*, *46*, 1176 (1985).
220. C. M. Lieber, C. M. Gronet, and N. S. Lewis, *Nature (London)*, *307*, 533 (1984).
221. R. T. Ross and A. J. Nozik, *J. Appl. Phys.*, *53*, 3813 (1982).
222. A. J. Nozik and F. Williams, *Nature (London)*, *312*, 21 (1984).
223. G. Cooper, J. A. Turner, B. A. Parkinson, and A. J. Nozik, *J. Appl. Phys.*, *54*, 6463 (1983).
224. C. A. Koval and P. R. Segar, *J. Am. Chem. Soc.*, *111*, 2004 (1989).
225. C. A. Koval and P. R. Segar, *J. Phys. Chem.*, *94*, 2033 (1990).
226. B. K. Ridley, *Rep. Prog. Phys.*, *54*, 169 (1991).
227. R. Cingolani and K. Ploog, *Adv. Phys.*, *40*, 535 (1991).

228. B. A. Parkinson, T. E. Furtak, D. Canfield, K.-K. Kam, and G. Kline, *Faraday Discuss. Chem. Soc.*, *70*, 233 (1980).
229. G. Razzini, L. P. Bicelli, G. Pini, and B. Scrosati, *J. Electrochem. Soc.*, *128*, 2134 (1981).
230. X. P. Li, N. A. Vante, and H. Tributsch, *J. Electroanal. Chem. Interfacial Electrochem.*, *242*, 255 (1988).
231. B. J. Skromme, C. J. Sandroff, E. Yablonovitch, and T. Gmitter, *Appl. Phys. Lett.*, *51*, 2022 (1987).
232. S. Gayen, W. C. Ermler, and C. J. Sandroff, *J. Phys. Chem.*, *95*, 7357 (1991).
233. S. R. Lunt, G. N. Ryba, P. G. Santangelo, and N. S. Lewis, *J. Appl. Phys.*, *70*, 7449 (1991).
234. S. R. Lunt, P. G. Santangelo, and N. S. Lewis, *J. Vac. Sci. Technol.*, *B*, *9*, 2333 (1991).
235. C. W. Sheen, J.-X. Shi, J. Mårtensson, A. N. Parikh, and D. L. Allara, *J. Am. Chem. Soc.*, *114*, 1514 (1992).
236. O. S. Nakagawa, S. Ashok, C. W. Sheen, J. Märtensson, and D. L. Allara, *Jpn. J. Appl. Phys.*, *30*, 3759 (1991).
237. C. J. Sandroff, F. S. Turco-Sandroff, L. T. Florez, and J. P. Harbison, *J. Appl. Phys.*, *70*, 3632 (1991).
238. K. Uosaki, Y. Shigematsu, H. Kita, and Y. Umezawa, *Anal. Chem.*, *61*, 1980 (1989).
239. C. J. Murphy and A. B. Ellis, *J. Phys. Chem.*, *94*, 3082 (1990).
240. J. Z. Zhang and A. B. Ellis, *J. Phys. Chem.*, *96*, 2700 (1992).
241. G. J. Meyer, G. C. Lisensky, and A. B. Ellis, *J. Am. Chem. Soc.*, *110*, 4914 (1988).
242. G. C. Lisensky, R. L. Penn, C. J. Murphy, and A. B. Ellis, *Science*, *248*, 840 (1990).
243. G. J. Meyer, L. K. Leung, J. C. Yu, G. C. Lisensky, and A. B. Ellis, *J. Am. Chem. Soc.*, *111*, 5146 (1989).
244. C. J. Murphy and A. B. Ellis, *Polyhedron*, *9*, 1913 (1990).
245. C. J. Murphy, G. C. Lisensky, L. K. Leung, G. R. Kowach, and A. B. Ellis, *J. Am. Chem. Soc.*, *112*, 8344 (1990).
246. A. Henglein, *Chem. Rev.*, *89*, 1861 (1989).
247. M. L. Steigerwald and L. E. Brus, *Annu. Rev. Mater. Sci.*, *19*, 471 (1989).
248. M. L. Steigerwald and L. E. Brus, *Acc. Chem. Res.*, *23*, 183 (1990).
249. T. Dannhauser, M. O'Neil, K. Johansson, D. Whitten, and G. McLendon, *J. Phys. Chem.*, *90*, 6074 (1986).
250. B. A. Parkinson, A. Heller, and B. Miller, *Appl. Phys. Lett.*, *33*, 521 (1978).
251. B. A. Parkinson, A. Heller, and B. Miller, *J. Electrochem. Soc.*, *126*, 954 (1979).
252. B. J. Tufts, I. L. Abrahams, L. G. Casagrande, and N. S. Lewis, *J. Phys. Chem.*, *93*, 3260 (1989).

253. R. J. Nelson, J. S. Williams, H. J. Leamy, B. Miller, H. C. Casey, Jr., B. A. Parkinson, and A. Heller, *Appl. Phys. Lett.*, *36*, 76 (1980).
254. P. Allongue and H. Cachet, *J. Electrochem. Soc.*, *131*, 2861 (1984).
255. G. N. Ryba, Ph.D. Thesis, ''Time-Resolved Photoluminescence Studies of Metal Ion Treated n-GaAs in Electrolytes,'' California Institute of Technology, Pasadena, CA, 1992.
256. M. X. Tan, C. Newcomb, A. Kumar, S. R. Lunt, M. J. Sailor, B. J. Tufts, and N. S. Lewis, *J. Phys. Chem.*, *95*, 10133 (1991).
257. B. J. Tufts, I. L. Abrahams, C. E. Caley, S. R. Lunt, G. M. Miskelly, M. J. Sailor, P. G. Santangelo, N. S. Lewis, A. L. Roe, and K. O. Hodgson, *J. Am. Chem. Soc.*, *112*, 5123 (1990).
258. A. Heller, H. J. Leamy, B. Miller, and W. D. Johnson, Jr., *J. Phys. Chem.*, *87*, 3239 (1983).
259. J. M. Bolts and M. S. Wrighton, *J. Am. Chem. Soc.*, *101*, 6179 (1979).
260. M. S. Wrighton, R. G. Austin, A. B. Bocarsly, J. M. Bolts, O. Haas, K. D. Legg, L. Nadjo, and M. C. Palazzotto, *J. Am. Chem. Soc.*, *100*, 1602 (1978).
261. J. M. Bolts, A. B. Bocarsly, M. C. Palazzotto, E. G. Walton, N. S. Lewis, and M. S. Wrighton, *J. Am. Chem. Soc.*, *101*, 1378 (1979).
262. A. B. Bocarsly, E. G. Walton, and M. S. Wrighton, *J. Am. Chem. Soc.*, *102*, 3390 (1980).
263. N. S. Lewis, A. B. Bocarsly, and M. S. Wrighton, *J. Phys. Chem.*, *84*, 2033 (1980).
264. S. Chao, J. L. Robbins, and M. S. Wrighton, *J. Am. Chem. Soc.*, *105*, 181 (1983).
265. R. N. Dominey, N. S. Lewis, J. A. Bruce, D. C. Bookbinder, and M. S. Wrighton, *J. Am. Chem. Soc.*, *104*, 467 (1982).
266. N. S. Lewis and M. S. Wrighton, *Science*, *211*, 944 (1981).
267. H. Van Ryswyk and A. B. Ellis, *J. Am. Chem. Soc.*, *108*, 2454 (1986).
268. R. Dabestani, A. J. Bard, A. Campion, M. A. Fox, T. E. Mallouk, S. E. Webber, and J. M. White, *J. Phys. Chem.*, *92*, 1872 (1988).
269. N. Vlachopoulos, P. Liska, A. J. McEvoy, and M. Grätzel, *Surf. Sci.*, *189/190*, 823 (1987).
270. B. A. Parkinson and M. T. Spitler, *Electrochim. Acta*, *37*, 943 (1992).
271. R. K. Bunting, *The Chemistry of Photography*, Photoglass Press, Normal, IL, 1987.
272. W. West and P. B. Gilman, Jr., in *The Theory of the Photographic Process*, 4th ed., T. H. James, Ed., Macmillan, New York, 1977, pp. 251–290.
273. H. Gerischer and B. Bressel, *Ber. Bunsenges. Phys. Chem.*, *89*, 1083 (1985).
274. R. Memming, *Photochem. Photobiol.*, *16*, 325 (1972).
275. M. Spitler and B. A. Parkinson, *Langmuir*, *2*, 549 (1986).
276. B. A. Parkinson, *Langmuir*, *4*, 967 (1988).
277. M. Matsumura, Y. Nomura, and H. Tsubomura, *Bull. Chem. Soc. Jpn.*, *50*, 2533 (1977).

278. N. Alonso, V. M. Beley, P. Chartier, and V. Ern, *Rev. Phys. Appl.*, *16*, 5 (1981).
279. M. D. Archer, *J. Appl. Electrochem.*, *5*, 17 (1975).
280. M. T. Spitler, *J. Electroanal. Chem. Interfacial Electrochem.*, *228*, 69 (1987).
281. R. Eichberger and F. Willig, *Chem. Phys.*, *141*, 159 (1990).
282. K. Kalyanasundaram, N. Vlachopoulos, V. Krishnan, A. Monnier, and M. Grätzel, *J. Phys. Chem.*, *91*, 2342 (1987).
283. O. Enea, J. Moser, and M. Grätzel, *J. Electroanal. Chem. Interfacial Electrochem.*, *259*, 59 (1989).
284. H. Frei, D. J. Fitzmaurice, and M. Grätzel, *Langmuir*, *6*, 198 (1990).
285. N. Vlachopoulos, P. Liska, J. Augustynski, and M. Grätzel, *J. Am. Chem. Soc.*, *110*, 1216 (1988).
286. E. Vrachnou, M. Grätzel, and A. J. McEvoy, *J. Electroanal. Chem. Interfacial Electrochem.*, *258*, 193 (1989).
287. Y. M. Xu, P. E. Ménassa, and C. H. Langford, *Chemosphere*, *17*, 1971 (1988).
288. H. Al-Ekabi, A. Safarzadeh-Amiri, W. Sifton, and J. Story, *Inter. J. Environ. Pollution*, *1*, 125 (1991).
289. C. Minero, C. Aliberti, E. Pelizzetti, R. Terzian, and N. Serpone, *Langmuir*, *7*, 928 (1991).
290. Y. Mao, C. Schöneich, and K.-D. Asmus, *J. Phys. Chem.*, *95*, 10080 (1991).
291. C. Kormann, D. W. Bahnemann, and M. R. Hoffmann, *Environ. Sci. Technol.*, *25*, 494 (1991).
292. A. L. Pruden and D. F. Ollis, *Environ. Sci. Technol.*, *17*, 628 (1983).
293. E. Pelizzetti, C. Minero, V. Carlin, M. Vincenti, and E. Pramauro, *Chemosphere*, *24*, 891 (1992).
294. H. Hidaka, K. Nohara, J. Zhao, N. Serpone, and E. Pelizzetti, *J. Photochem. Photobiol. A*, *64*, 247 (1992).
295. H. Hidaka, H. Kubota, M. Grätzel, N. Serpone, and E. Pelizzetti, *Nouv. J. Chim.*, *9*, 67 (1985).
296. H. Hidaka, J. Zhao, K. Kitamura, K. Nohara, N. Serpone, and E. Pelizzetti, *J. Photochem. Photobiol. A*:, *64*, 103 (1992).
297. C. D. Jaeger and A. J. Bard, *J. Phys. Chem.*, *83*, 3146 (1979).
298. D. Lawless, N. Serpone, and D. Meisel, *J. Phys. Chem.*, *95*, 5166 (1991).
299. R. B. Draper and M. A. Fox, *Langmuir*, *6*, 1396 (1990).
300. R. C. Chambers and C. L. Hill, *Inorg. Chem.*, *30*, 2776 (1991).
301. M. Bideau, B. Claudel, L. Faure, and H. Kazouan, *J. Photochem. Photobiol. A*:, *61*, 269 (1991).
302. M. Muneer, S. Das, V. B. Manilal, and A. Haridas, *J. Photochem. Photobiol. A*:, *63*, 107 (1992).
303. H. Gerischer and A. Heller, *J. Phys. Chem.*, *95*, 5261 (1991).
304. H. Gerischer and A. Heller, *J. Electrochem. Soc.*, *139*, 113 (1992).
305. H. Gerischer, *J. Phys. Chem.*, *88*, 6096 (1984).

306. D. Duonghong, E. Borgarello, and M. Grätzel, *J. Am. Chem. Soc.*, *103*, 4685 (1981).
307. E. Yesodharan and M. Grätzel, *Helv. Chim. Acta*, *66*, 2145 (1983).
308. D. E. Aspnes and A. Heller, *J. Phys. Chem.*, *87*, 4919 (1983).
309. M. A. Fox, in *Photocatalysis: Fundamentals and Applications*, N. Serpone and E. Pelizzetti, Eds., Wiley, New York, 1989, pp. 421–455.
310. J. L. Muzyka and M. A. Fox, *J. Org. Chem.*, *55*, 209 (1990).
311. M. A. Fox, in *Homogeneous and Heterogeneous Photocatalysis*, E. Pelizzetti and N. Serpone, Eds., Reidel, Dordrecht, 1986, pp. 363–383.
312. J. L. Muzyka and M. A. Fox, *J. Photochem. Photobiol. A:*, *57*, 27 (1991).